The optical polarisation of m42 and m43

Bahram Khalesse

THE OPTICAL POLARISATION OF M42 AND M43

by

BAHRAM KHALESSE

A Thesis presented at the

University of Durham

For the Degree of Ph.D.

June 1978

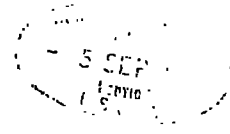

To my wife

ABSTRACT

This thesis contains a description of the technique used to measure the optical linear polarisation of the Orion Nebula and the nebula, M43, and the results obtained from these measurements. This work was undertaken while the author was a member of the Durham University Astronomy Group.

The first chapter is an outline of the differing states of polarisation and the method used to describe these states via the Stokes Parameters. A short review of the mechanisms producing linear polarisation of the optical radiation from astronomical objects is included.

Chapter 2 describes briefly the mechanisms producing plane polarisation and dust scattering and also contains a description of Rayleigh and Mie Scattering.

Chapter 3 contains a brief account of the design and operation of the Durham University nebular polarimeter used to detect and measure optical linear polarisation, along with a short description of the electronographic camera used as a recording device. Also, the technique for the reduction of the data, from its initial electronograph to the final extraction of the Stokes parameters for over 8550 points in the Orion Nebula is described.

The next chapter contains an account of gaseous nebulae, particularly the Orion Nebula, where a review of the present properties of this object and some general remarks on M43 are made.

In Chapter 5 of this thesis, the technique employed to measure the optical linear polarisation of these nebulae, together with a final map of the polarisation for each of them, and a comparison of the results obtained by the present method for the Orion Nebula with those measurements of Hall (1974) and Pallister et al (1977) are described

which confirm the success of the present technique.

In the following chapter, some interpretation of the results and the geometry of the Orion Nebula and M43 are described. Also a simple model of the Orion Nebula as a spherically symmetric dust cloud with θ^1ori at the centre is presented. A comparison between this model considering the constant dust density case, and the polarisation measurements, is made in this chapter and some possible causes of the disagreement between this model and observational results are presented. In conclusion, the success of the technique is confirmed for the production of high resolution, accurate polarimetric measurements.

PREFACE

The work presented in this thesis was carried out during the period 1975 - 1978 while the author was a research student under the supervision of Dr. S.M. Scarrott in the Physics Department of the University of Durham. During this period the author visited the Royal Greenwich Observatory (R.G.O.) several times, also the Florence and George Wise Observatory, University of Tel Aviv, Israel in November 1976, and the Massachusetts Institute of Technology (MIT) in December 1977, U.S.A.

CONTENTS

Page No.

LIST OF FIGURES

Page No.

Page No.

LIST OF TABLES

INTRODUCTION

In my country, Iran, during the course of the history of science, astronomy has been ascribed the role of mother of science. stronomy has reached this important status because it has always been an area from which new knowledge and insight has been forthcoming. This is still true today, much of the 'new' physics of the past few decades has arisen from astronomical observations.

The techniques of twentieth century astronomy are very different from those of the past eras. As technology has progressed then astronomers have capitalised on these advances and have utilised them in their own particular domain. The topics of radio, microwave, infra-red, ultra violet, x-ray and γ-ray astronomy have become possible because of these advances and even the older form of astronomy, optical astronomy has benefited accordingly with the advent of sensitive detectors, on-line computer etc. Furthermore, the application of technological improvements in telescope manufacture and operation have considerably assisted in making the observations.

The role of the astronomer has also changed. At the present time the acquisition of data is rapid and usually the astronomer spends much less time in integrating the data.

In optical astronomy obviously the medium by which information is gleaned about astronomical objects is visible light, the usual techniques being polarimetry and spectroscopy. However light carries considerable information about its history in the form of polarisation. Linear polarisation is a commonly observed form of polarisation

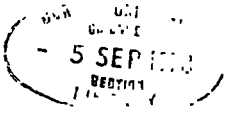

and this thesis is devolved to the description of the measurement and interpretation of the linear polarisation in the Orion Nebula, M42 and M43.

Before embarking on the description of this work, it is worth recording the major events in the discovery and understanding of the polarisation of light, in particular where astronomical implications are involved. In chronological order I feel the important advances have been as follows:

1809 D.F.J. Arago found that the light from the sunlit sky is partially polarised.

1845 Michael Faraday discovered the rotation of the plane in a beam of linearly polarised light traversing certain media parallel to magnetic lines.

1852 Sir George G. Stokes described the four stokes parameters (this will be discussed in Chapter 1).

1869 D. Tyndall established the fact that the character of the polarisation of light scattered by particles changes strongly with the dimensions of the particles.

1896 Pieter Zeeman found that spectral lines can be broadened when the radiating atoms are in the presence of an intense magnetic field. Observation of the splitting of spectral lines by magnetic fields and their associated polarisation (Zeeman effect) was observed a few years later.

1908 Gustav Mie, and Peter Debye independently developed the theory of light scattering by spherical particles or arbitary size (this will be discussed in Chaper 2).

1929 Bernard Lyot published his thesis containing major discoveries on the linear polarisation of light from planets and terestrial substances.

1949 J.S. Hall and W.A. Hiltner discovered linear interstellar polarisation. Subsequent work produced a wealth of information on the polarisation of starlight which lead to a better understanding of the role of magnetic fields in the structure of the galaxy.

1954 V.A. Dombronskij disovered large polarisation in the Crab Nebula predicted with synchrotron radiation a year before by I.S. Shklovskij.

1959 Strong wavelength dependence was found for the linear polarisation of planets, stars and nebulae (see Coffeen, D.L. and Hanson, J.E.).

The reader who is interested in the above chronology is referred to T. Gehrels (1974, and references therein).

It is clear that observation of polarisation in astronomical objects might play an important role in understanding the physical mechanisms occurring in such objects. With this aim in mind, the Durham group have constructed a nebular polarimeter. Used in conjunction with the electronographic camera it is possible to map out the linear polarisation in extended astronomical objects. This thesis describes the polarimeter and its use to observe the Orion Nebula in an attempt to elucidate the illumination and dust distribution within the nebula.

CHAPTER ONE

POLARISED LIGHT

1.1 Discovery of Polarisation

The polarisation of light was discovered by Huygens in 1690, while experimenting with Iceland spar. He found that a ray of light was, by passage through the crystal, divided into two separate rays of equal intensity, except when the light traversed in a direction parallel to the crystallographic axis.

Then he stated that polarised light is such that its properties are not symmetrical with respect to the direction of propagation. This lack of symmetry is proved by the fact that a rotation of the ray about the direction of propagation as axis produces a change in the observed optical phenomena.

1.2 States of Polarisation

From the standpoint of classical physics, light consists of electromagnetic waves whose vibration are transverse to the propagation direction and characterised by the electric vector E. If the electric vector vibrates randomly in a plane perpendicular to the direction of propagation the light is called natural or unpolarised light.

Polarised light is light whose vibration exhibits a preference as to transverse direction, or a preference as to the associated handedness. When the orientation of the electric vector is constant although its magnitude and sign varies in time, the light is described as being linearly polarized or plane-polarised.

The result of the superposition of specific amounts of natural and polarised light is described as being partially polarised, then the degree of polarisation is defined as the ratio of the intensity of the polarised light and the total intensity.

The amplitude of the electric vector can be divided into two orthogonal components which are sinusoidal and exactly in phase, so that the resultant of these components is at a fixed angle in the plane of vibration.

When the two component beams have a phase difference α introduced between them, the electric vector traces out an ellipse in both time and position along the curve (Fig. 1.1). The ratio of the semi-minor axis and semimajor axis, i.e. b/a is called the ellipticity, and the eccentricity, less commonly referred to is given by $(a^2 - b^2)^{\frac{1}{2}}/a$. In the case where the two components have equal amplitudes, and in addition, their relative phase difference $\alpha = 2m\pi \pm \pi/2$ where $m = 0, \pm 1, \pm 2, \ldots$ the radiation is described as being circularly polarised.

By defining the sectional pattern, as seen by an observer who is situated in the path of the radiation and looking toward the light source, which is at the origin of coordinates, θ the angle of between the major semiaxis of ellipse and the x-direction is called the Azimuth of the sectional pattern or orientation of the ellipse (Fig. 1.1).

The plane of polarisation means the plane containing both E and K, the electric vector and the propagation vector in the direction of propagation.

1.3 Mathematical Specification of a Polarised Wave Train

As far as the mathematical description is concerned, both linear and circularly polarised light may be considered to be special cases of elliptically polarised. As previously described (Section 1.2), this means that, in general, the resultant electric fector E will both rotate and change its magnitude. In such cases the endpoint of E will trace out an ellipse, in a fixed plane perpendicular to K (propagation vector), as the wave sweeps by. In order to see this and then find the expressions of elliptical, circular and linear polarisation, we may write an expression for the curve traversed by the tip of E. That is:

$$E_x = E_{ox} \cos (kz - \omega t) \tag{1.1}$$

and

$$E_y = E_{oy} \cos (kz - \omega t + \alpha) \tag{1.2}$$

where α is the relative phase difference between the two bean components, k the wave number = $2\pi/\lambda$, z the position along the axis of propagation and ω the angular frequency. The equation of the curve we are looking for should neither be a function of position nor time, i.e. should be independent of $(kz - \omega t)$. Expand the expression for E_y into

$$\frac{E_y}{E_{oy}} = \cos (kz - \omega t) \cos\alpha - \sin (kz - \omega t) \sin\alpha$$

and combine it with $\frac{E_x}{E_{ox}}$ to yield

$$\frac{E_y}{E_{oy}} - \frac{E_x}{E_{ox}} \cos\alpha = -\sin (kz - \omega t) \sin\alpha \tag{1.3}$$

It follows from equation (1.1) that

$$\sin(kz - \omega t) = \left[1 - \left(\frac{E_x}{E_{ox}}\right)^2\right]^{\frac{1}{2}}$$

and so equation (1.1) leads to

$$\left(\frac{E_y}{E_{oy}} - \frac{E_x}{E_{ox}}\cos\alpha\right)^2 = \left[1 - \left(\frac{E_x}{E_{ox}}\right)^2\right]\sin^2\alpha$$

Finally then, on rearranging terms we have

$$\left(\frac{E_y}{E_{oy}}\right)^2 + \left(\frac{E_x}{E_{ox}}\right)^2 - 2\left(\frac{E_x}{E_{ox}}\right)\left(\frac{E_y}{E_{oy}}\right)\cos\alpha = \sin^2\alpha \qquad (1.4)$$

This is the equation of an ellipse for elliptical polarisation making an angle θ (orientation of ellipse), with the (E_x, E_y) coordinate system (Fig. 1.1) such that

$$\text{Tan } 2\theta = \frac{2\,E_{ox}\,E_{oy}\cos\alpha}{E_{ox}^2 - E_{oy}^2} \qquad (1.5)$$

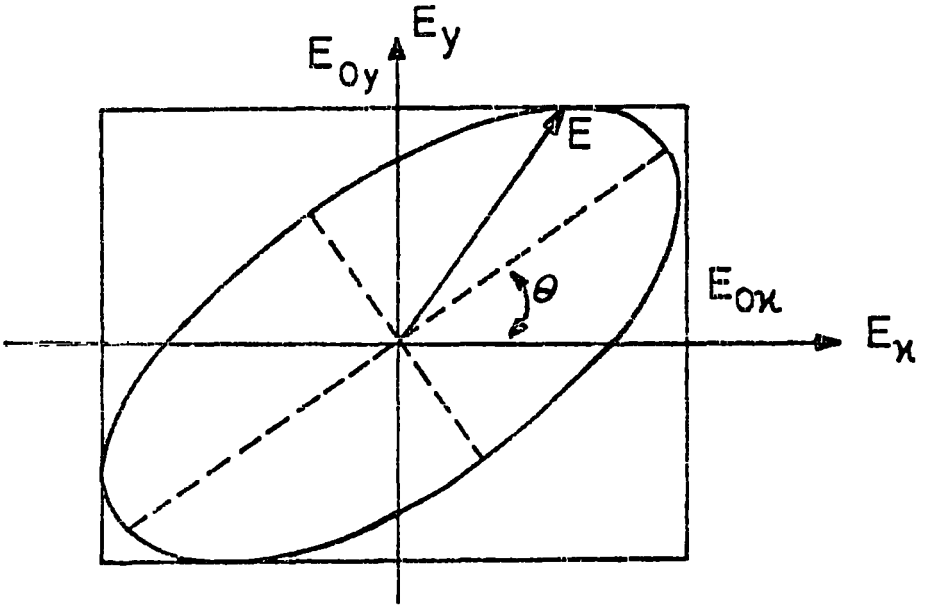

Figure 1.1: Elliptical polarisation. The direction of propagation is into the paper.

Equation (1.4) might be a bit more recognizable if the principal axes of the ellipse were aligned with the coordinate axes, i.e. $\theta = 0$ or equivalent $\alpha = \pm\pi/2, \pm 3\pi/2, \pm 5\pi/2, \ldots\ldots$, in which case we have the familiar form

$$\frac{E_y^2}{E_{oy}^2} + \frac{E_x^2}{E_{ox}^2} = 1 \qquad (1.6)$$

Furthermore, if $E_{oy} = E_{ox} = E_o$ this reduces to

$$E_y^2 + E_x^2 = E_o^2 \qquad (1.7)$$

which is equation of a circle for circular polarisation.

If $\alpha = n\pi$ where $n = 0, \pm 1, \pm 2, \ldots\ldots$, equation (1.4) then becomes

$$E_y = \pm \frac{E_{oy}}{E_{ox}} E_x \qquad (1.8)$$

which are equations of lines for linear polarisation having slopes of $\pm E_{oy}/E_{ox}$

1.4 Methods of Describing Polarised Light

The modern description of polarised light actually had its origins in 1852 in the work of G.G. Stokes. He introduced four quantities which are functions only of observables of the electromagnetic wave and are now known as the Stokes parameters. The state of polarisation of a beam of light can be described in terms of these quantities. The four parameters have the dimensions of intensity; each corresponds not to an instantaneous intensity, but to a time-averaged intensity,

the average being taken over a period long enough to permit practical measurement.

For quasimonochromatic light with elliptical polarisation, in general we have:

$$\vec{E}_x(t) = \vec{i}\, E_{ox}(t) \cos\left[(\vec{k}z - \vec{\omega}t) + \alpha_x(t)\right] \tag{1.9}$$

and

$$\vec{E}_y(t) = \vec{j}\, E_{oy}(t) \cos\left[(\vec{k}z - \vec{\omega}t) + \alpha_y(t)\right] \tag{1.10}$$

where $\vec{i}$ and $\vec{j}$ being the unit vectors along the x and y axes, and $\underline{\vec{E}}(t) = \vec{E}_x(t) + \vec{E}_y(t)$. Using these and the fact that $\alpha = \alpha_y - \alpha_x$, the Stokes parameters are:

$$I = \langle E_{ox}^2 \rangle + \langle E_{oy}^2 \rangle \tag{1.11a}$$

$$Q = \langle E_{ox}^2 \rangle - \langle E_{oy}^2 \rangle \tag{1.11b}$$

$$U = \langle 2E_{ox} E_{oy} \cos\alpha \rangle \tag{1.11c}$$

$$V = \langle 2E_{ox} E_{oy} \sin\alpha \rangle \tag{1.11d}$$

For the hypothetical case of perfectly monochromatic light $E_{ox}(t)$, $E_{oy}(t)$, and $\alpha(t)$ are time independent and by dropping the $\langle\rangle$ brackets in equation (1.11), the applicable Stokes parameters can be obtained.

The measured intensities of an actual beam of light are a superposition of many simple waves with independent phases. Thus the Stokes parameters of entire beam are:

$$I = \Sigma I_j \qquad Q = \Sigma Q_i \qquad U = \Sigma U_i \qquad V = \Sigma V_i \,.$$

In general the four parameters satisfy the inequality

$$I^2 \geq (Q^2 + U^2 + V^2) \qquad (1.12)$$

If the beam is entirely unpolarised, $Q = U = V = 0$. If it is completely polarised, $I^2 = Q^2 + U^2 + V^2$. The degree of polarisation may be defined as:

$$P_e = \frac{(Q^2 + U^2 + V^2)^{\frac{1}{2}}}{I} \qquad (1.13)$$

The parameter V is positive for right handed circular polarisation, negative for left circular polarisation, and zero for all linear forms.

In the case of linear polarisation where $V = 0$, the degree of polarisation is

$$P = \frac{(Q^2 + U^2)^{\frac{1}{2}}}{I} \qquad (1.14)$$

and in the case of time independence for the ratio of $\frac{U}{Q}$ we have:

$$\frac{U}{Q} = \frac{2 E_{ox} E_{oy} \cos\alpha}{E_{ox}^2 - E_{oy}^2}$$

It follows from equation (1.5)

$$\tan 2\theta = \frac{U}{Q}$$

$$\theta = \tfrac{1}{2} \tan^{-1} \left(\frac{U}{Q}\right) \qquad (1.15)$$

REFERENCES

CHAPTER 1

Coffeen, D.L. and Hansen, J.E., 1974, Plants, Stars and Nebulae, p.518, ed. T. Gehrels

Gehrels, T., 1974, Plants, Stars and Nebulae, pp. 4 & 40, ed. T. Gehrels

Huygens, C.' Treatise on Light, Dover Pub. Inc., N.Y. 1962 (1690).

Stokes, G.G. 1852, Trans. Cambridge Phil. Soc. 9, 399

CHAPTER TWO

POLARISATION BY SCATTERING FROM DUST

2.1 Mechanisms producing plane polarisation

For the past three decades astronomers have made measurements of the plane polarisation of light from many astronomical objects.

From these measurements it is possible to deduce, in many cases, the mechanism responsible for the production of polarisation. Magnetic fields have an important role in the polarising mechanisms, either directly in the emission process or indirectly by the alignment of scattering particles. In astrophysical phenomena partially plane polarised light can arise in processes such as synchrotron emission, Zeeman effect, reflection from solid surfaces and most important of all, by scattering as listed below.

(1) Scattering by molecules (Raleigh Scattering), for example, by the molecules in the atmosphere of Venus (Coffeen and Hansen 1974).

(2) Scattering by small particles, or grains of finite size (Mie scattering), e.g. in the central region of Orion Nebula (Pallister et al 1977).

(3) Scattering by free electrons (Thompson Scattering) as seen in the solar corona (Aller 1953).

Obviously Rayleigh and Mie scattering are relevant to the Orion nebula and will be discussed in detail later in this chapter.

2.2 Theory of Scattering

When a plane electromagnetic wave of frequency ν_o falls upon

a charged particle, the particle is set into motion and radiates secondary waves with the same frequency ν_o. The phenomenon is called Scattering.

Generally the term scattering is used when small particles are involved, particularly when they are irregularly arranged in space. Scattering is not a practical means of polarising light, because in practice the polarisation usually is not complete in any direction and the intensity is quite low. The study of polarisation effects in the light scattered by small particles, however, gives information on the nature of the particles and is a means of investigating the scattering particles in remote astronomical objects.

2.3 Rayleigh Scattering

The first quantative study of the laws of scattering by small particles was made in 1871 by Rayleigh, and such scattering is frequently called Rayleigh scattering.

The scattering of light by particles which are small in comparison to the wavelength of the incident light is known as Rayleigh scattering; an example is the scattering of sunlight by air molecules.

Details of the mathematical investigation of the problem which gives a general law for the intensity of scattered light, applicable to any particles or grains with index of refraction different from that of the surrounding medium are given in Van De Hulst 1957.

The scattering properties of grains depend on the dimensionless quantity

$$x = \frac{2\pi d}{\lambda} \qquad (2.1)$$

where d = radius of the grain

λ = wavelength of the light.

In the case of Rayleigh scattering, the restriction is that the linear dimensions of the particles be considerably smaller than the wavelength

$$d << \lambda$$

or

$$x << 1$$

The scattered intensity is found to be proportional to the incident intensity and to the square of the volume of the scattering particle. The most interesting result, however, is the dependence of scattering on wavelength. For scattering at an angle θ (Figure 2.2), the scattered intensity is proportional to $I/\lambda^4 \ (1 + \cos^2\theta)$. For more detail see Chandresakhar 1960, Jenkins and White (1957).

For a given size of the particles, the longer wavelengths would be expected to be less effectively scattered than short ones, because the particles present obstructions to the waves which are smaller compared with those for longer wavelengths, so the radiation of shorter (blue) wavelength is most strongly scattered, see Figure 2.1.

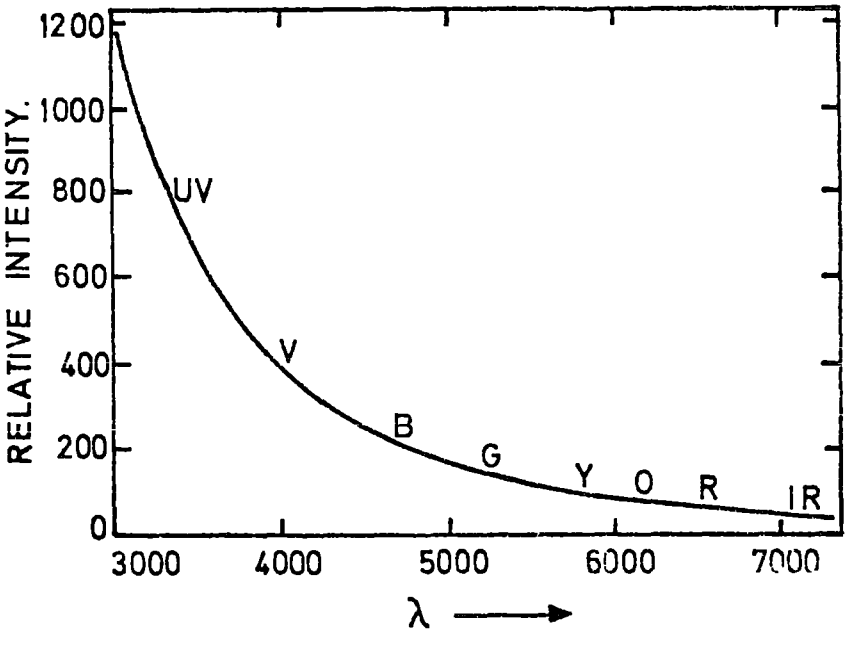

Figure 2.1: Intensity of scattering vs. wavelength according to Rayleigh's law (Jenkins and White 1957).

Now if we consider a small particle to be at the origin of a cartesian coordinate system, and a quasi-monochromatic plane wave whose wavelength is much larger than the dimensions of the particle travelling in the positive z direction, the scattered wave is to be observed at a point P whose polar coordinates are r, θ and ϕ, as is shown in Figure 2.2.

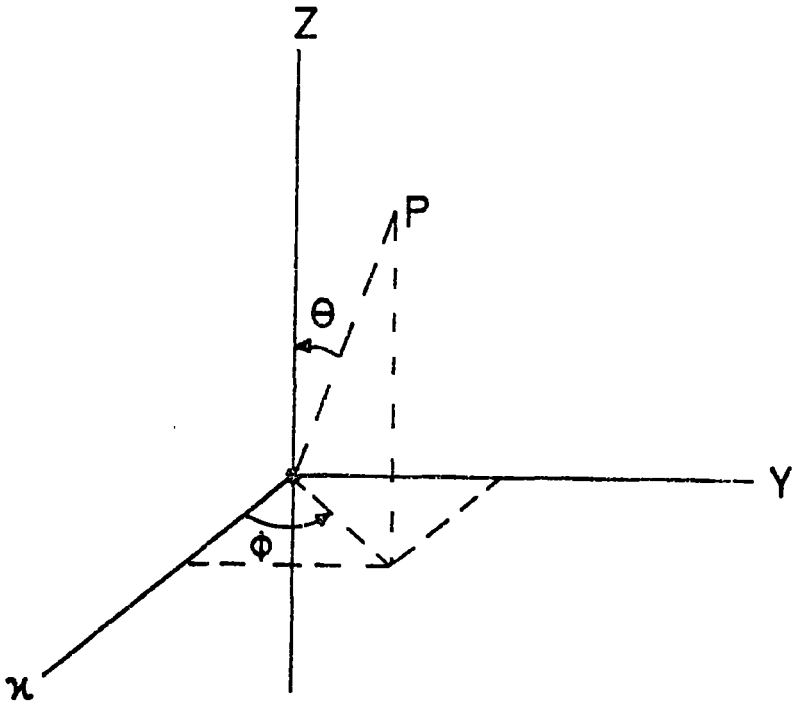

Figure 2.2: The scattering particle is at the origin, and an incident plane wave travels in the positive z direction.

To find the nature of the scattered wave at the point P when the incident wave is quasi-monochromatic and whether there is any polarisation represented by a set of Stokes parameters, we consider the case of an unpolarised incident wave which will be represented by:

$$(I, Q, U, V) = (I, O, O, O) \tag{2.2}$$

The parameters of the scattered wave are found to be (see Born 1963):

$$I_p = \frac{K^4 |\alpha|^2}{2r^2} (\cos^2\theta + 1) I \tag{2.3}$$

$$Q_p = \frac{K^4 |\alpha|^2}{2r^2} (\cos^2\theta - 1) I \tag{2.4}$$

$$U_p = V_p = 0 \tag{2.5}$$

Where α is the polarisability and is defined by $p = \alpha e$; (p is the dipole moment of the particle and e is the electric field at point P) and K is the wave number ($K = \frac{2\pi}{\lambda}$).

The polarisation is identical to that produced by Thompson scattering from free electrons. From equations (2.5) and (1.14) the degree of polarisation is found to be

$$P = \frac{|Q_p|}{I_p} \tag{2.6}$$

By substituting equations (2.3) and (2.4) into (2.6), we have:

$$P = \frac{1 - \cos^2\theta}{1 + \cos^2\theta} \tag{2.7}$$

The scattered wave is therefore unpolarised in the forward and backward directions, and completely polarised in the directions at right angles to the incident beam ($\theta = 90^o$). It can also be seen that the scattered intensity is symmetric about $\theta = 90^o$, as is shown in Figure 2.3.

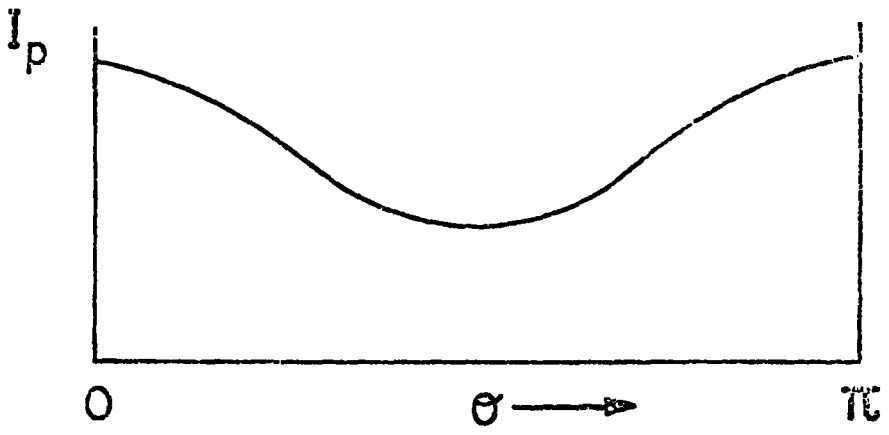

Figure 2.3: The scattering diagram for Rayleigh scattering from an unpolarised beam.

2.4 Mie Scattering

An important case in the scattering of light by particles is that by spheres, such as drops of water in fog or rain, or metal spheres in colloidal suspension.

Gustave Mie in 1908 published a rigorous solution of the scattering problem for homogeneous spherical particles of any size. Single scattering by spheres of a finite size is called Mie Scattering.

The Mie theory shows that when the wavelength is comparable to the diameter of a sphere, the scattering pattern shows details quite sensitive to size. In general, the scattering in any direction is described by four amplitude functions, S_1, S_2, S_3 and S_4, all functions of θ and ϕ (see Figure 2.2) which form a matrix $S(\theta,\phi)$ of four elements called the Scattering Matrix.

The electric vector is represented by:

$$E = \mathrm{Re}\left(E_{\ell} m + E_{q} n\right) \tag{2.8}$$

Where E_{ℓ} and E_{q} are complex, oscillating functions, m and n are the unit vectors.

By considering E_o and E to be electric field vectors of incident and scattered radiation, we can write:

$$\begin{pmatrix} E_{\ell} \\ E_{q} \end{pmatrix} = \begin{pmatrix} S_2 & S_3 \\ S_4 & S_1 \end{pmatrix} \frac{e^{-iKr + iKz}}{iKr} \begin{pmatrix} E_{o\ell} \\ E_{oq} \end{pmatrix} \tag{2.9}$$

Where q and ℓ refer to the electric fields perpendicular to and parallel with the plane of scattering.

Spherical particles have $S_3 = S_4 = 0$. So two complex amplitude functions occur for any direction. These functions are $S_1(\theta)$ and $S_2(\theta)$; they depend only on the scattering angle θ. The matrix equation for an arbitrary direction $\theta \neq 0$ now gives the two relations:

$$E_q = S_1(\theta) \frac{e^{-iKr + iKz}}{iKr} E_{oq} \tag{2.10}$$

$$E_{\ell} = S_2(\theta) \frac{e^{-iKr + iKz}}{iKr} E_{o\ell} \tag{2.11}$$

by taking the squares of the moduli we obtain for perpendicular polarisation:

$$I = \frac{I_1}{K^2 r^2} I_o \tag{2.12}$$

For parallel polarisation:

$$I = \frac{I_2}{K^2 r^2} I_o$$

For incident natural light:

$$I = \frac{{}^1/_2 (I_1 + I_2)}{K^2 r^2} I_o \qquad (2.14)$$

where $I_1 = |S_1(\theta)|^2$ and $I_2 = |S_2(\theta)|^2$

In which the terms I_1 and I_2 refer respectively to the intensity of light vibrating perpendicularly and parallel to the plane through the direction of propagation of the incident and scattered beams, and the degree of polarisation is $\frac{(I_1 - I_2)}{(I_1 + I_2)}$.

Quite generally the computational problem involved in the Mie problem is to compute the values of I_1 and I_2. In this situation, various definitions and complicated mathematical calculations are required in order to obtain the coefficients (see Van de Hulst 1957).

REFERENCES

CHAPTER 2

Aller, L.H., 1953, The Atmospheres of the Sun and Stars, Chap. 4.

Chadrasekhar, S. 1960, Radiative Transfer.

Coffeen, D.L. and Hansen, J.E., 1974, Plants, Stars and Nebulae, p.518, ed. T. Gehrels

Jenkins, F.A. and White, H.E., 1957, Fundamentals of Optics, Chap. 22

Mie, G., 1908, Ann Physik, 25, 377

Pallister, W.S. et al, 1977, 178 MNRAS pp.93-95

Rayleigh, J.W.S., 1871, Phil. May, 41, pp.107, 274 and 447 (Sci. Papers 8 and 9)

Stone, J.M., 1963, Radiation and Optics, Chap. 13 and 14

Van De Hulst, H.C., 1957, Light Scattering by Small Particles

CHAPTER THREE

TECHNIQUE

3.1 The Electronographic Camera

The conventional techniques for photometric measurements of astronomical objects are the photographic plate and photoelectric devices. Photographic plates allow extended images to be recorded but have low photometric accuracy due to the logarithmic response of the emulsion and consequent calibration. Another difficulty with the photographic process is the limited dynamic range of the recording medium.

Photoelectric photometers have the required range and accuracy but measure a small area at a time so that photometric mapping of an extended object is laborious and the combination in a way both the above processes incorporating the individual desired features. The electronographic camera is linear, has a wide dynamic range and records all areas of an extended field simultaneously.

Electronographic cameras are devices, which produce pictures and have sensitivity close to that of photoelectric devices. Of these the 4-cm. McMullan Camera, built at the Royal Greenwich Observatory was used for the present observation.

The basic idea of the electronographic camera is that the photon image is converted into electrons, and these are accelerated and recorded to give an amplified image. A diagram of the camera is shown in Figure 3.1.

The light image is focussed on the photocathode, which is a

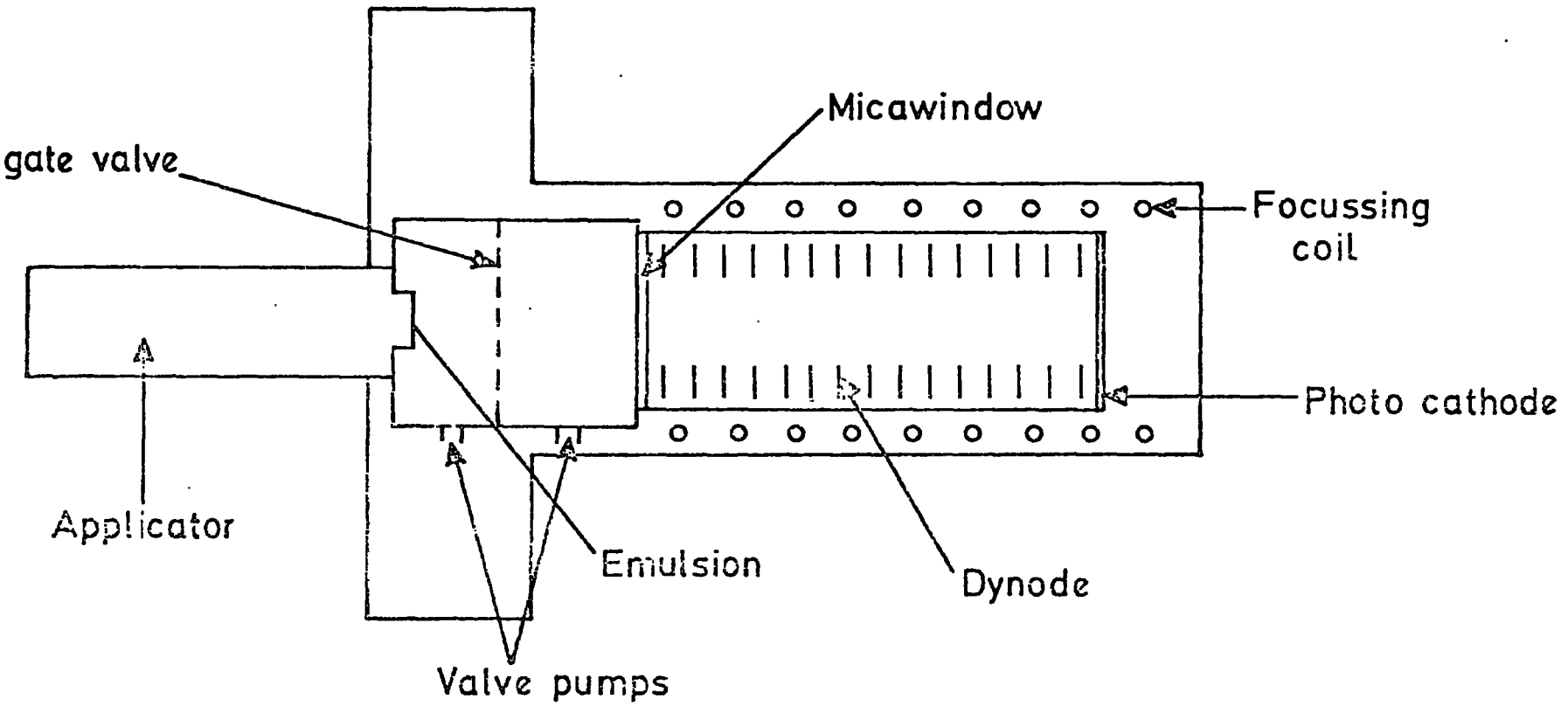

FIG 3·1 SCHEMATIC DIAGRAM OF THE ELECTRONOGRAPHIC CAMERA.

thin layer of compound of Na-K-Cs-Sb, and is formed on the inside surface of a glass window at the end of the camera. The photocathode is affected by small amounts of oxygen or water vapour, and as a result a mica window is introduced between the photocathode and the inserted electronographic film. Window and film are placed in the vacuum surroundings, by means of an ion appendage pump.

Each incident photon of light from the object produces an electron which has relatively zero energy (electron energy - energy of photon - work function $\sim$ eV), the electrons are electrostatistically accelerated down the camera by a large potential difference along the tube ($\sim$ 40 Kv). The electric field is produced by electrodes made of titanium annuli spaced by soda lime glass cylinders 10 mm long. The whole structure is fused together with solder glass. Metal oxide-glaze resistors forming the potential divider are mounted on the electrode structure.

An external coil produces a magnetic field, which constrains the accelerated-electrons to tight spiral paths. Then the electron image is formed at the thin transparent mica window (with a diameter of 40 mm and a thickness of 4 μ), which has the property of transmitting at least 70 per cent of the accelerated-electrons.

The difficulty in practice is that the mica window, which must be very thin to be transparent to the electrons, will not resist atmospheric pressure on one side, and a high vacuum on the chamber side. This difficulty has been overcome in the McMullan electronographic camera. On the film side of the window (nuclear emulsion 10 μ thick, on melinex 50 μ thick), the air pressure is maintained at 1 torr by a mechanical pump, and the film is mounted in a film

holder and brought into contact by a pneumatic activator, through and gate valve which acts as a vacuum lock.

The mechanism for loading and unloading the [illegible] automatic. Each of the high energy electrons have a track in the nuclear emulsion, which can later be developed to reveal an apparent optical negative of the object.

The detector quantum efficiency of the electronographic is wavelength dependent. Each electron incident on the emulsion causes the same amount of development along its track because all of them are at the same high energy ($\sim$ 40 KV). In comparison to photographic plates, the grain size is much smaller, so saturation occurs at a much greater density. The main advantage is the fact that the density on the plate is linearly proportional to the intensity of incident radiation, and this linearity law is exhibited over a range of at least 5 in density.

For the present series of observations Ilford L4, a fine grain emulsion was used.

3.2 Polarimeter and Operation

Many kinds of polarimeter have been designed and used for measurement of optical polarisation from astronomical objects. Some examples of these can be seen in the thesis of Lyot (1929) and Dollfus (1958), also in the work of Öhman (1939) and Hiltner (1949, 1951).

Öhman used a doubly refracting prism to produce two adjacent images in orthogonally polarised light. For these studies, the Durham polarimeter was used, which is based on the ideas of Öhman (1939) and Pickering (1873).

The Durham polarimeter has been designed so as to be as flexible as possible in its optical configuration, mechanical construction and detection system (of which full details are given i Pallister 1976, Axon 1977). The figures of 3.2 and 3.3 respectively are schema diagrams of the polarimeter (showing the passage of a light ray) and a photograph of the Durham polarimeter.

When a particular object is imaged on the grids (where these grids (opaque bars) by necessity block out half the field view), the polarimeter 'sees' the part of image contained in the series of vertical gaps formed by the grids. The light from those parts of the image which are formed behind the opaque bars, is absorbed.

The light from the image contained in the vertical gaps passes through the polarising components of the polarimeter, and is finally reimaged by the relay lens. This image can then be recorded by means of a photographic plate or, as used in the present case, an electronographic camera. Grids are attached to a brass rod, which, when operated externally moves the grid system, transverse to the axis of the polarimeter by exactly one grid spacing. The width of the grid (3.2 mm) is chosen such that the Wollaston prism (4 cm width) will produce two adjacent images with a mutual displacement of one grid spacing.

By using a field lens (2.0 cm focal length and f5), all the light is constrained to pass through the optical system and then, an achromatic 'half wave ($\lambda/2$) plate', in a rotatable mounting is required. When in its initial position 0^{o}, its optic axis is aligned North-South.

The step of the half-wave plate is $22\frac{1}{2}^{o}$, so when it is rotated through $22\frac{1}{2}^{o}$ the plane of polarisation of the light rotates through 45^{o}.

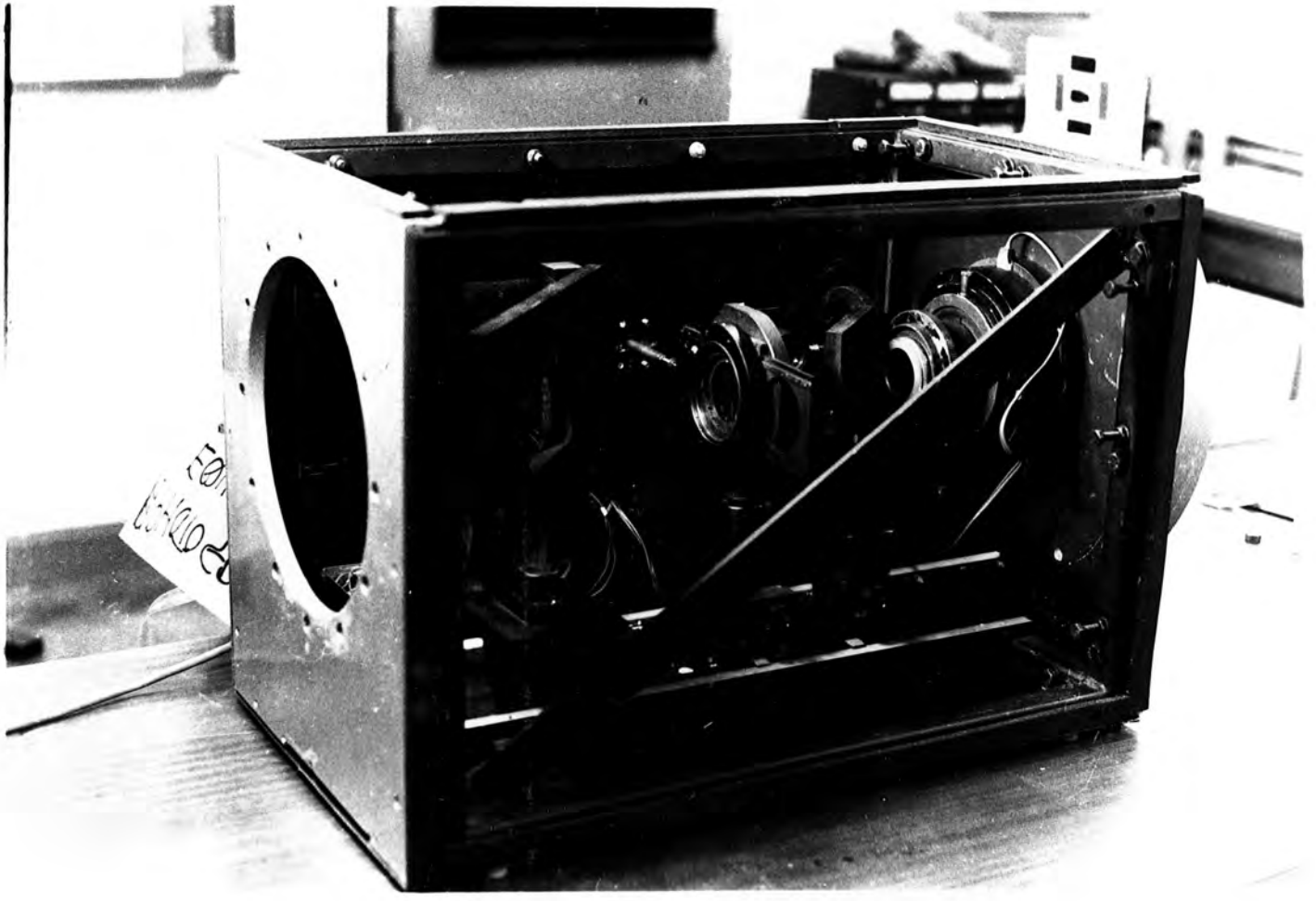

Figure 3.3: The Durham Polarimeter

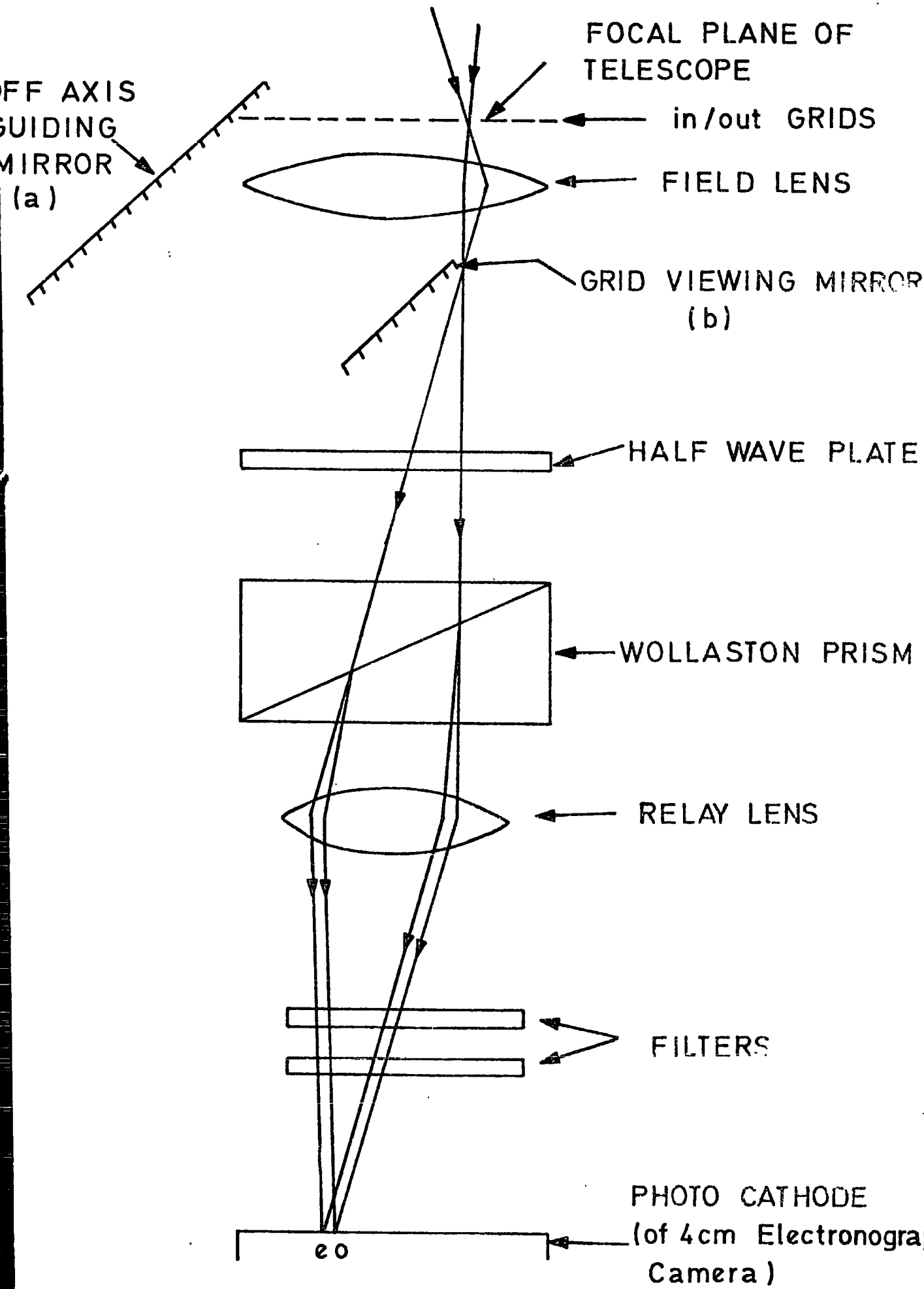

IG. 3·2 SCHEMATIC DIAGRAM OF THE POLARIMETER SHOWING PASSAGE OF LIGHT RAY

In separate observations, different $\lambda/2$ plates which are achromatic over the ranges of $(4500\ \text{Å} \pm 500\ \text{Å})$ and $(5400\ \text{Å} \pm 600\ \text{Å})$ are used. Also both B and V filters of UBV system are placed between the grids and the corresponding $\lambda/2$ plate, to limit the waveband of the incident light.

By then, two adjacent images in orthogonally polarised light will be produced by the Wollaston prism. If we rotate the $\lambda/2$ plate in steps of $22\frac{1}{2}^{\circ}$, we can obtain the four electronographs of an object in planes of polarisation of 0° and 90° on one film and 45°, 135°; 90°, 0°; 135°, 45° on the other three films. Now all the information required to calculate the degree and angle of polarisation, can be obtained from these four electronographs.

An externally operating electronic shutter is used to regulate the exposure time of each electronograph. Because of some long exposure time, a relay lens is used in the system to demagnify the image, and focus it on the photocathode of the McMullan Camera.

The relay lens is a Nikon f/1.4 camera lens of focal length 50 mm, and is bloomed to reduce unwanted reflection. The focal length, and positioning of the relay lens, demagnifies 4 x linearly, which means sixteen times in area. Therefore, the exposure time is reduced by a factor of 16. In addition to the main components of the polarimeter mentioned here, two mirrors which are made of aluminised perspex have been used in operation.

The first mirror, the off axis guiding mirror, mounted at 45° to the principle axis of the polarimeter, is such that its distance from the viewing telescope is the same as the distance from its centre front fact to the grids. The mirror has an elliptical hole of mirror

axis ~ 5 Cm in the centre to allow the axial light to reach the polarimeter.

The second mirror, the grid-image viewing mirror, can be rotated into the light path at 45° between the grids and half wave plate to deliver the light to a telescope mounted on the control panel so that the astronomical image formed on the grids can be viewed, Figure 3.2. This is necessary before an exposure is taken, to ensure that the object is centrally placed in the field of view. It is also used to focus the telescope image on to the grid system. Eyepieces of 2 cm focal length are used in the polarimeter.

The whole system is enclosed in a box with a one inch steel framework and aluminium sides of 570 x 380 x 410 mm in dimensions. All the controls and knobs for the $\lambda/2$ plate and the rotatable mirror, the grids, relay lens and shutter, are situated on the side of the casing.

In operation, without moving the position of the telescope, the grids can be moved into two positions, viz: IN and OUT, and in each case an electronograph of one half of the object under view can be taken. For the grids to be focussed, 20 micron gold wires are attached to them. By viewing these through the relay lens, it is possible to tell, if the prism is not in square since the two images of the wire are mutually vertically displaced. When the images of the wire form a straight line, we have the correct position (see Figure 3.4).

The polarimeter is mounted on the telescope by an aluminium adaptor plate and the electronographic camera is connected to the polarimeter in this position.

The grids are finely focussed on the photocathode, when the thin wire is sharply in focus. This is achieved by adjusting the relay

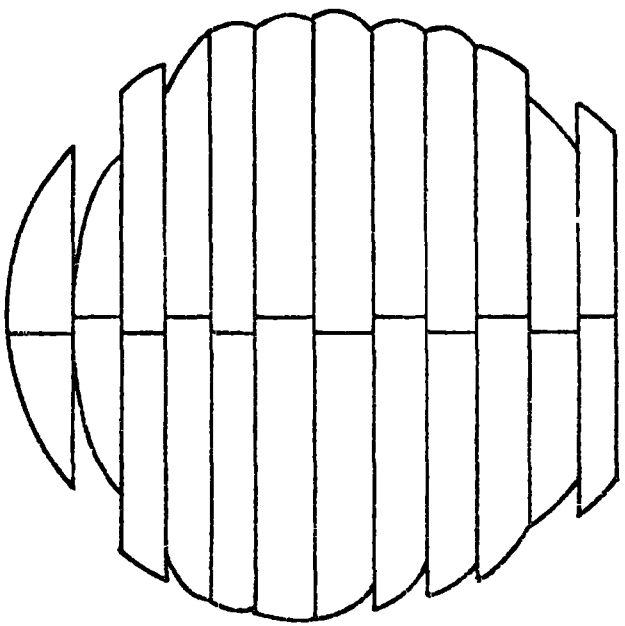

PRISM NOT IN SQUARE

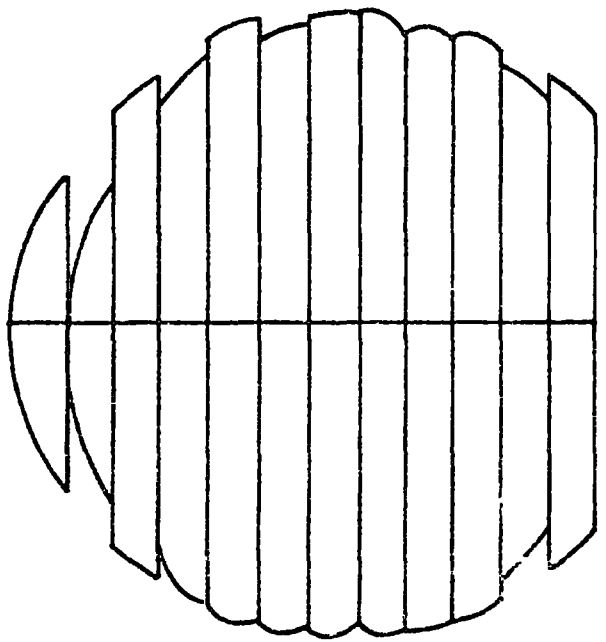

PRISM IN SQUARE

FIG. 3.4

lens position and taking some electronographs.

The telescope is focussed so that the grids lie in the focal plane of the secondary mirror. To check that north is at the top of the grids, and that the grids lie North-South, a star may be imaged on the edge of a grid spacing, using the grid viewing mirror and eye-piece. If the telescope is now driven in declinations, the star will be seen to move up and down the grid, while remaining exactly on the edge of the grid, if the alignment is correct.

After focussing the telescope, the system is ready for operation. Figure 3.5 shows a diagram of a typical electronograph.

3.3 Digitisation of the plates

The information on the developed-electronographic plates has first to be converted to a digital form. The electronographs were digitised on the P.D.S. machine at the Royal Greenwich Observatory, with an aperture size of 24 μ x 24 μ, and steps of 26 μ, over an area of 512 pixels x 512 pixels, where each pixel corresponds to an area of 1.4 arc sec x 1.4 arc sec (more details are given in Pallister 1976).

As mentioned in Section 3, the density on the plate is linearly proportional to the intensity of the incident light. After a small correction has been made for the microdensitometer-response, the digital results are directly proportional to the actual intensity of the light from the object.

3.4 Reduction of the Data

There are a series of eight plates for the object, four from each position ('in', 'out') of the grids. We assume that the intensity

FIG. 3·5 DIAGRAM SHOWING A SKETCH OF AN ELECTRONOGRA

I WITH THE WOLLASTON PRISM REMOVED

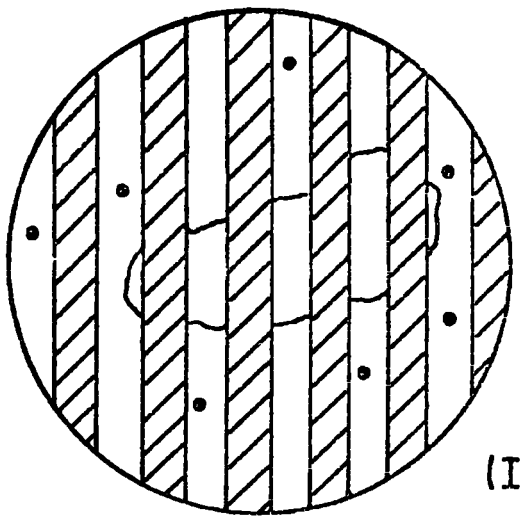

(I)

II WITH THE WOLLASTON PRISM.

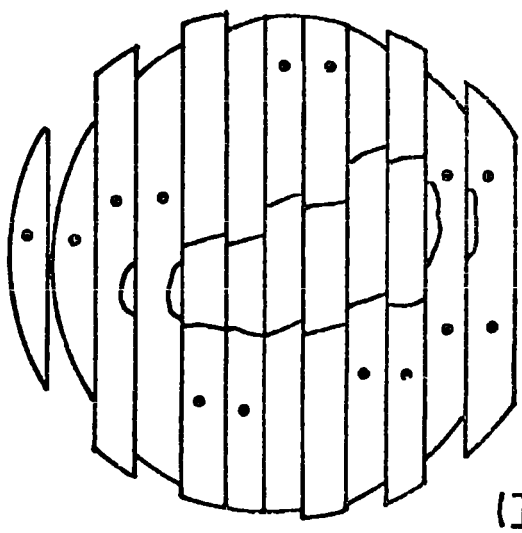

(II)

of the left hand strip is i_1, which corresponds to the intensity of the unpolarised component plus the polarized component, component at angle θ , and the intensity of the clear plate. Its adjacent strip has intensity i_2 and similarly we define i_3, i_4; i_5, i_6; i_7, i_8 for the other three plates.

Consider a beam of light with intensity consisting of a linearly polarised component of intensity I_p, whose E vector makes an angle θ with North (see Figure 3.6), and an unpolarised component of intensity $(I - I_p)$.

In this case the component of the E vector parallel to the reference direction, ($\theta = 0^o$) from the polarised light will be $I_p \cos^2\theta$. The unpolarised light will be divided equally between $\theta = 0^o$ and $\theta = 90^o$, therefore

$$i_1 = I_p \cos^2(-\theta) + \frac{I - I_p}{2}$$

or

$$i_1 = I/2 + I_p/2 \cos 2\theta \qquad (3.1)$$

Similarly for the plane of polarisation at 90^o to the first i.e. for orthogonal image of i_1 we have:

$$i_2 = I_p \cos^2(90 - \theta) + \frac{I - I_p}{2}$$

or

$$i_2 = I/2 - I_p/2 \cos 2\theta \qquad (3.2)$$

3.4.1 Photocathode Response

As the sensitivity of the photocathode is not constant in position, there is a variation in the photocathode response between

FIG. 3.6

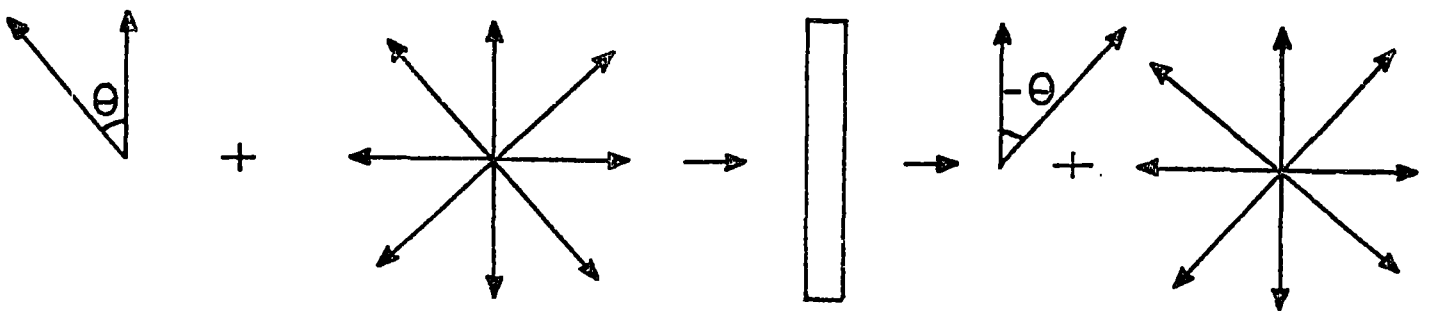

POLARISED COMPONENT Ip AT ANGLE θ

UNPOLARISED COMPONENT

λ/2 PLATE

POLARISED COMPONENT TURNED THROUGH 2θ

UNPOLARISED. COMPONENT

left hand strip and its adjacent strip (right hand strip). These deviations which are quoted by manufacturers, are small $\mp$ 5%. But as we need to compare the intensity of a point with the same position in both left hand and right hand strips, we need to make a correction the correction coefficient called the f-factor.

If we called the photocathode response of the right hand strip at some point 1 and that of the left hand strip at the corresponding point f, by rotating the half wave plate in steps of $22\frac{1}{2}^{o}$, the situations in Table 3.1 are obtained, showing directions of the E vectors of the light.

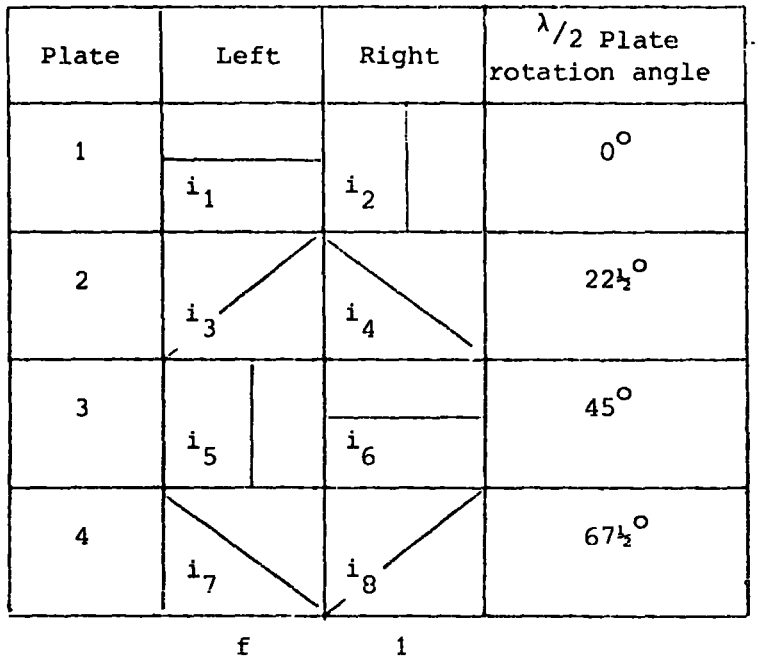

Table 3.1: The direction of the E vector recorded at each $\lambda/2$ plate setting (black line).

With regard to this table, the intensity of i_1 on plate 1 must correspond to the intensity of i_6 on plate 3, i_2 to i_5 and so on.

For plates 1 and 3 we have:

$$i_1 = \frac{i_6}{f_1} \qquad \text{and} \qquad i_5 = \frac{i_2}{f_1}$$

so

$$f_1 = \left(\frac{i_6 i_2}{i_5 i_1}\right)^{\frac{1}{2}} \tag{3.3}$$

Plates 2 and 4 give:

$$i_3 = \frac{i_8}{f_2} \qquad \text{and} \qquad i_7 = \frac{i_4}{f_2}$$

so

$$f_2 = \left(\frac{I_4 I_8}{I_3 I_7}\right)^{\frac{1}{2}} \tag{3.4}$$

hence the variation of the photocathode response at each point may be calculated.

When the photocathode response is constant, $f_1 = f_2 = 1$. But in practice this is not the case and for the present series of observations, the restriction on points used is that $|f_1 - f_2| \leq 0.05$. Therefore the factor used is the average of f_1 and f_2.

$$f = \frac{f_1 + f_2}{2} \tag{3.5}$$

and all the right strips normalised by a factor f, as $\frac{i_2}{f}$ in plate 1.

3.4.2 Exposure Factor

As the observed intensity on the plates depends on the time of exposure and sky-brightness, which could change over the time taken for all plates to be obtained, total intensity is not constant from plate to plate.

To allow for this, we use the exposure factors e_1, e_2, e_3 which are defined later, to normalise from plate 1 to the other three plates.

The exposure factor e_1 is the ratio of the total intensity on plate 2 to plate 1 and similarly for e_2 and e_3, where we define:

$$e_1 = (i_3 + i_{4/f}) / (i_1 + i_{2/f}) \tag{3.6}$$

$$e_2 = (i_5 + i_{6/f}) / (i_1 + i_{2/f}) \tag{3.7}$$

$$e_3 = (i_7 + i_{8/f}) / (i_1 + i_{2/f}) \tag{3.8}$$

As mentioned in Section 3.2, when the half wave plate is rotated through $22\frac{1}{2}^{\circ}$, the plane of polarisation of the light is rotated through twice this angle, so with regard to the last column of Table 3.1, our original equations are:

$$i_1 = I/2 + I_p/2 \cos 2\theta \tag{3.9}$$

$$i_2 = f\left[I/2 - I_p/2 \cos 2\theta\right] \tag{3.10}$$

$$i_3 = e_1\left[I/2 + I_p/2 \cos 2(45 - \theta)\right] \tag{3.11}$$

$$i_4 = fe_1\left[I/2 - I_p/2 \cos 2(45 - \theta)\right] \tag{3.12}$$

$$i_5 = e_2\left[I/2 + I_p/2 \cos 2(90 - \theta)\right] \tag{3.13}$$

$$i_6 = fe_2\left[I/2 - I_p/2 \cos 2(90 - \theta)\right] \tag{3.14}$$

$$i_7 = e_3\left[I/2 + I_p/2 \cos 2(135 - \theta)\right] \tag{3.15}$$

$$i_8 = fe_3\left[I/2 - I_p/2 \cos (135 - \theta)\right] \tag{3.16}$$

Now, defining the Stokes parameters in terms of intens: (i_1, i_2, ... i_8), we have:

$$I = i_1 + \frac{i_2}{f} \tag{3.17}$$

$$Q_1 = i_1 - \frac{i_2}{f} = I_p \cos 2\theta \tag{3.18}$$

$$U_1 = \frac{i_3}{e_1} - \frac{i_4}{fe_1} = I_p \cos 2(45 - \theta) = I_p \sin 2\theta \tag{3.19}$$

and then the degree of polarisation is:

$$P_1 = \frac{\left(Q_1^2 + U_1^2\right)^{\frac{1}{2}}}{I} \tag{3.20}$$

with angle of

$$\theta_1 = \tfrac{1}{2} \tan^{-1} \frac{U_1}{Q_1} \tag{3.21}$$

By using the equations 3.13 - 3.16 we can find another definition of the Stokes parameters - call these Q_2 and U_2. Hence:

$$Q = \frac{Q_1 + Q_2}{2} \tag{3.22}$$

and

$$U = \frac{U_1 + U_2}{2} \tag{3.23}$$

Therefore our equations for degree and angle of polarisation become:

$$P = \frac{\left(Q^2 + U^2\right)^{\frac{1}{2}}}{I} \tag{3.24}$$

and

$$\theta = \tfrac{1}{2} \tan^{-1} \frac{U}{Q} \tag{3.25}$$

3.5 Computer Procedure

After digitisation of the electronographic plates and storage of output on 7 track unlabelled tapes, the data must be translated from 7 to 9 track magnetic tapes in the Cambridge Computing Laboratory. Then the 9 track tapes are forwarded to the Northumbrian Universities Multiple Access Computer at Newcastle.

When the tapes are finally read by the Durham Computer the data is transferred from tape to disk storage for convenience.

3.5.1 Computer Analysis

We will describe the computer analysis in the following sections. Figure 3.7 shows a flow chart of the reduction techniques (of which a full description is given by Pallister 1976).

3.5.2 Primary Contour Map and Star Positions

With regard to the number of scans (512) during digitisation, and the data sets of 512 elements in each scan, each of our plates contains 512 pixels x 512 pixels data points. Firstly to be able to see what the digital information actually looks like, the plates are shortened to contain 128 pixels x 128 pixels data points. Then we produce a visual contour map of the data.

Secondly we obtain visual contour maps of 512 x 512. The plates are shortened to contain 384 pixels x 384 pixels to reduce storage in the computer.

As we need to obtain corresponding points on each of the plates, we need to align the plates exactly. Using the 384 x 384 computer output, which is in the form of a visual contour map, (for each plate)

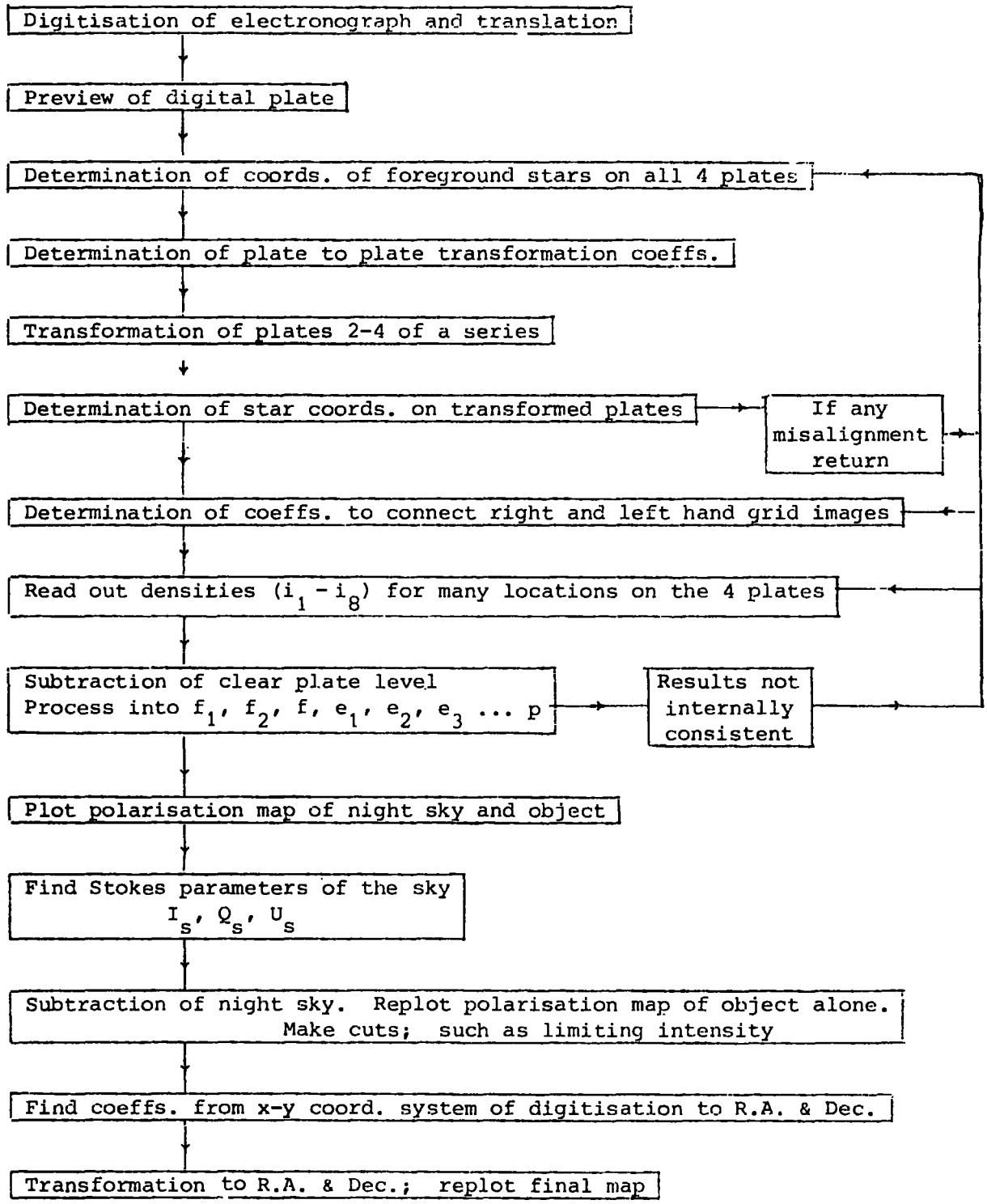

Figure 3.7: Flowchart of the Reduction Technique

the positions of the stars are found roughly by eye and then more accurately by computer.

3.5.3 Transformation Coefficients

By use of these star co-ordinates and a minimising routine, the transformation coefficients A, B, C, D, E, F from one set of co-ordinates X1, Y1 on plate 2 to the co-ordinates of the same stars, X, Y on plate 1 is found, so that

$$X = A + BX1 + CY1 \tag{3.26}$$

$$Y = D + EX1 + FY1 \tag{3.27}$$

and in this way the coefficients are found for X2, Y2 on plate 3, X3, Y3 on plate 4.

3.5.4 Plates - Transformation

In this stage, by using Transformation Coefficients, all positions on plates 2, 3, 4 are transformed to plate 1, and the star positions are again found on the transformed plates. The star co-ordinates on plate 1 and on the transformed plates, should be the same, the acceptable level of difference being within ½ pixel.

3.5.5 Strips Comparison Coefficients

These coefficients are used to establish the relationships of the position of points on one strip to the corresponding points on the adjacent strip. For this we need to find the strips comparison co-efficients, which will be found by using the same minimising routine as in Section 3.53. The star co-ordinates on one strip are compared

to the star co-ordinates on the adjacent strips.

3.5.6 Extraction Values of i_1 to i_8

By using the computer print out of the data of plate 1, which has 384 pixels x 384 pixels dimensions, from right to left, the positions on the odd strips are found at distances of 5 pixels apart. The same positions are obtained on the other three plates. Grid overlaps are avoided.

With these positions, a computer program is used to add the points in 5 pixels x 5 pixels areas in steps of 5 pixels. Thus producing the values of i_1, for all points on the odd strips in integrated area of 7" x 7".

For finding the values of i_2 for all points corresponding to the odd strips on the even strips, the Strip Comparison Coefficients are used.

3.5.7 Clear Plate Levels

To obtain the intensity of the clear plate, from the data on each of 512 x 512 plates a histogram is drawn. Firstly if the distribution is narrow, a constant clear plate level is calculated and then subtracted from the $i_1 - i_8$ values.

Secondly if the distribution is broad, and the residual density down the plate is not constant, then it is necessary to subtract a variable background. This is done by using a program similar to that used in Section 3.5.6. Thus, the correct clear plate intensity is removed from each point on the plates.

3.5.8 Values of the Stokes Parameters for the "Object + Sky"

By a combination of the clear plate subtraction and using the $i_1 - i_8$ values from Section 3.5.6, the photocathode response (f_1 and f_2 factors) is obtained having the mean value of f. Also in this way the three factors e_1, e_2, e_3, the total intensity I, the three values Q_1, Q_2 and U_1, U_2, U are calculated. Then by using these, P_1, P_2, P and θ_1, θ_2, θ for all points of the "object + Sky" are obtained.

3.5.9 Stokes Parameters for the Sky

Firstly to check the quality of the observations, and effect of sky on both observed intensity and polarisation, the output of the preceding section is used. Then to check the distribution of f_1, f_2, f_3, e_1, e_2, e_3 various histograms are drawn. When the distributions are narrow, the quality of data is good.

The parameters and histograms corresponding to the present series of observations will be described and shown in more detail in Chapter Five. The Stokes parameters for the sky (I_s, Q_s, U_s) in a wide area of the plate containing sky only, are obtained from these histograms.

3.5.10 Stokes Parameters of the Object

By subtracting the sky values of I_s, Q_s, U_s from the I, Q, U of all points on the plates, which were obtained in Section 3.5.8, the Stokes parameters of the Object are calculated. Using these parameters, the degree and angle of polarisation can be found for many points of the object.

3.6 Instructmental Errors

The errors on the measurements will be discussed in Chapter Five. Here, the instrumental errors will be mentioned.

As a test, to determine if any systematic error was induced by the equipment itself, a number of standard polarised stars (whose degree and angle of polarisation are known from other photoelectric measurements), were observed, slightly defocussed, on the same observing run as the object in this thesis was observed.

Star	Tabulated value		Our measurements	
	P%	θ^{o}	P%	θ^{o}
HD 43384	2.7	170	2.3	172
HD 122945	0.1	56	0.3	69
HD 155528	4.6	93	4.3	90
HD 80083	0.13	140	1.4	128

Table 3.2: Comparison between our measurements and published values for polarised stars (Mathewson and Ford 1970).

Inspection of Table 3.2 which gives the present and previcus determinations for the standard stars indicates that there is no evidence for any systematic effect being present and the agreement is extremely good, so we can conclude that our technique for measuring nebular polarisation is valid.

REFERENCES

CHAPTER 3

Axon, D.J. 1977, Thesis, University of Durham

Dollfus, A. 1958, C.R., 246, 2345

Hiltner, W.A. 1949, Ap.J., 109, 471

Hiltner, W.A. 1951, Ap.J., 114, 241

Loyt, B. 1929, Ann. Obs. Paris (Meudon), 8, 102

Mathewson, D.S. and Ford, V.L. 1970, MEMBRAS, Vol.74, 139-182

Öhman, Y. 1939, M.N.R.A.S. 78, 553

Pallister, W.S. 1976, Thesis, University of Durham

Pickering, 1873 American Academcy of Arts and Sciences
Vol. IX, 1

CHAPTER FOUR

THE ORION NEBULA

4.1 An Introduction of Gaseous Nebulae

Gaseous nebulae are observed as bright extended objects in the sky. They have an emission line spectrum which is dominated by the forbidden lines of ions of common elements, such as [OIII] λλ 4959, 5007. Gaseous nebulae also have a weak continuous spectrum, consisting of atomic and reflection components.

Many nebulae have reflection continua consisting of starlight scattered by dust, and the strength of this continuum fluctuates correspondingly. In the infrared, the nebular continuum is largely thermal radiation emitted by dust. The source of energy that enables emission nebulae to radiate is, in almost all cases, ultra violet radiation from stars in the nebulae.

The ultra violet photons which these stars emit, transfer energy to the nebula medium by photoionisation. In nebulae, hydrogen is by far the most abundent element, and photoionisation of H is thus the main energy input mechanism (see Orterbrock 1974).

In nebulae in which the central star has an especially high temperature the radiation field has a correspondingly high number of high energy photons, and the nebular ionisation is therefore high.

Diffuse nebulae or HII regions as they are called, are regions of interstellar gas in which the exciting star or stars are O - or early B-type stars of population I, which are the main source of

ionisting radiation and have formed fairly recently from interstellar matter. In many nebulae dense neutral condensations are scattered throughout the ionised volume. There is a tendency for the hot ionised gas to expand into the cooler surrounding neutral gas, thus decreasing the density within the nebulae and increasing the ionised volume.

The outer edges of these nebulae are surrounded by ionisation fronts running out into the neutral gas, so that the ionisation front is a zone which separates two regions of ionised and neutral gas.

4.2 Present Properties of the Orion Nebula

The Orion Nebula, (NGC 1976) which was discovered by Fabri de Peiresc in 1610 (see Dufay 1968), is one of the brightest emission nebulae in the sky. It is a cloud of gas (mainly hydrogen) and dust in which are embedded massive young stars that provide the energy to produce the light emanating from the nebula itself.

For some of the astrophysical quantities of the Orion Nebula (M42) see Table 4.1.

RA (1950)		Dec (1950)		Diameter		Distance from the earth	Mass $M_\odot$	Visual magnitude (m_v) mag.
h	m	o	′	′	PC	PC		
05	32.9	-05	15	35	5	460	300	4

Table 4.1: Showing some astrophysical quantities of the Orion Nebula (M42) (Allen 1973).

The Orion Nebula is the most studied of all HII regions. An HII region in the Orion Nebula is partially embedded in the near edge of a large neutral complex which contains the molecular cloud and infrared sources.

The optically visible portions of Orion consist of the bright nebula M42 in the southern part of this region along with the smaller nebula M43, which lies to the NE of M42. The electron density distribution consists of a Gaussian distribution with a width of 3′ or 4′ (0.5 PC) and central density of $\sim 10^{3.5}$ cm^{-3} centred very close to the Trapezium and optical centre (Balick et al 1974).

Optically, structure can be found with all size scales (e.g. Münch and Wilson 1962). The core region is the dark area near the centre, which its boundaries vary differently and give us their relationship to the neutral and ionised medium (e.g. Gull 1974). The brightest optical nebulosity is found in the western part of the core.

The prominent Dark Bay, which is a thick cloud of neutral gas which has not yet been ionised by the stars, the optical filament or 'bar' said to be an ionisation front of the dark cloud behind the ionised region (e.g. Münch and Taylor 1974; Gull 1974) just above θ^2 Ori, and the Dark Lane which seaparates M42 and M43, can all be seen in Figure 4.1.

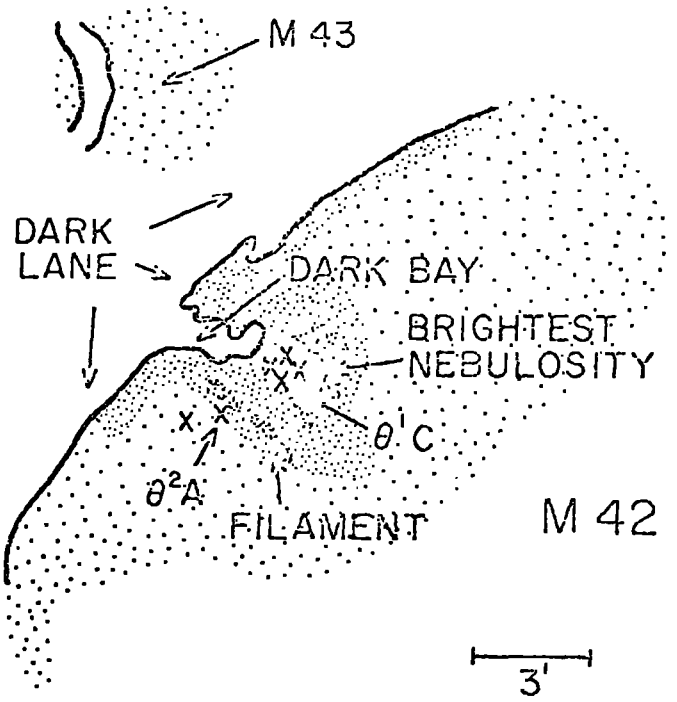

Figure 4.1: The positions of the important optical features are indicated schematically (Balick et al 1974)

At the centre of the core, the four so-called "Trapezium stars" are located. The southernmost of these, θ^1 ori is an O6 star thought to provide all of the ultra-violet excitation for M42 (Balick et al 1974). At radio frequency studies, Hjellming and Gordon (1971) have reported that the electron densities are, Ne $\sim 10^{4.3}$ cm^{-3} and electron temperatures, Te $\sim 10^4$ K in those regions, which contribute most of the line radiation.

The work of Brocklehurst and Seaton (1972) who have made a careful analysis of the radio line and continuum observations, indicates a good fit to the data, for a peak of Ne $\sim 10^{4.2}$ cm^{-3}, with the density falling to a value of $10^{3.7}$ cm^{-3} at a distance of 0.15 PC which is approximately 1′ and to 10^3 cm^{-3} at 0.4 PC (3′) where Tc is 9500 K throughout.

Optical determinations of Ne and Te yield similar results. Forbidden lines of O^+ and S^+ show peak densities reaching 10^5 cm^{-3} over small distances in the brightest regions (Danks and Mea[illegible] 1974; Osterbrock and Flather 1959). It appears that the temperature rises by $\sim$20% (or more) from the centre of the core to the edge (Bohuski et al 1974; Osterbrock 1974).

It has been indicated by Balick et al (1974) that, the boundary of the nebula is quite cold ($T < 50$ K) and dynamically quiescent compared to the HII region.

Feibelman (1976) has drawn attention to a structure in the Orion Nebula which exhibits a proper motion of $\sim$3.6″/century. Several nebulae features with large proper motions have been identified within the Orion Nebula where the proper motions correspond to tangential velocities of up to $\sim$70 Km sec^{-1} (Cudworth and Stone 1977). A photograph of the Orion Nebula is shown in Figure 5.25 (with the polarisation map superimposed on it.) In the following sections we are going to describe some other important physical aspects of the Orion Nebula.

4.2.1 Radial Velocity

At radio frequencies, the work of Balick et al (1974) shows, kinematically, that the core region is very active showing a wide range of velocities both as a function of position and of line excitation. The velocities change from 8 Km s^{-1} (relative to the LSR) at about 5′ NE of the peak near M43, to -2 Km s^{-1} at the peak of the core, to $\sim$ -5 Km s^{-1} 5′ toward the SW. Further to the west, the velocities become increasingly positive (Mezger and Ellis 1968).

Optically, kinematic study of Orion shows that velocities can change rapidly between regions separated by only several seconds (Wilson et al 1959; Elliot and Meaburn 1973).

Radial velocity of the HII region = -2.8 K ms^{-1} (Gordon and Churchwell 1970), average radial velocity of the Trapezium stars $\approx$ + 11 K ms^{-1} (Johnson 1965) and densest HI gas observed in front of the Orion Nebula has a radial velocity of $\sim$6 K ms^{-1} (Radhakrishnan et al 1972). The difference in average radial velocity between the Trapezium and the molecular cloud may be due to their mutual gravitational attraction (see Zukerman 1973).

On the basis of the relative radial velocities of the HII region, the HI region and the Trapezium stars, previous investigators (e.g. Wilson et al 1959) have suggested that the Orion Nebula is a sphere expanding about the Trapezium.

4.2.2 Gas and Molecular Cloud

Behind the Orion Nebula is a large cloud of molecular hydrogen which gives out no light but can be seen by radio telescopes. The southern peak of this cloud is known as OMC1, which lies fairly close to the Trapezium cluster and contains some 500 $M_\odot$ of hydrogen (Mitton and Ryle 1977). The northern peak of this cloud is known as OMC2.

At the centre of each of these clouds there are clusters of infrared protostars and OH and H_2O masers, all of which are probably the result of the collapse of the molecular clouds.

The temperature and density of the molecular clouds is highest close to the infrared sources, and it therefore seems very likely that there are the parts of the clouds where gravitational collapse and star

formation have been happening most recently.

Most of the dust in the Orion Nebula has probably come from the molecular cloud. Based on measurements of scattered light O'Dell and Hubbard (1965) concluded that the gas-to-dust ratio is higher in regions near the Trapezium (inner parts) than in regions far from it (outer parts). The gas-to-dust ratio for the inner and outer parts of the Orion Nebula are 1.4×10^{22} cm^{-2} and 5×10^{20} cm^{-2}, where in addition to OH and H_2O, the molecules CO, CN, CS, HCN, H_2CO and CH_3OH have been detected and shows that the dust is significantly less abundant in the inner part. This may be the result of the presence of hot stars there (Osterbrock 1974).

From observations of O'Dell and Hubbard (1965) and calculations of Weedman (1966) it appears very unlikely that the relatively large colour excess observed in the Trapezium stars $E(B-V) = 0.35$ (Schiffer III and Mathis 1974) can be due to dust distributed uniformly between the stars and the edge of the HII region closest to the earth.

There is a fairly small HI cloud known to exist (Radhakrishnan et al 1972) between the Earth and the Orion Nebula that could produce the observed $E(B-V)$, with which the Trapezium is reddened.

The existence of a massive cloud of neutral gas lying behind the HII region is established by Kutner and Thaddeus (1971), and the mass of this cloud within 2′ (0.26 PC) of the KL Nebula has been estimated to be at least 10^3 $M_\odot$ with an upper limit of $\sim 2 \times 10^4$ $M_\odot$ (Zuckerman 1973). A schematic picture of the Orion Nebula and molecular cloud which has been considered by Zuckerman (1973) is presented in Figure 4.2.

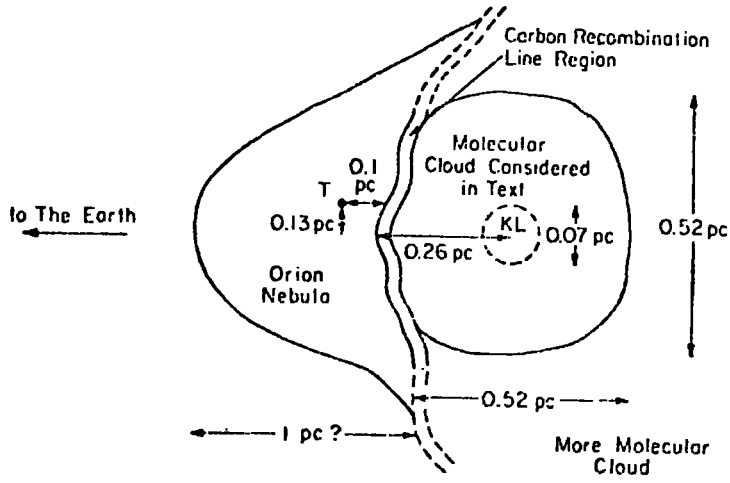

Figure 4.2: Orion Nebula and molecular cloud.
KL stands for Kleinman-Low nebula. T for Trapezium, on the assumption that the Orion Nebula is located at a distance of 460 PC; thus, 1 arc minute = 0.13 PC (Zuckerman 1973).

4.2.3 Scattering

The Scattering by dust in the Orion Nebula has been discussed by many observers (e.g. Schiffer III and Mathis 1974). They have analysed the scattered starlight component in the continuum of the Orion Nebula by means of a composite model consisting of the front portion of a spherically symmetric dust distribution surrounding the star, plus a slab of dust at the front surface of the HI region behind the star and nebula. Their optical data lead them to an estimate of an optical depth at Hβ of 1.5 - 2. They have indicated that most of

the scattered light at visual wavelengths arises from a foreground shell of optical depth ~ 2. The neutral condensations, which seem to exist near the Trapezium, must therefore not scatter efficiently, presumably because they are very small and possible optically thick in dust.

Savage (1973) suggests that the ultra-violet scattered light from the nebula does not dominate the stars.

Polarisation studies of the Orion Nebula (e.g. Hall 1974; Pallister et al 1977) which is the subject of this thesis, indicates the effect of scattering by dust in the Orion Nebula, and will be discussed in the next chapter.

4.2.4 Ionisation Front

A ridge or bar of emission at 10 μ has been found which is parallel and adjacent to the HI - HII interface in the Orion Nebula 2' southeast of the Trapezium (Becklin et al 1976). The bar structure is nearly as bright as the brightest part of the nebula (Gull 1974). Becklin et al (1976), interpreted the emission coming from heated dust whose density at the interface is an order of magnitude higher than that inside the HII region, where the source of luminosity for this emission is shown to be the Trapezium stars.

This ionisation front has been shown in the work of Pallister et al (1977), and their interpretation suggested that the bar is physically closer to θ^1 than to θ^2 in spite of its projects position. θ^2 and the regions it illuminates, particularly to the east, are then at different distances. Results of the present series of observations

is in agreement with them and will be discussed in the next chapter.

The ionisation front is in an ideal configuration for studying the distributions of dust and gas near the boundary of an HII region. As the optical radio and infrared observations indicate, the HI - HII interface is seem almost edge-on (see, e.g. Zuckerman, 1973).

4.2.5 Infrared Sources

There are at least two infrared unresolved 'point' sources in the Orion Nebula, both of which apparently are highly luminous, heavily reddened stars. In addition, two extended peaks of intensity are measured at 10 μ and 20 μ (Osterbrock 1974). One, the Ney Allen source is centred approximately on the Trapezium stars while the second region is centred approximately on the brighter infrared point source (often called the Becklin-Neugehaur object) and lies in the centre of OMC1 about 1′ northwest of Trapezium.

Both these peaks, or 'infrared nebulae', as they have been called (the first is known as the Trapezium nebula, the second is known as the Kleinmann-Low nebula), have angular sizes of the order of 30″ to 1′.

Another complex of infrared and molecular emission which is ∿12′ northeast of the Trapezium has been found by Gatley et al (1974), and they have labelled it as the Orion Molecular Cloud 2 (OMC2). It has been detected with a peak intensity of 3×10^{-23} W m^{-2} Hz^{-1} at 69 μ (Fazio et al 1974) and appears to be smaller than 1.5′, where the position of the peak is RA (1950) = $5^h\ 33^m\ 0^s$, Dec (1950) = $-5^o\ 12.3'$. It seems that in the infrared Trapezium nebula, the dust particles are heated by the absorption of ultraviolet (giving rise to the colour temperature, T_C) and optical radiation from the Trapezium stars, and possibly also from the

nearby nebular gas that is ionised by these same stars. Likewise the dust observed as the Kleinmann-Low nebula is heated by absorption of shorter wavelength radiation probably emitted by, or ultimately due to, the Becklin-Neugebare star (see e.g. Osterbrock 1974, Gnedin and Mitrofanov 1975).

4.2.6 Polarisation Studies and Magnetic Field in the Infrared Sources

Polarisation studies of infrared sources in the Orion Nebula indicate that the extended regions of the Kleinmann-Low nebula may emit polarised radiation in the far-infrared (~ 100 μm) which is estimated to be as large as 8% (Dennison 1977). The alignment of dust grains in the KL nebula may be responsible for the polarisation effects.

Also high linear polarisation $P_\ell \approx 15\%$ and circular polarisation $P_C \approx 1\%$ in the BN source has been detected near the absorption lines at $\lambda \approx 3\ \mu$ and $10\ \mu$ (Gendin and Mitrofanov 1975), where their polarimetric data has yielded an estimate $M_{KL} \approx 10^4\ M_\odot$ for the mass of KL nebula. They indicated the fact that the polarisation is related to the absorption and the fact that circular as well as linear polarisation is observed implies that the polarisation develops when the BN radiation passes through an ensemble of absorbing, aspherical, aligned grains, which act like a phase plate, converting the linear polarisation to circular polarisation.

In the optical polarisation studies of Orion Nebula, Pallister et al (1977), have shown that in the KL infrared nebula, the direction of the infrared polarisation is similar to that observed optically.† The polarising mechanisms may differ, since the optical polarisation can

†See page 78.1

arise from scattering of light by randomly aligned particles whereas the infrared effect has been attributed, by Dyck and Beichman (1974), to a polarising screen of aligned grains.

Dyck and Beichman (1974) assumed that the alignment was caused by magnetic fields, but Pallister et al (1977) indicate that there is no evidence for this at optical wavelength.

In the work of Beichman and Chaisson (1974) it has been suggested that the infrared nebula/molecular cloud in Orion is permeated by a magnetic field of milligauss strength. In the neighbourhood of the KL nebula Gendin and Mitrofanov (1975) have concluded that a weak ($\approx 3 \times 10^6$ gauss) regular magnetic field exists perpendicular to the line of sight.

4.3 General Remarks on M43

NGC 1982 (M43), is a small diffuse nebulae in the sky, with approximately the same distance as M42 from the earth and lies 10′ to the N.E. of M42.

Although it is partly cut off from NGC 1976 by foreground extinction, radio-frequency measurements show that there is a real density minimum between the two nebulae (Osterbrock 1974).

NUOr$_i$ is the exciting star of M43 which is a BlVstar and in studies of far-infrared emission from HII regions (Harper 1974), IRe4 is a source which has been observed in the Orion Nebula region at infrared wavelengths with the 91 μ emission from the region near NUOr$_i$.

M43 has been detected with a peak intensity of $(1 \pm 0.5) \times 10^{-16}$ $Wm^{-2}\ H_z^{-1}\ Sr^{-1}$ (Fazio et al 1974) where the size of the source is

3′ ± 1′. A photograph of the M43 is shown in Figure 5.32 taken in the red with a polarisation map of M43 superimposed on it, and for some astrophysical quantities of M43 see Table 4.2 (Allen 1973, Schraml and Merzger 1969).

RA (1950)				Distance from the earth PC	Mass of the ionised Hydrogen (M_{HII}) $M_\odot$	Radial velocity of HII region (V_{LSR}) K m sec^{-1}	Visual magnitude (M_V) mag	Diameter of the HII region 2 R_S P_C
h	m	o	′					
05	33.1	-05	18	460	1.3	8.4	9	0.56

Table 4.2: Showing some astrophysical quantities of M43 (Allen 1973, Schraml and Mezyer 1969) where:

Electron Density ≡ N_e = 610 cm^{-3}

Electron Temperature ≡ T_e = 5800 K

As most observers have studied the diffuse nebulae in the Orion region about M42 rather than M43, very little is known about NGC 1982 (M43), but in the present series of data we are going to present an optical polarisation map of this object.

REFERENCES

CHAPTER 4

Allen, C.W. 1973, Astrophysical Quantities, Athlone Press, pp. 260 & 301

Balick, B. et al 1974, Pub. A.S.P. 86, 616

Beckline, E.E. et al 1976, Ap. J. 207, 770

Beichman, C.A. and Chaisson, E.J. 1974, Ap. J. 190, L21

Bohuski, T.J. et al. 1974, Ap. J. 188, 529

Brocklehurst, M. and Seaton, M.J. 1972 M.N.R.A.S. 157, 179

Cudworth, K.M. and Stone, R.C. Pub. A.S.P. 89, 627

Danks, A.C. and Meaburn J. 1971, Ap. and Space Sci. 11, 398

Denniosn, B. 1977, Ap. J. 215, 529

Dufay, J. 1968, Galactic Nebulae and Interstellar Matter, Dover Pub. Chap. 1

Dyck, H.M. and Beichman, C.A. 1974, Ap. J. 194, 57

Elliot, K.H. and Meaburn, J. 1973, Astr. and Ap. 27, 367

Elliot, K.H. and Meaburn, J. 1974, Astr. and Ap. 34, 473

Fazio, G.G. et al 1974, Ap. J. 192, L23

Feibelman, W.A. 1976, Pub. A.S.P. 88, 677

Gatley, I. et al 1974, Ap. J. 191, L.121

Gnedin, Yu. N. and Mitrofanov I.G. Astron. Zh. 1975 52, 1121

Gordon, M.A. and Churchwell, E. 1970, Astr. and Ap. 9, 307

Gull, T.R. 4-7 June 1974, Eight Eslah Symposium Ed. A.F.M. Moorwood

Hall, R. 1974, I.A.U. Coll. 23, Planets, Stars and Nebulae, p.881 ed. T. Gehrels

Harper, D.A. 1974, Ap. J. 192, 557

Hjellming, R.M. and Gordon, M.A. 1971, Ap. ~ 164, 47

Johnson, H.M. 1965, Ap. J. 142, 964

Kutner, M.L. and Thaddens, P. 1971, Ap. J. 168, L67

Mezger, P.G. and Högland, B. 1967, Ap. J. 147, 490

Mitton, S. and Ryle, M. 1977, The Cambridge Encyclopaedia Astronomy, Sec. 14, Pub. Trewin Copplestone

Münch, G. and Taylor, K. 1974, Ap. J. 192, L93

Münch, G. and Wilson, O.C. 1962, Z. Ap. J. 56, 127

O'Dell, C.R. and Hubbard, W.B. 1965, Ap. J. 142, 591

Osterbrock, D.E. 1974, Astrophysics of Gaseous Nebulae, Pub. Freeman and Company

Osterbrock, D.E. and Flather, E. 1959, Ap. J. 129, 26

Pallister, W.S. et al, 1977, M.N.R.A.S. 178, 93P

Radhakrishnan, V. et al, 1972, Ap. J. Suppl. 24, 1

Savage, B.D. 1973, I.A.U. Symposium 52, Albany, New York

Schiffer III, F.H. and Mathis, J.S. 1974, Ap. J. 194, 597

Schradml, J. and Mezger, P.G. 1969, Ap. J. 156, 269

Weedman, D.W. 1966, Ap. J. 145, 965

Wilson, O.C. et al 1959, Ap. J. Supple. 4, 199

Zuckerman, B. 1973, Ap. J. 183, 863

CHAPTER FIVE

PRESENT OBSERVATION OF THE OPTICAL LINEAR POLARISATION OF THE ORION NEBULA

5.1 Introduction

The Orion Nebula is the nearest HII region to Earth and is the one that has received the greatest attention from astronomers. In the Orion regions, a large number of observations have been carried out at optical, infrared and radio frequencies.

The nebular light has two components: one is intrinsic to the gas itself and consists of emission radiation seen as a line spectrum; the second is the light reflected by the dust, but originating in the illuminating stars themselves.

Also, the observations of the HeII λ 4686 absorption line in the continuous spectrum of M42, where the atomic contribution (nebular atomic continuum caused by bound-free and free-free emission) is subtracted from the observed continuum, represent the dust-scattered continuum. The observations show, in the Orion Nebula, that the infrared radiation is far greater than the free-free and bound-free continuous radiation predicted from the observed H β radio-frequency intensities (Osterbrock 1974).

Solid particles or dust grains in the Orion Nebula give rise to a variety of effects that can be studied optically, in particular they scatter the light from stars embedded in the nebula and polarise it in the process (see for instance, Hall et al, 1974 and references therein).

Information on polarisation coupled with spectral data (on both direct and scattered stellar continuum and nebular emission) will yield information on the number density, size and composition of the particles. This will lead to an indication as to how the particles are formed and also clarify their role in the formation of protostars in the nebula.

The great wealth of observational evidence in the Orion Nebula makes it an ideal subject to study with the nebular polarimeter described in Chapter 3 of this thesis.

Accordingly in November 1976, a series of thirty two plates of the Orion Nebula were taken (eight plates for the Central region plus eight plates for the Dark Bay region, plus eight plates for the Fan Edge region), with varying positions of the half-wave plate. The Durham polarimeter was used with a 4 cm. McMullen electronograph camera, on the 1 meter telescope of the Wise Observatory, Tel Aviv University, Israel. The V waveband of the UBV system was used. Each of the eight plates combined, in two series of four plates, one for each half of the region observed (Central, Dark Bay and Fan Edge), gave sufficient information to obtain the degree and angle of polarisation for over 8550 points in the Orion Nebula.

5.2 Technique

The technique used to reduce the data, from the original electronograph to the Stokes parameters, which give the degree and angle of polarisation of radiation from the Orion Nebula, was described in Chapter 3 of this thesis.

The final optical linear polarisation map of the Orion Nebula, will be the combination of the results from three groups of plates.

The procedure for the reduction of each set of eight plates is the same.

The four electronographs, for one half of the region observed, give intensities i_1 - i_8 corresponding to components 0^o, 90^o ; 45^o, 135^o ; 90^o, 0^o ; 135^o, 45^o ; of the radiation measured from the north, called plates 1, 2, 3, 4 respectively. The procedure adopted is shown in diagramatic form in Figure 5.1, and is described as follows.

5.2.1 Photocathode Response

The first step in the reduction is to calculate the two independent estimates of the sensitivity factor 'f_1' and 'f_2' given by equations 3.3 and 3.4. These two estimates, which are of the same quantity, must agree with each other, unless one of the densities (i_1 - i_8) from which they were calculated is inaccurate. As there is no straightforward way to deduce which is the incorrect value, the complete set of eight component densities must be omitted from the summation.

The photocathode response factor 'f' used was the average of f_1 and f_2, and is shown by equation 3.5. Figures 5.2 and 5.3 show the distributions of the estimates f_1 and f_2 of the photocathode sensitivity for the points of the central regions in the map of the Orion Nebula. The scatter plot of f_1 against f_2 which is shown in Figure 5.4 yields the expected straight line at an angle of 45^o.

5.2.2 Exposure Factors e_1, e_2, e_3

The exposure factor 'e_1' is the ratio of the total amount of light received on electronograph 2 to electronograph 1, which normalises

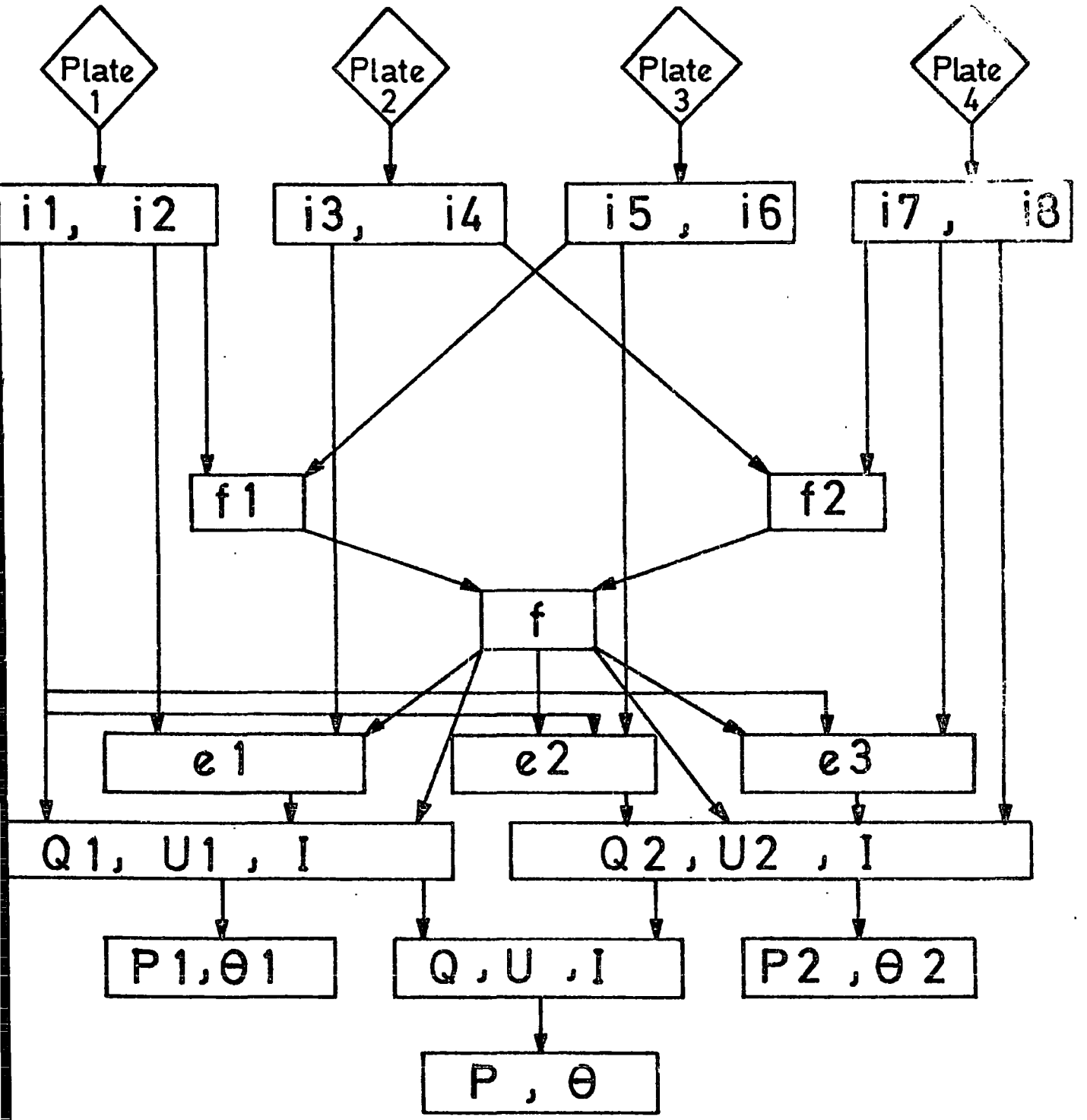

FIG.5.1 FLOW DIAGRAM OF THE FOUR PLATES ANALYSIS.

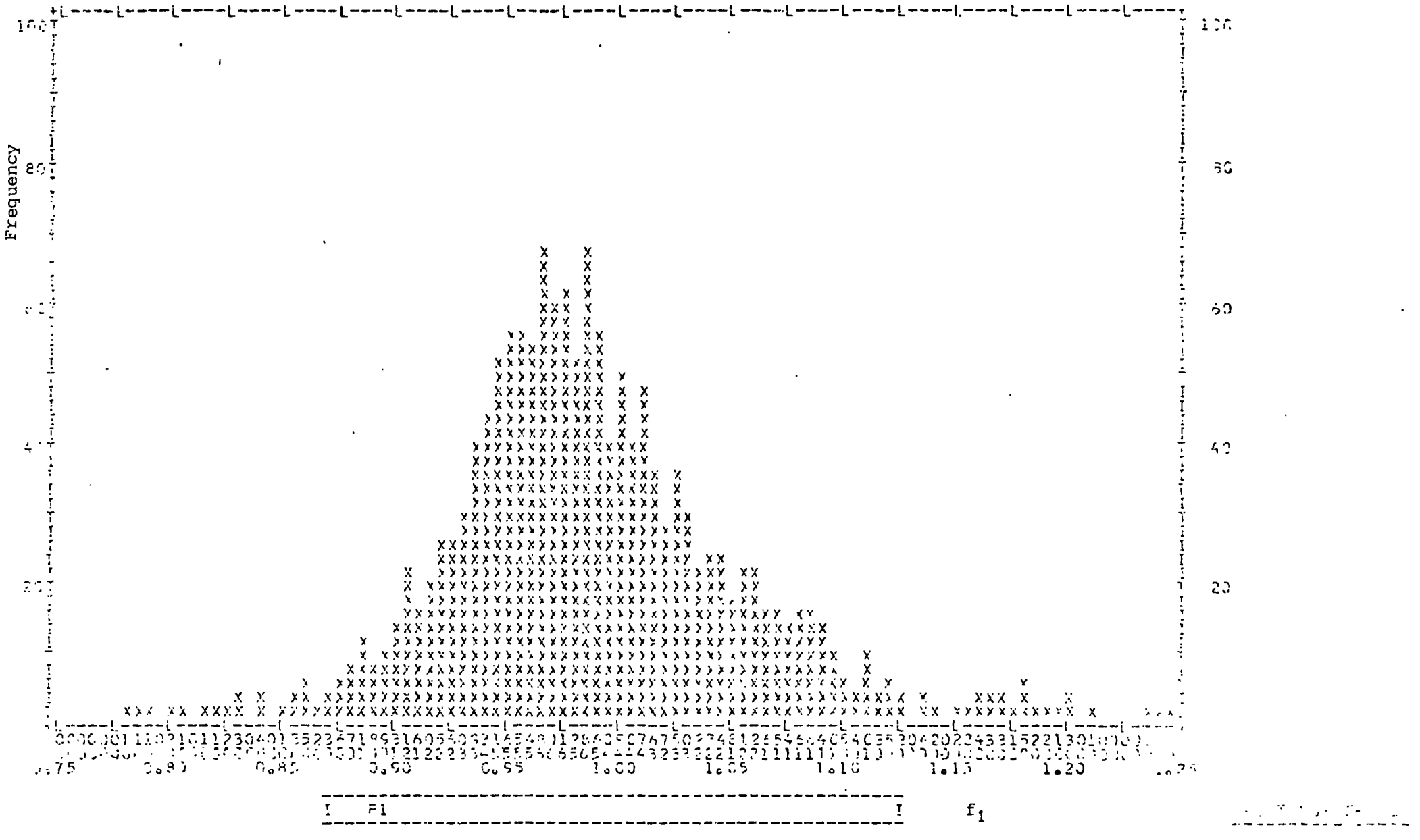

Figure 5.2: Frequency distribution of the photocathode sensitivity factor 'f_1'

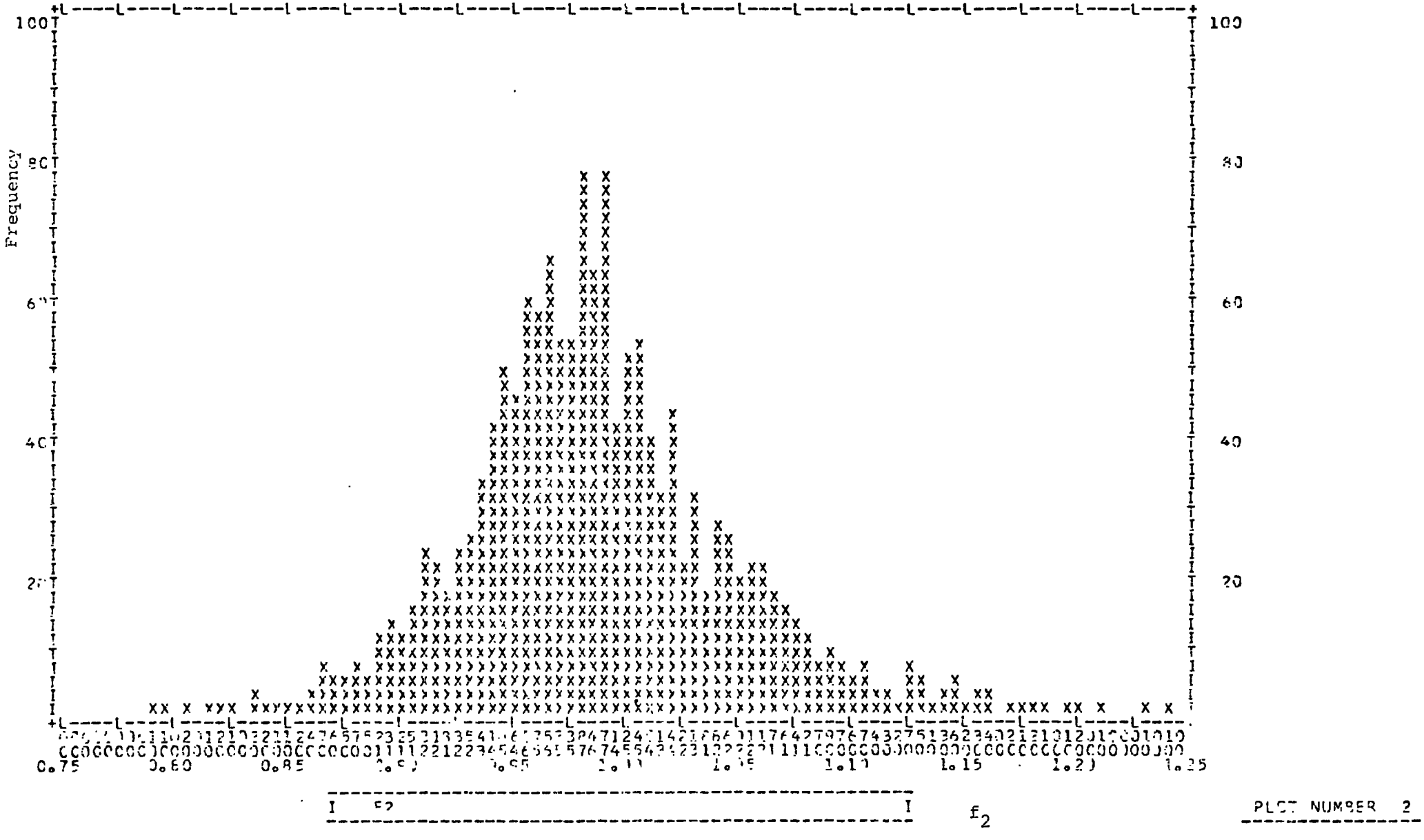

Figure 5.3: Frequency distribution of the photocathode sensitivity factor 'f_2'

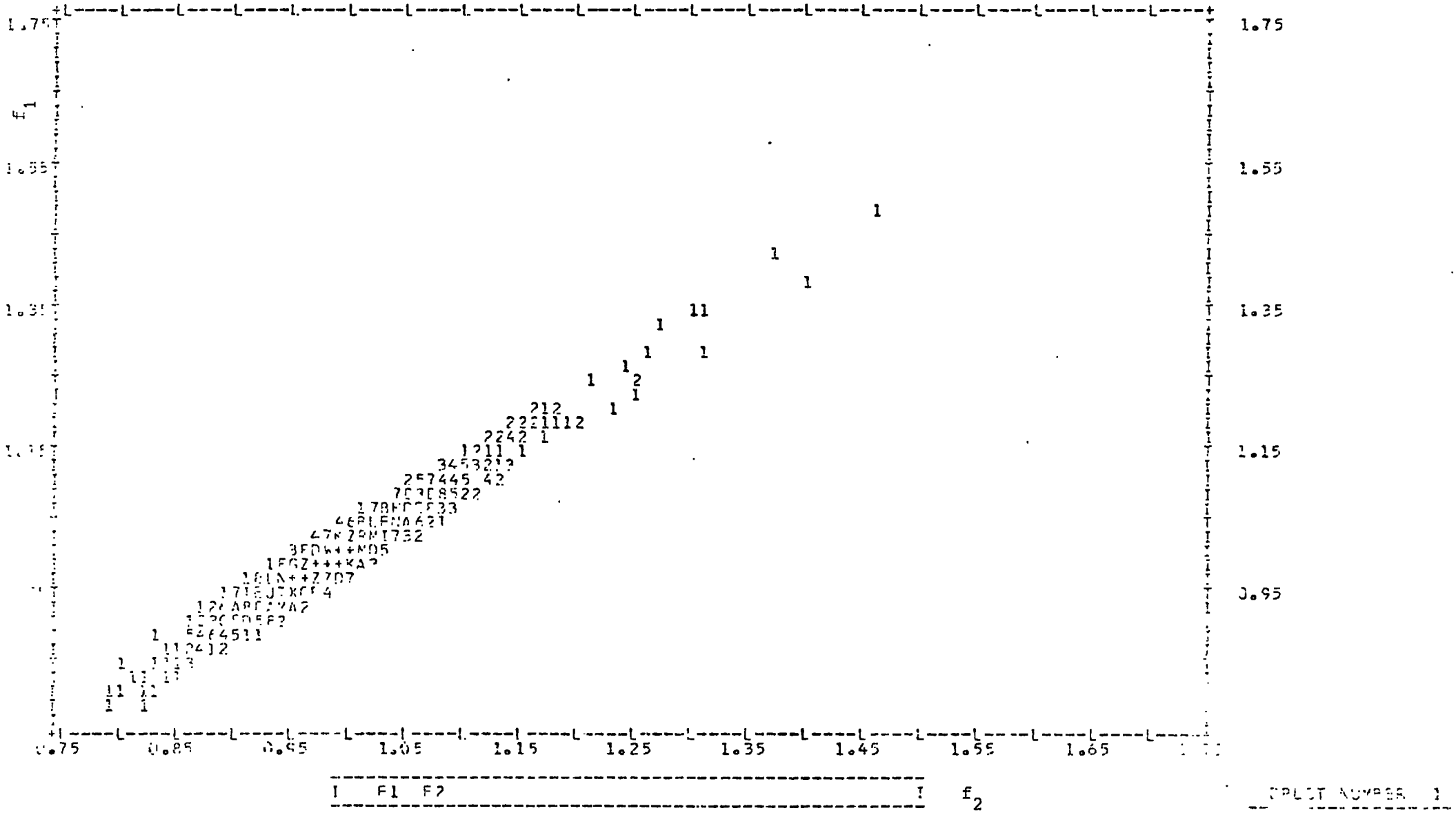

Figure 5.4: Scatter plot of 'f_1' v 'f_2'

the intensity from plate 1, to the intensity of plate 2 and is g. . by equation 3.6.

For plates 3 and 4, the exposure factors 'e_2' and 'e_3' were used and are given by equations 3.7 and 3.8. Figures 5.5, 5.6 and 5.7 show a frequency distribution of the estimates of the exposure factors e_1, e_2 and e_3. The distributions are of the expected form, and each of them are centred around a mean value.

As the clear plate level should be removed correctly, a check was made by plotting the value of the exposure factor against the position from north to south down the plate (Y position). A variable level for the clear plate was removed and the Figures 5.8, 5.9 and 5.10 indicate that the correct clear plate was removed since the exposure factors do not very with Y positions.

5.2.3 Stokes parameters

By using equations 3.9 to 3.19 for the intensities, of the four plates, the values of I, Q_1, Q_2, U_1, U_2 were calculated. Since $Q = (Q_1 + Q_2)/2$ and $U = (U_1 + U_2)/2$, the Stokes parameters I, Q, and U for objects combined with the sky are obtained and indicated by I_T, Q_T and U_T. Then a histogram of sky intensities gave the intensity level of the sky I_S. Q_S and U_S factors for the sky alone were determined from the histgrams of Q_S and U_S at the intensity level of the sky (I_S).

By subtracting the values of I_S, Q_S and U_S from the I_T, Q_T and U_T, the Stokes parameters of the object itself (I, Q, U) were calculated.

Figures 5.11, 5.12 and 5.13 show the distribution of the Stokes parameters for the object alone, the distributions of the Stokes

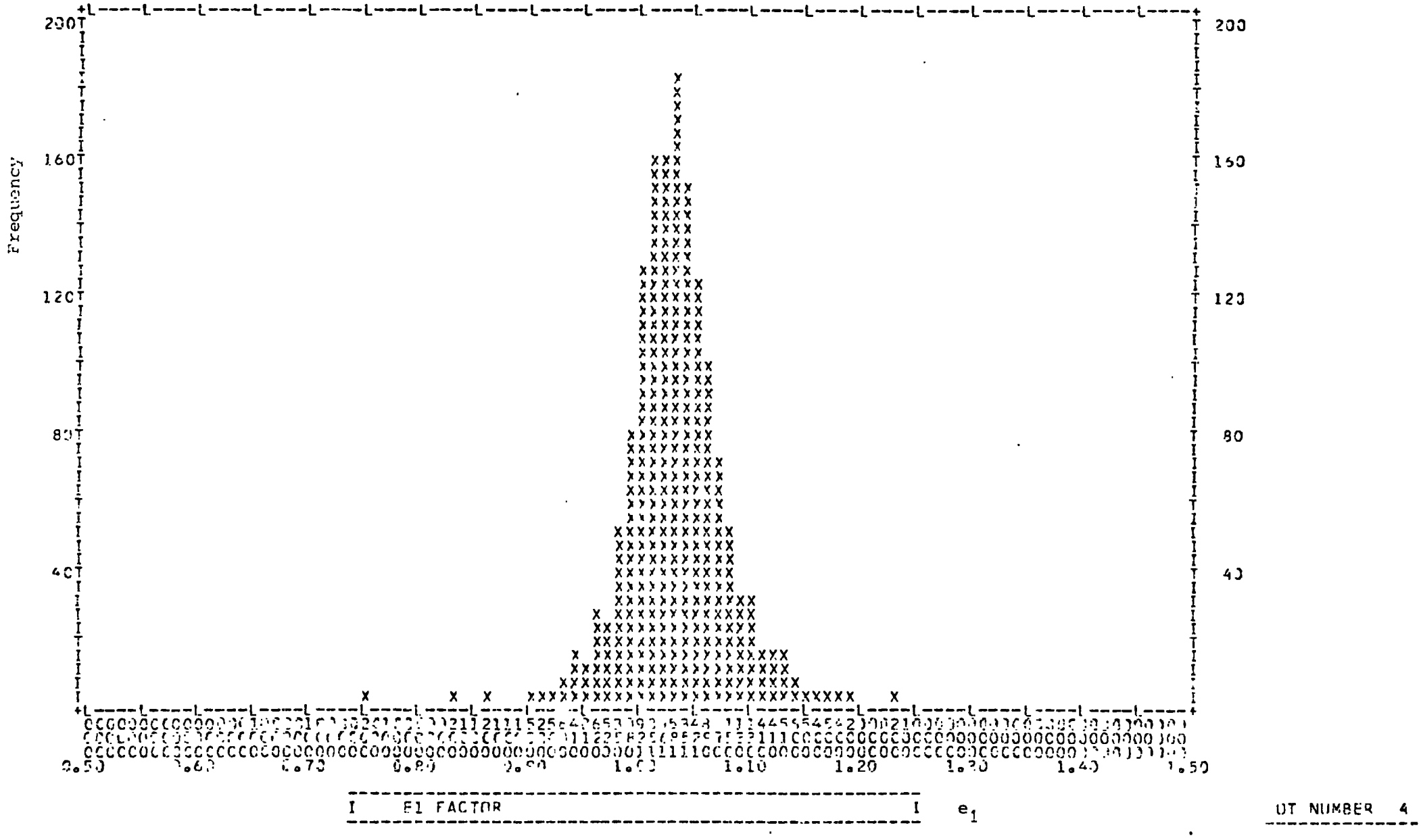

Figure 5.5: Frequency distribution of the exposure factor 'e_1'

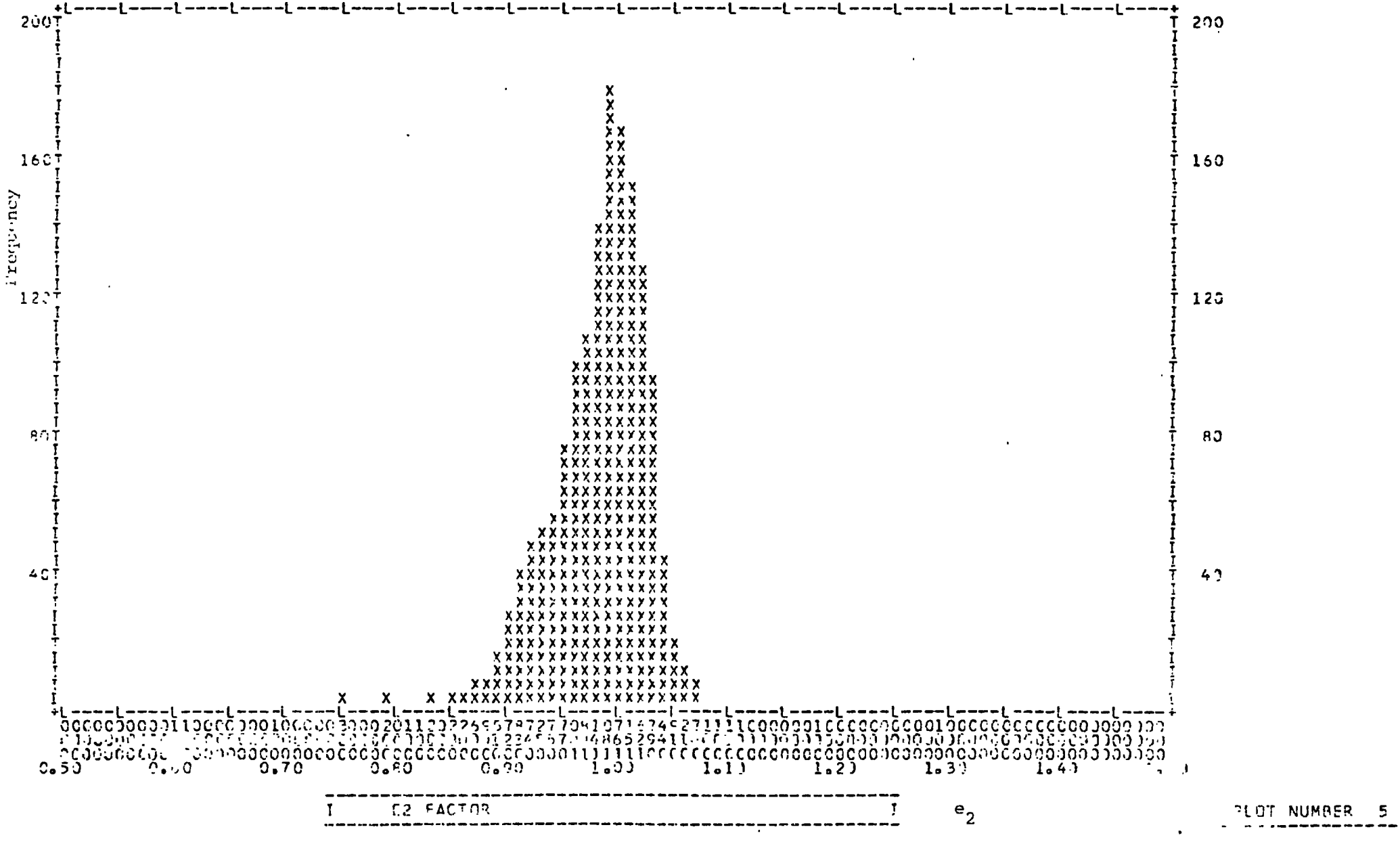

Figure 5.6: Frequency distribution of the exposure factor 'e_2'

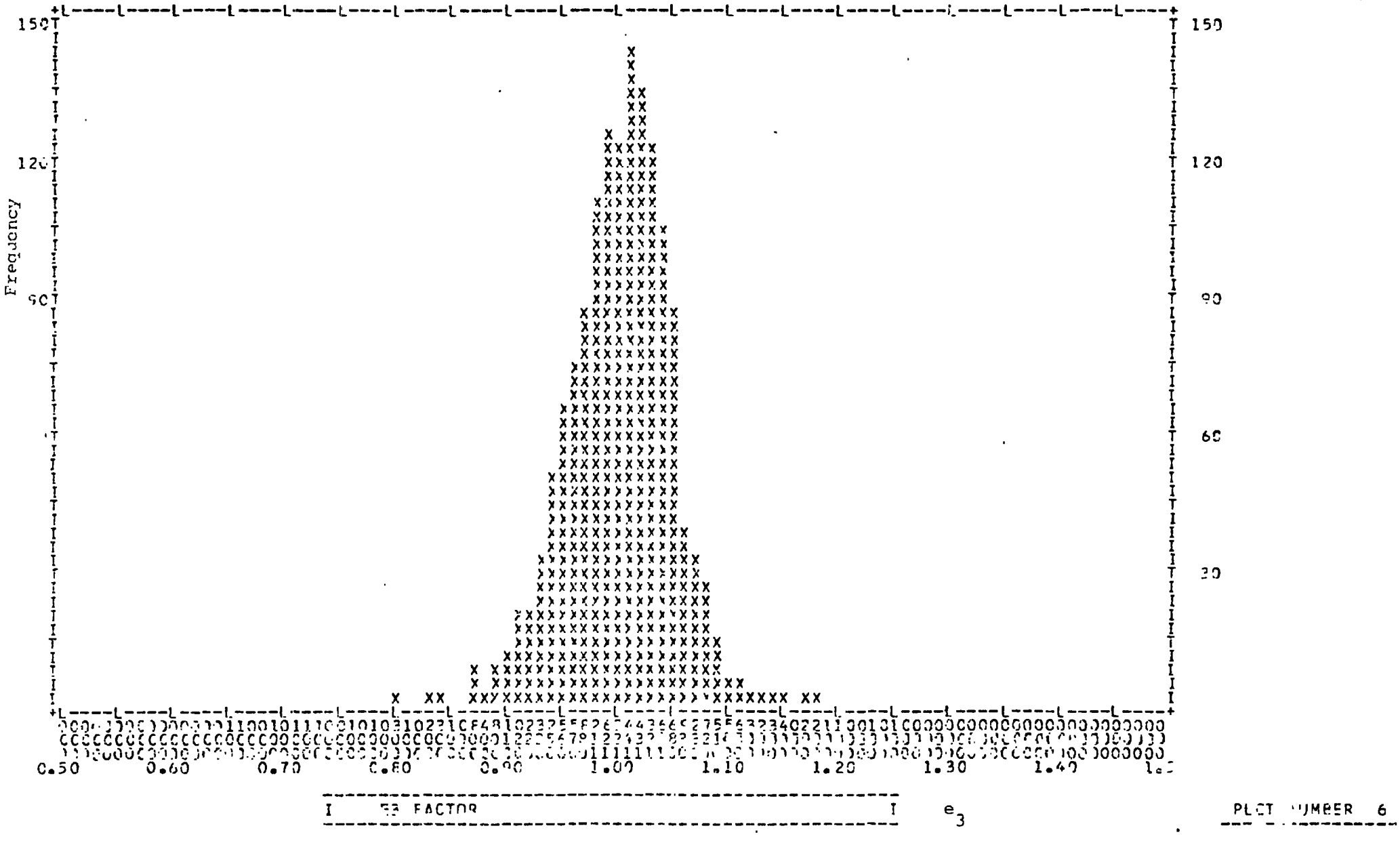

Figure 5.7: Frequency distribution of the exposure factor 'e_3'

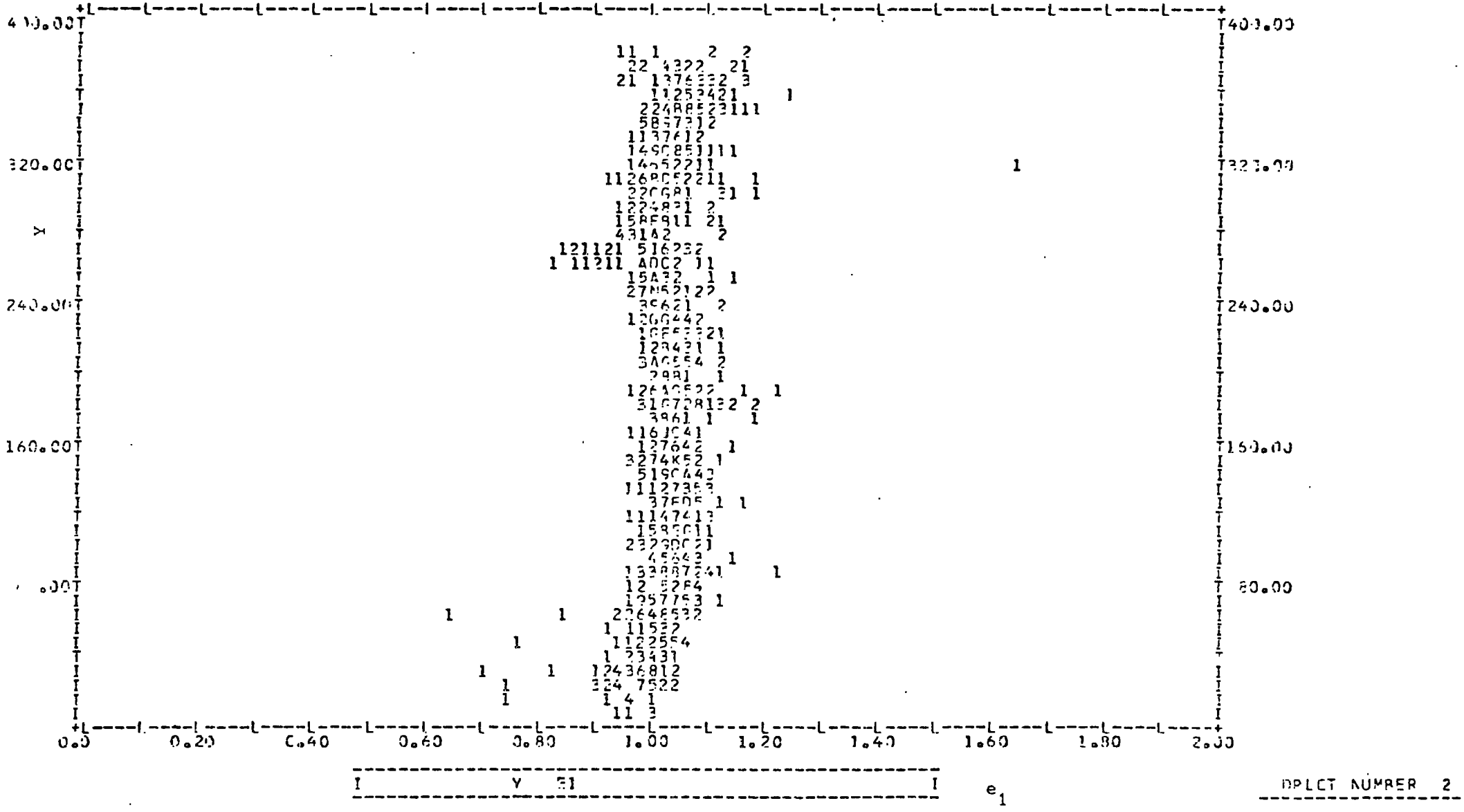

Figure 5.8: Scatter plot of the 'e_1' v Y

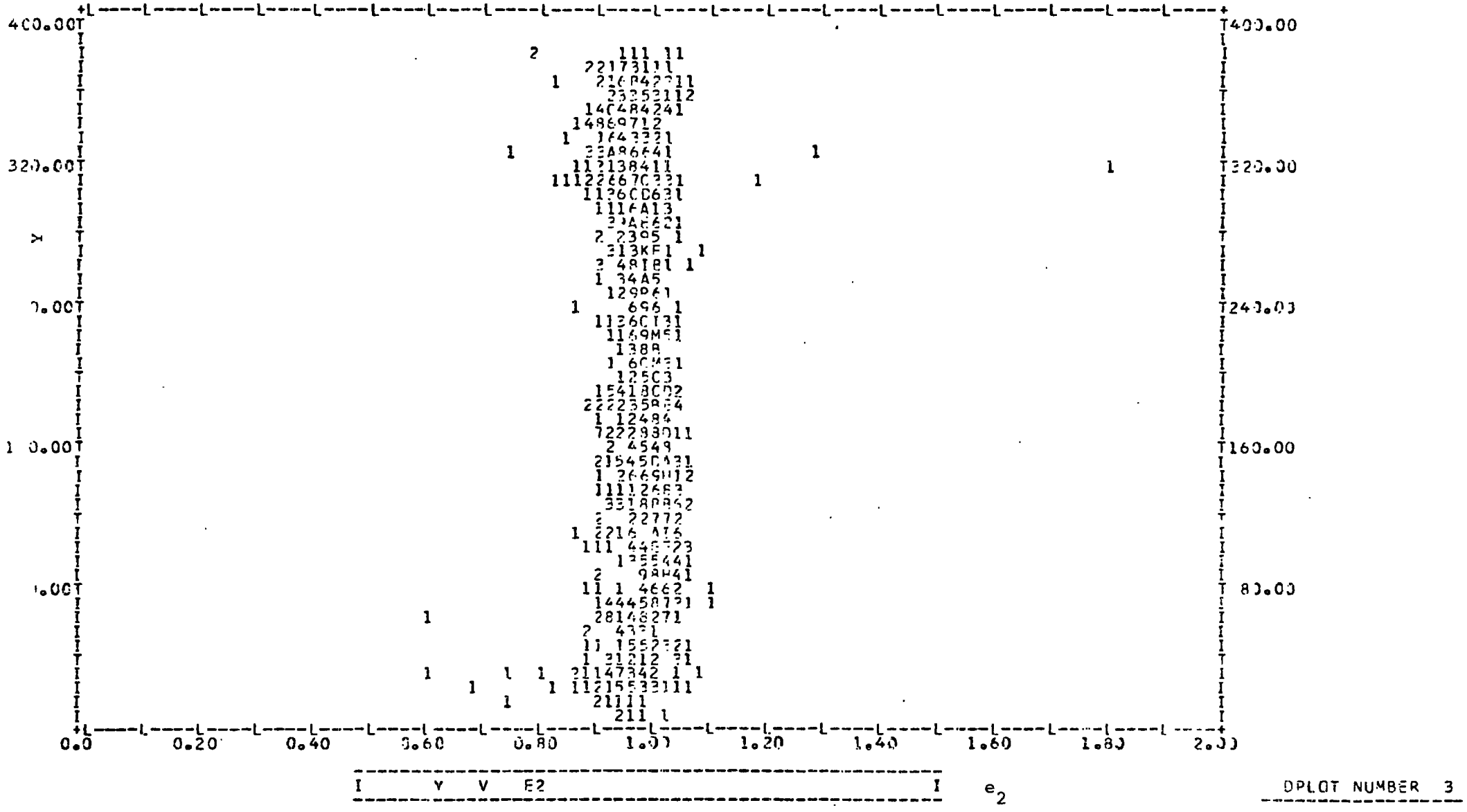

Figure 5.9: Scatter plot of the 'e_2' v Y

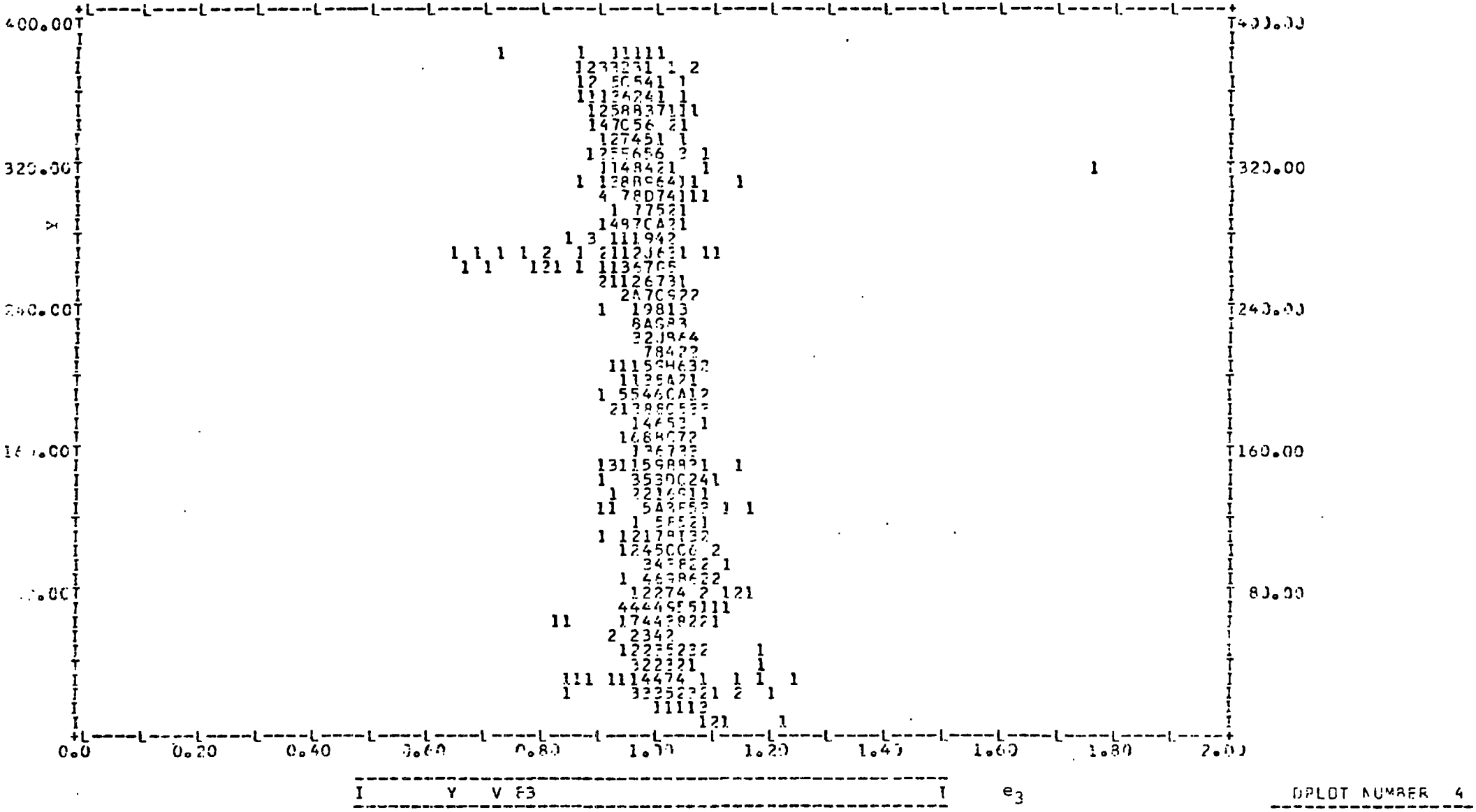

Figure 5.10: Scatter plot of the 'e_3' v Y

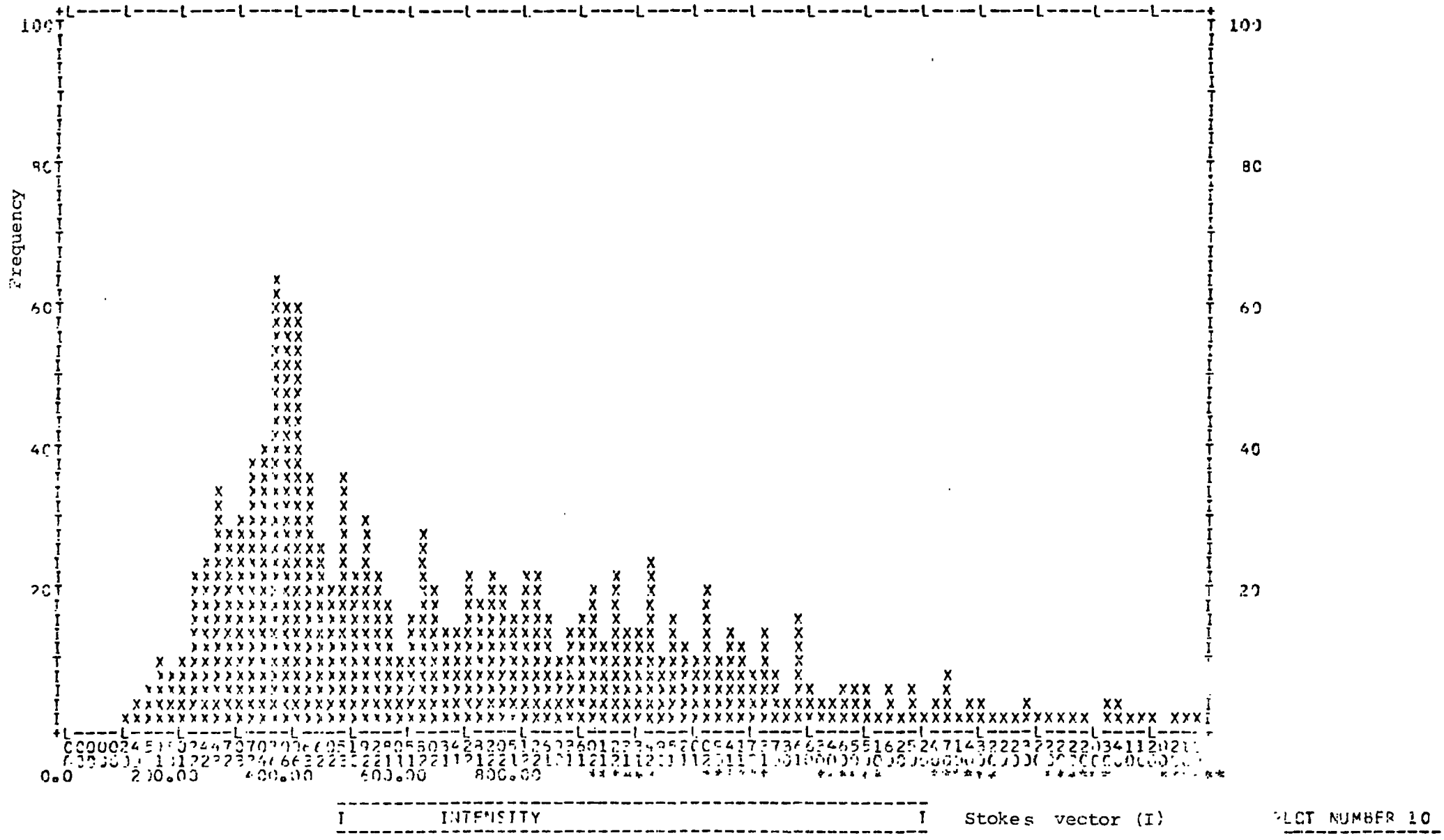

Figure 5.11: Distribution of the Stokes vector (I)

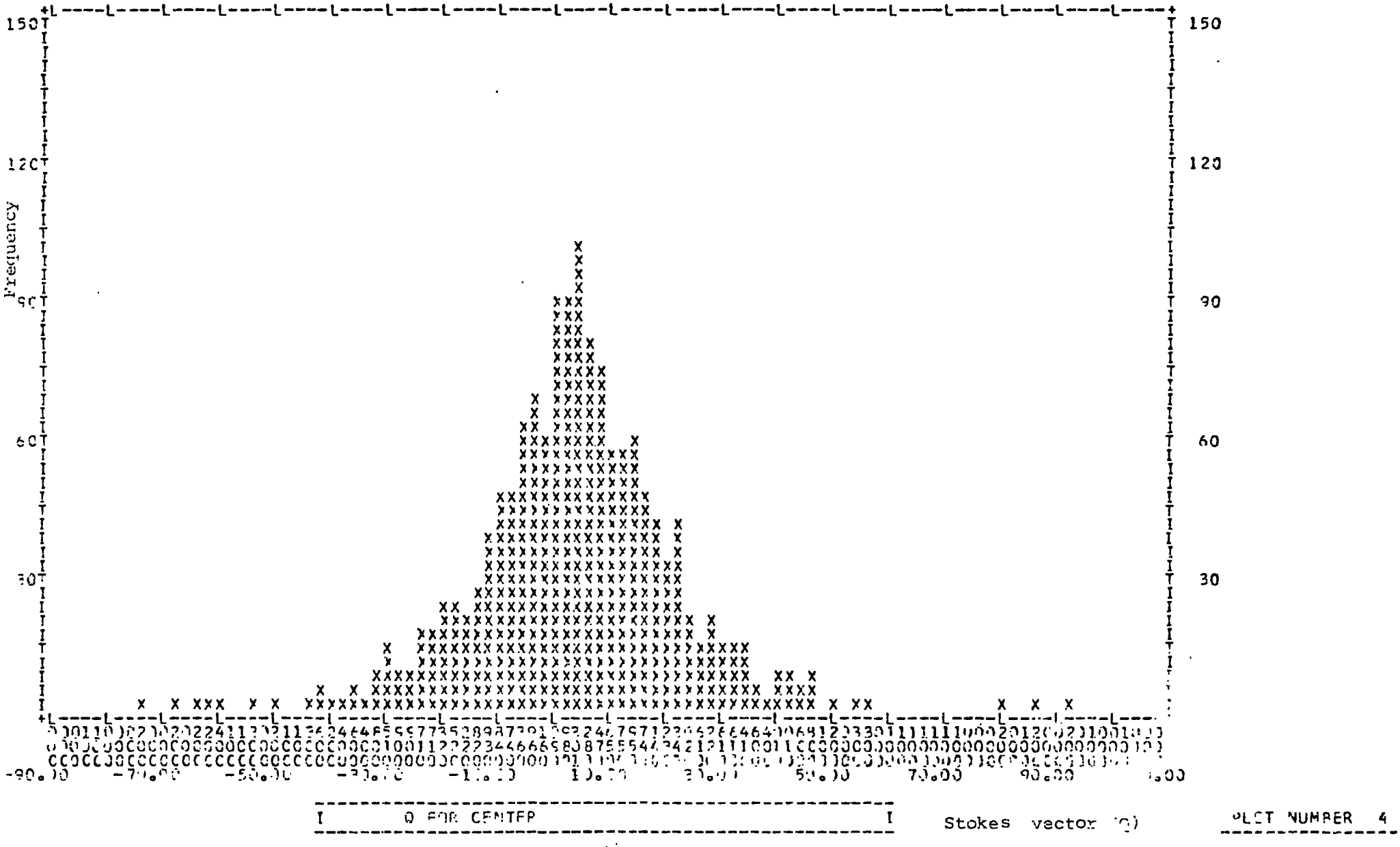

Figure 5.12: Distribution of the Stokes vector (Q)

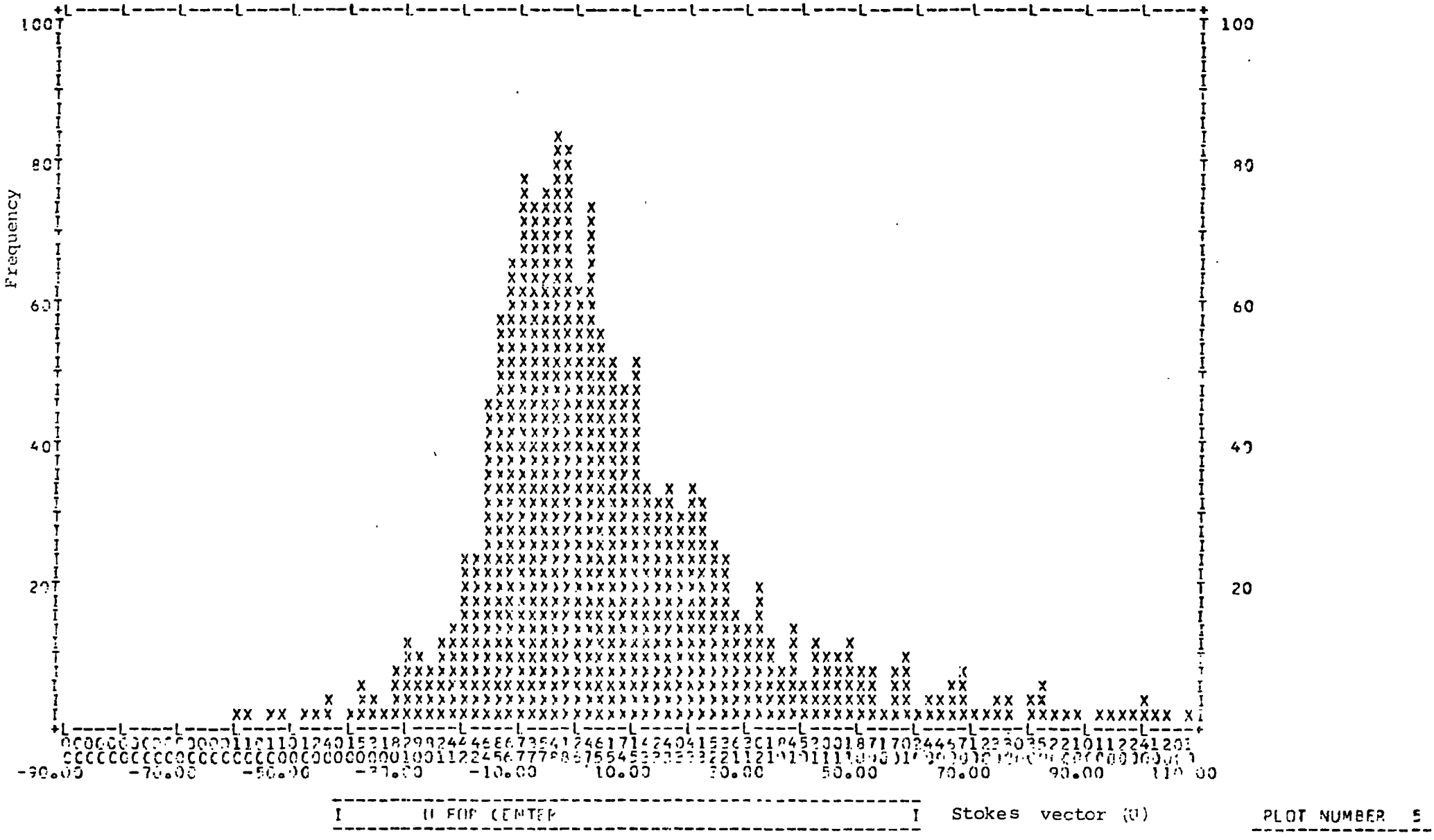

Figure 5.13: Distribution of the Stokes vector (U)

parameters for the sky are represented in Figures 5.14, 5.15 and 5.16.

5.2.4 The Degree of Polarisation P and Angle θ

Since $P_1 = (Q_1^2 + U_1^2)^{\frac{1}{2}}/I$, and $P_2 = (Q_2^2 + U_2^2)^{\frac{1}{2}}/I$, the two estimates of the degree of polarisation P_1, P_2 are obtained, and the two estimates of the angle θ_1, θ_2 are calculated from $\theta_1 = \frac{1}{2} \tan^{-1} \frac{(U_1)}{(Q_1)}$ and $\theta_2 = \frac{1}{2} \tan^{-1} \frac{(U_2)}{(Q_2)}$. By using the equations 3.24 and 3.25, the degree of polarisation P at the angle θ is calculated.

Figure 5.17 shows some of the polarisation parameters as line printer output.

5.2.5 Transformation to an Absolute Co-ordinate System

The two halves of the map which are completely independent of each other have been shown in Figures 5.18 and 5.19. But Figure 5.20 shows the two halves aligned by eye, to give the complete polarisation map of the Central region of the Orion Nebula.

As each half is plotted in terms of the different arbitary x-y co-ordinate systems which are positions through the East/West and North/South direction on each electronograph, so it is necessary to transform each half in order that the entire map is plotted in the usual absolute co-ordinate system of right ascension and declination.

At $f/_{13.5}$ focus, for the central part of the telescope image, plane geometry will be sufficiently accurate to describe the transformation from the x-y co-ordinate system to the RA(α) and Dec (δ) system. By using the same procedure described in Section 3.5.3 and the two equations:

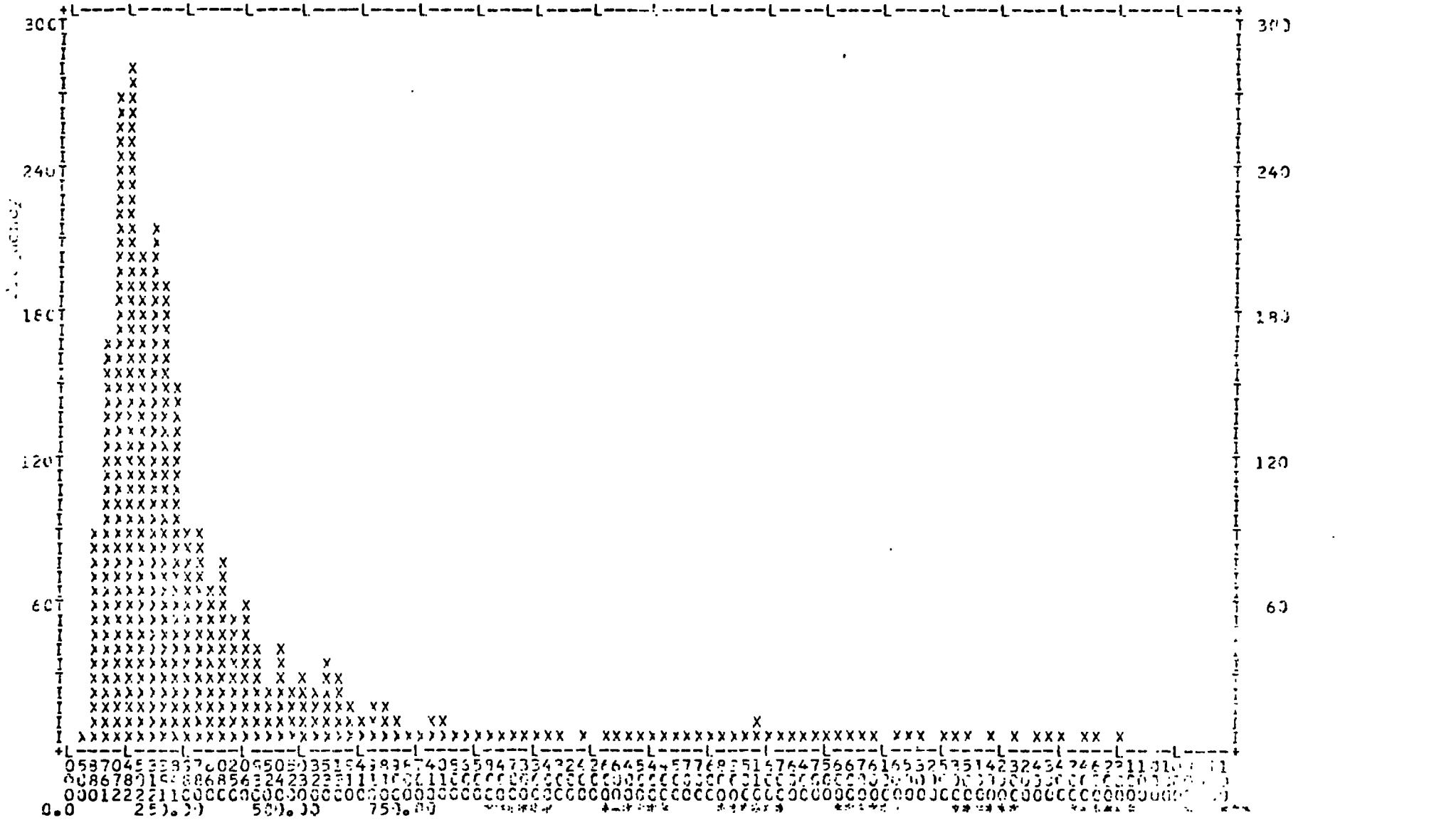

Figure 5.14: Distribution of the Stokes vector (I_S)

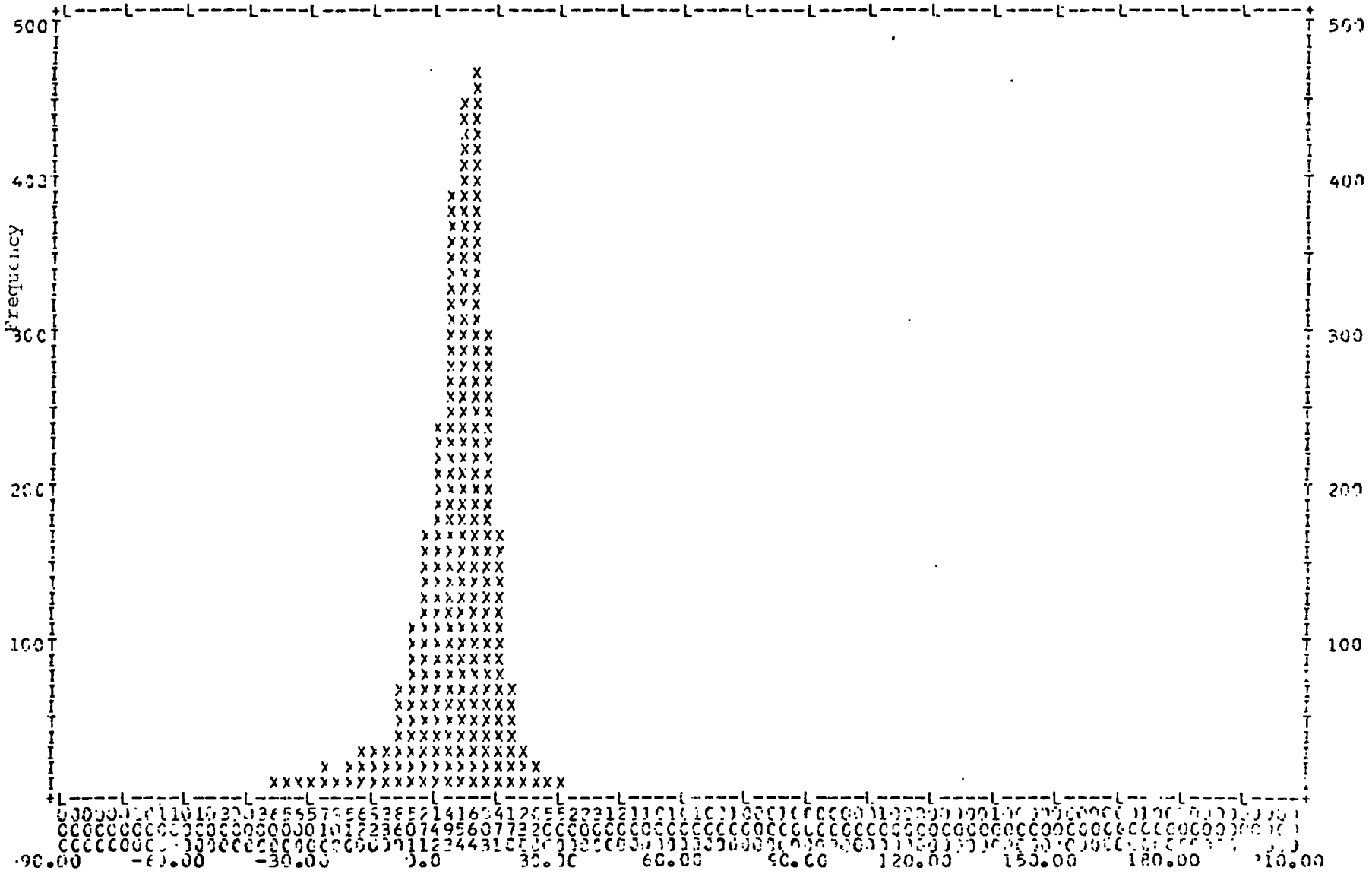

Figure 5.15: Distribution of the Stokes vector (Q_S)

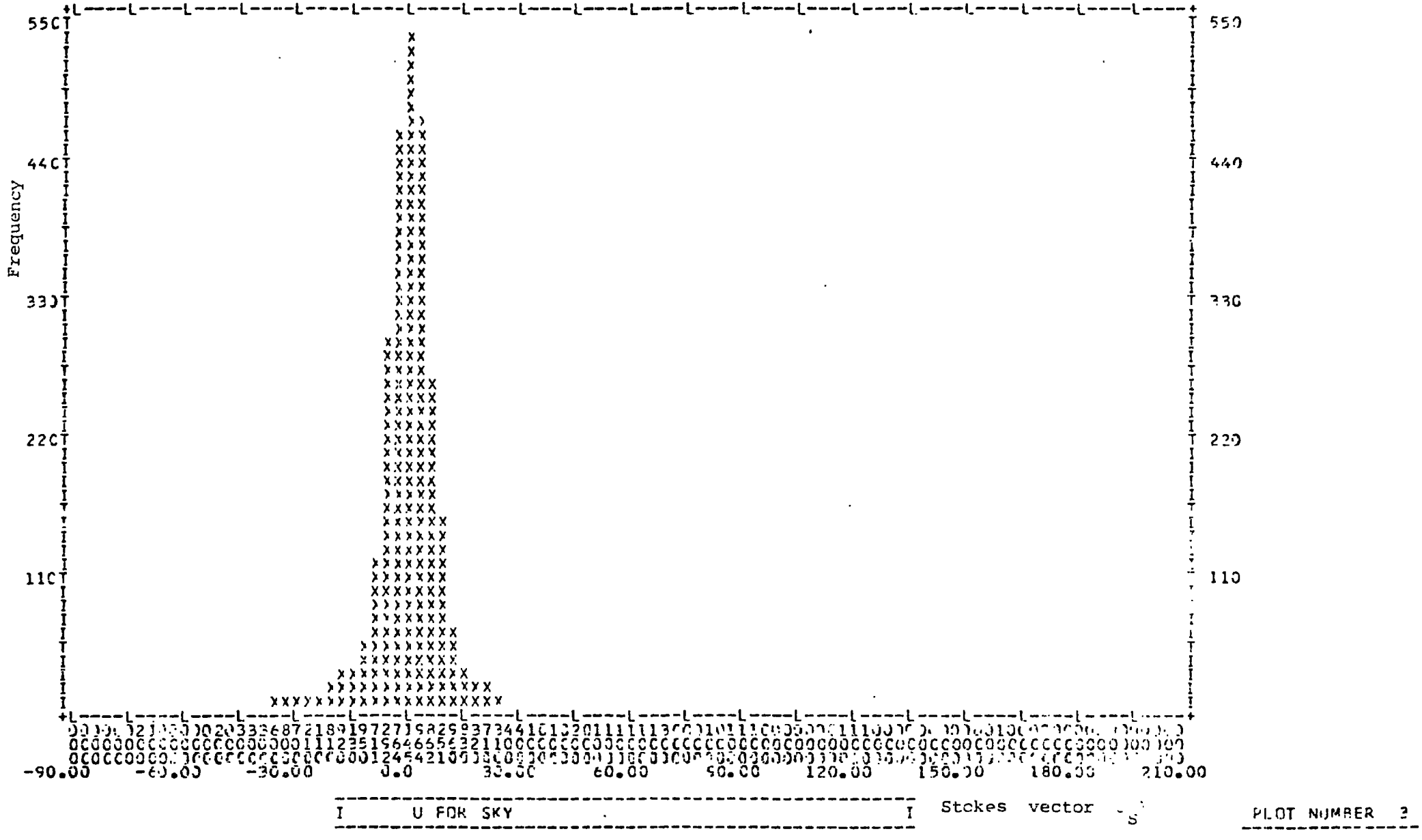

Figure 5.16: Distribution of the Stokes vector (U_S)

		I_1	I_2	I_3	Q_1	Q_2	Q_3	I	U_1	U_2	U	V_1	V_2	V	θ_1	θ_2	θ_3
128	101	1.06	1.07	1.07	1.01	0.94	0.94	749.	11.	7.	9.	-11.	-6.	-8.	2.1	1.2	1.7	21.5	20.9	21.3
128	106	1.06	1.07	1.07	0.99	0.92	0.90	739.	13.	9.	11.	-10.	-6.	-8.	2.2	1.5	1.8	18.9	17.2	18.2
128	111	1.09	1.08	1.08	0.97	0.91	0.93	787.	1.	3.	2.	-21.	-23.	-22.	2.7	3.0	2.8	43.8	41.0	42.3
128	116	1.12	1.09	1.10	0.94	0.89	0.90	841.	1.	10.	6.	-12.	-21.	-16.	1.4	2.8	2.0	42.7	31.9	35.5
128	121	1.10	1.10	1.10	0.98	0.95	0.95	812.	2.	3.	2.	-13.	-14.	-13.	1.6	1.7	1.6	41.3	39.7	40.5
128	126	1.08	1.10	1.09	0.97	0.91	0.94	891.	13.	8.	10.	-30.	-25.	-27.	3.7	2.9	3.3	33.4	36.4	34.7
128	131	1.10	1.13	1.11	0.94	0.86	0.87	699.	17.	9.	13.	-20.	-12.	-16.	3.8	2.2	3.0	24.5	26.1	25.0
128	136	1.26	1.29	1.28	0.99	0.86	0.85	467.	3.	-4.	-0.	-18.	-11.	-15.	3.9	2.5	3.1	49.0	54.2	45.6
128	141	1.22	1.24	1.23	0.94	0.84	0.85	484.	10.	6.	8.	0.	5.	2.	2.1	1.5	1.7	-0.6	-20.1	-9.7
128	146	1.26	1.27	1.26	0.99	0.89	0.96	459.	8.	7.	8.	1.	3.	2.	1.9	1.7	1.7	-4.5	-9.9	-7.0
128	166	1.26	1.27	1.26	0.99	0.89	0.86	474.	8.	7.	7.	13.	15.	14.	3.3	3.4	3.3	-29.2	-32.8	-31.0
128	171	1.24	1.25	1.25	0.89	0.84	0.82	565.	1.	-2.	-0.	1.	5.	3.	0.4	0.9	0.5	-23.0	-55.4	-46.6
128	176	1.14	1.16	1.15	0.97	0.89	0.89	626.	23.	17.	20.	0.	6.	3.	3.6	2.9	3.2	-0.4	-9.1	-4.3
128	186	1.11	1.08	1.10	0.93	0.92	0.94	1044.	-4.	11.	4.	-12.	-27.	-20.	1.2	2.8	1.9	53.9	33.7	39.5
128	191	1.07	1.07	1.07	0.95	0.90	0.88	1405.	11.	13.	12.	-14.	-16.	-15.	1.2	1.4	1.3	25.4	25.0	25.2
128	196	1.04	1.02	1.03	0.97	0.96	0.95	2481.	-31.	-2.	-16.	32.	3.	17.	1.8	0.1	1.0	-67.0	-62.0	-66.6
128	201	1.02	1.00	1.01	0.96	0.95	0.94	2901.	-31.	-2.	-16.	52.	23.	38.	2.1	0.8	1.4	-60.3	-47.3	-56.8
128	206	1.02	1.02	1.02	0.96	0.95	0.94	2691.	6.	7.	6.	26.	25.	26.	1.0	1.0	1.0	-38.5	-37.4	-37.9
128	211	1.03	1.01	1.02	0.96	0.96	0.95	2580.	5.	30.	17.	19.	-6.	7.	0.8	1.2	0.7	-38.0	5.7	-10.5
128	216	1.04	1.04	1.04	0.95	0.94	0.91	2431.	-2.	-4.	-3.	31.	34.	32.	1.3	1.4	1.3	-46.5	-48.6	-47.6
128	221	1.05	1.06	1.05	0.96	0.97	0.93	2157.	-8.	-27.	-18.	21.	39.	30.	1.0	2.2	1.6	-56.2	-62.4	-60.4
128	226	1.09	1.12	1.11	0.98	0.94	0.94	1826.	25.	0.	13.	11.	36.	23.	1.5	2.0	1.5	-11.5	-44.9	-30.6
128	231	1.10	1.09	1.09	0.99	0.91	0.92	1751.	17.	24.	21.	8.	-0.	4.	1.1	1.4	1.2	-12.5	0.0	-5.3
128	236	1.10	1.10	1.10	0.98	0.91	1.90	1966.	20.	15.	18.	34.	40.	37.	2.0	2.2	2.1	-29.8	-34.7	-32.3
128	241	1.10	1.09	1.09	0.97	0.86	0.86	2476.	-18.	-7.	-12.	28.	16.	22.	1.3	0.7	1.0	-61.5	-55.0	-59.6
128	246	1.07	1.06	1.07	0.98	0.88	0.88	2543.	-4.	12.	4.	4.	-12.	-4.	0.2	0.7	0.2	-69.0	23.2	24.3
128	251	1.07	1.06	1.06	1.01	0.97	0.96	2047.	-0.	14.	7.	2.	-12.	-5.	0.1	0.9	0.4	-49.7	21.1	19.4
128	256	1.05	1.06	1.06	1.00	0.95	0.93	1593.	11.	6.	9.	17.	23.	20.	1.3	1.5	1.4	-28.4	-38.0	-33.5
128	261	1.08	1.07	1.07	1.00	0.95	0.93	1156.	23.	28.	26.	7.	2.	4.	2.1	2.4	2.2	-9.0	-2.1	-4.9
128	266	0.87	0.89	0.88	0.99	0.97	0.93	958.	25.	12.	19.	-4.	10.	3.	2.7	1.6	2.0	4.1	-20.2	-4.8
128	271	0.97	0.96	0.96	0.98	0.94	0.92	828.	5.	12.	8.	11.	4.	7.	1.4	1.5	1.3	-37.9	-8.6	-20.4
128	276	1.03	1.05	1.04	0.98	0.95	0.95	803.	13.	6.	9.	16.	22.	19.	2.5	2.9	2.6	-25.7	-37.8	-32.2
128	281	1.07	1.04	1.06	1.01	1.01	0.93	748.	21.	30.	26.	23.	13.	18.	4.1	4.4	4.2	-23.5	-11.8	-17.4
128	286	1.01	1.02	1.01	0.99	0.96	0.91	736.	15.	12.	13.	16.	20.	18.	3.0	3.1	3.1	-23.5	-29.9	-26.8
128	291	1.02	1.01	1.01	0.96	0.92	0.91	696.	1.	6.	4.	12.	6.	9.	1.7	1.3	1.4	-42.7	-22.8	-34.1
128	296	1.02	1.02	1.02	0.96	0.92	0.94	599.	4.	4.	4.	20.	20.	20.	3.4	3.4	3.4	-39.3	-39.5	-39.4
128	301	1.00	1.00	1.00	0.97	0.91	0.92	585.	16.	17.	16.	13.	12.	13.	3.5	3.6	3.5	-19.8	-17.9	-18.9
128	306	1.03	0.99	1.01	0.95	0.91	0.93	573.	3.	14.	9.	22.	11.	16.	3.9	3.1	3.2	-40.5	-18.4	-30.7
128	311	1.00	1.03	1.01	0.96	0.91	0.89	553.	8.	3.	5.	16.	22.	19.	3.3	4.0	3.6	-31.3	-41.8	-37.1
128	316	1.04	1.01	1.02	0.93	0.85	0.89	526.	19.	24.	22.	10.	5.	8.	4.1	4.7	4.3	-14.5	-5.6	-9.7
128	321	1.04	1.04	1.04	0.99	0.89	0.84	462.	14.	13.	14.	24.	25.	24.	6.0	6.0	6.0	-30.2	-30.7	-30.5
128	326	1.05	1.01	1.03	0.97	0.85	0.81	424.	13.	21.	17.	11.	3.	7.	4.0	5.0	4.4	-19.2	-3.8	-10.7
128	336	0.84	0.86	0.85	0.86	0.77	0.81	396.	13.	9.	11.	15.	18.	17.	4.9	5.2	5.0	-24.5	-32.0	-28.3
128	341	1.02	1.00	1.01	0.93	0.81	0.84	311.	8.	11.	9.	7.	4.	5.	3.4	3.7	3.5	-20.6	-9.9	-15.0
128	346	1.07	1.07	1.07	0.89	0.77	0.75	293.	12.	12.	12.	11.	11.	11.	5.6	5.6	5.6	-21.9	-23.9	-22.9
128	351	0.97	1.00	0.99	0.87	0.76	0.73	282.	9.	4.	7.	6.	10.	8.	3.7	3.9	3.6	-16.3	-33.4	-25.1
128	356	1.04	1.02	1.02	0.83	0.80	0.70	263.	11.	13.	12.	17.	15.	16.	7.8	7.6	7.7	-29.3	-25.1	-27.2
128	366	0.88	0.90	0.89	0.81	0.78	0.67	254.	15.	13.	14.	7.	10.	8.	6.6	6.2	6.3	-12.2	-18.6	-15.3
133	36	1.04	1.08	1.06	0.94	0.89	0.69	144.	2.	0.	1.	-4.	-1.	-3.	3.0	1.0	1.9	29.6	44.2	32.7
133	41	1.08	1.07	1.07	0.99	0.82	0.73	160.	6.	6.	6.	-2.	-2.	-2.	3.7	4.1	3.9	8.3	10.3	9.6
133	51	1.10	1.11	1.11	1.09	0.82	0.75	193.	10.	8.	9.	-15.	-14.	-14.	9.2	8.3	8.8	29.1	29.2	29.8
133	56	1.09	1.08	1.08	0.97	0.82	0.85	220.	9.	10.	9.	-7.	-9.	-8.	5.1	6.1	5.6	19.3	20.2	20.0
133	61	1.09	1.06	1.08	0.96	0.88	0.88	265.	10.	13.	12.	-4.	-8.	-6.	4.1	5.9	5.0	11.9	15.3	13.9
133	66	1.10	1.07	1.08	0.99	0.95	1.00	325.	1.	6.	3.	-20.	-25.	-22.	6.1	7.9	6.9	43.7	38.2	40.6
133	71	1.04	1.02	1.03	0.96	0.88	0.90	417.	3.	6.	5.	-17.	-20.	-19.	4.3	5.1	4.6	39.4	36.4	37.8
133	76	1.06	1.10	1.08	0.98	0.86	0.86	462.	27.	19.	23.	-16.	-9.	-12.	6.7	4.5	5.6	19.6	12.3	14.3
133	81	1.12	1.12	1.12	1.04	0.92	0.94	500.	12.	11.	12.	-4.	-3.	-4.	2.5	2.3	2.4	8.2	7.9	8.6
133	86	1.10	1.13	1.12	0.98	0.89	0.92	608.	20.	13.	17.	2.	10.	6.	3.4	2.6	2.9	-2.8	-18.4	-9.6
133	91	1.09	1.08	1.08	0.99	0.92	0.92	659.	10.	13.	12.	-11.	-15.	-13.	2.2	3.0	2.6	24.2	23.8	24.0
133	96	1.07	1.06	1.07	1.01	0.93	0.91	731.	8.	11.	10.	-7.	-10.	-8.	1.4	2.0	1.7	19.8	20.7	20.3

Figure 5.17: The polarisation parametersas line printer output.

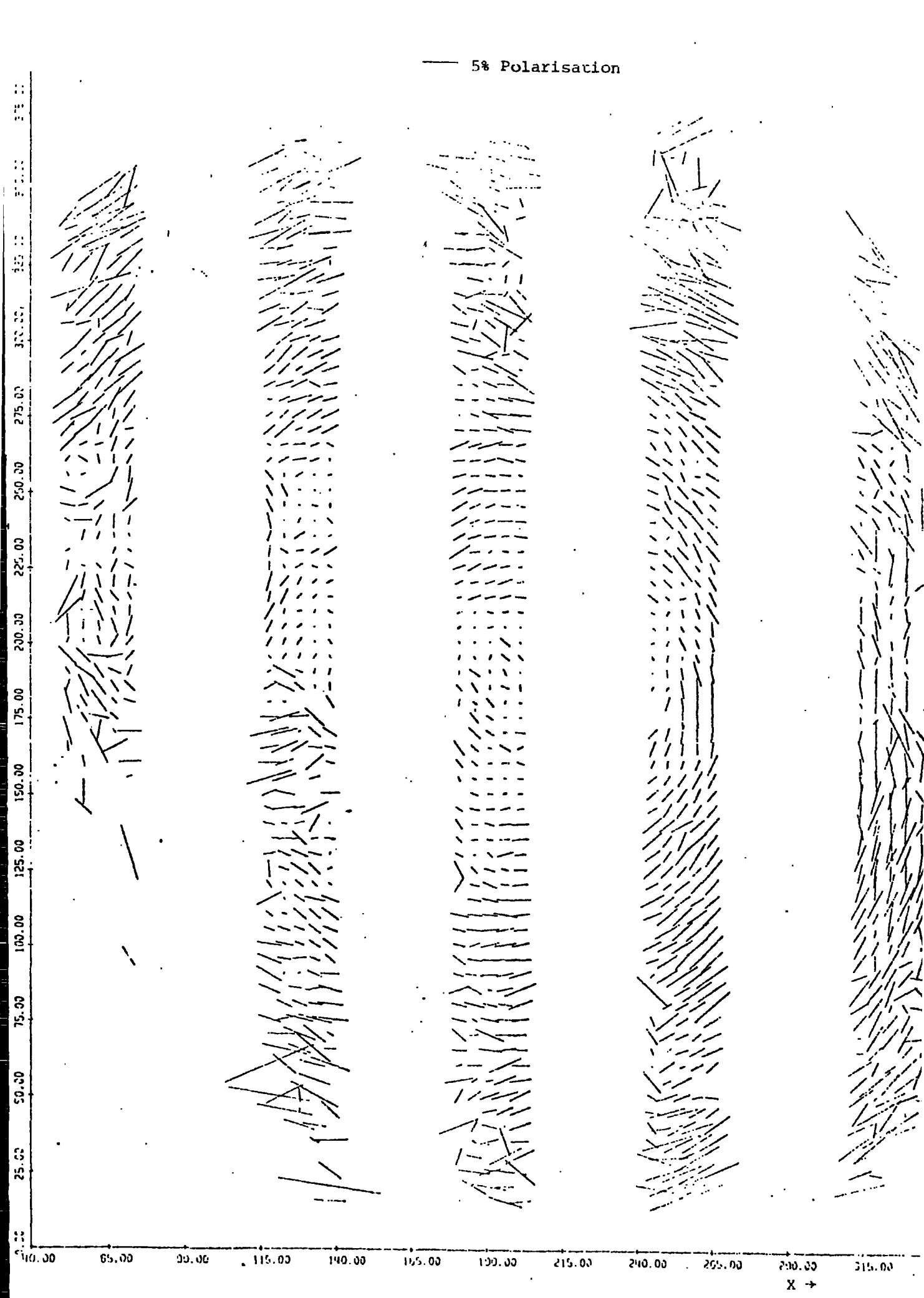

Figure 5.18: The polarisation map from electronographs 1-4.

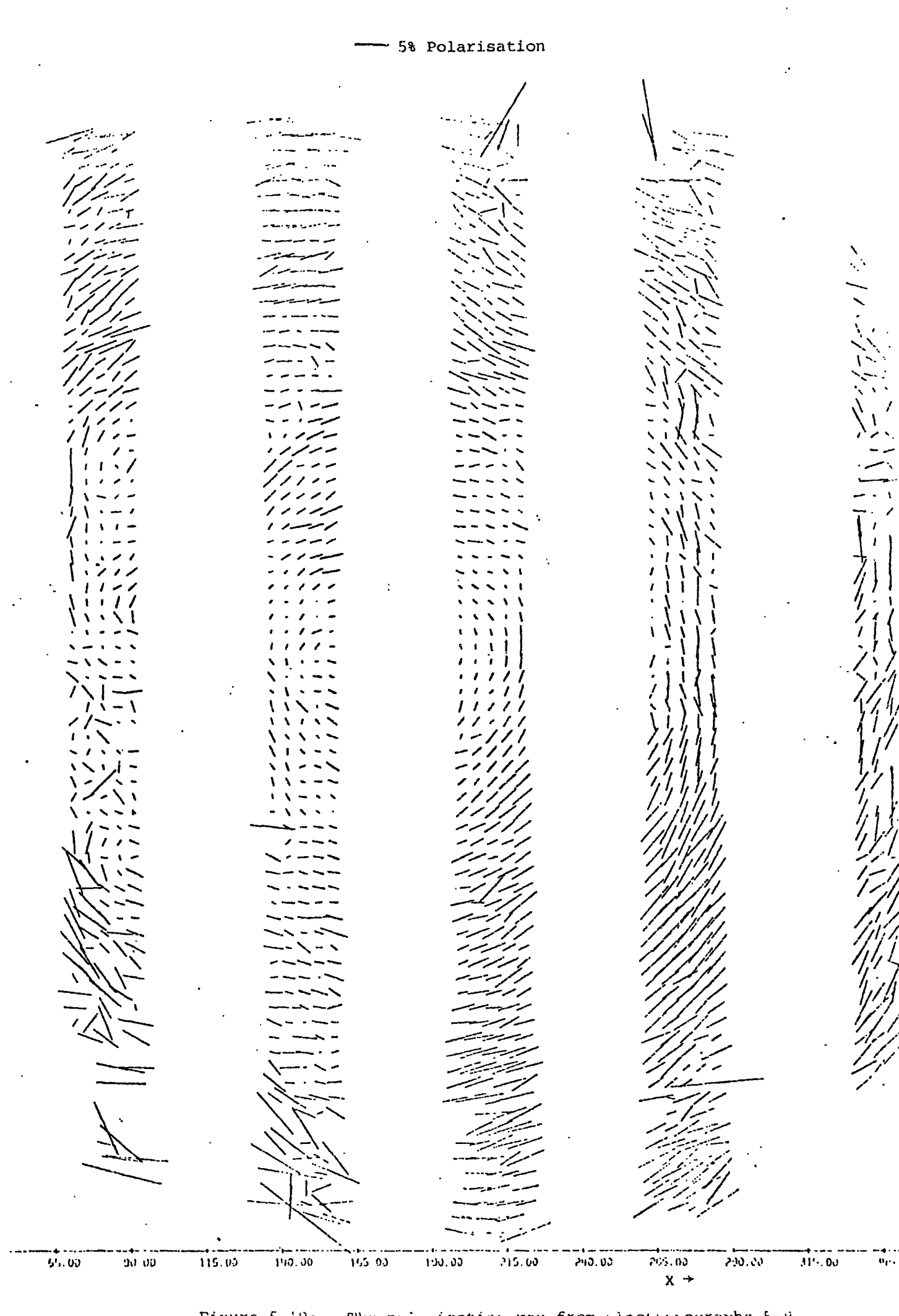

Figure 5.19: The polarisation map from electromagnetographs 5-8.

— 5% Polarisation

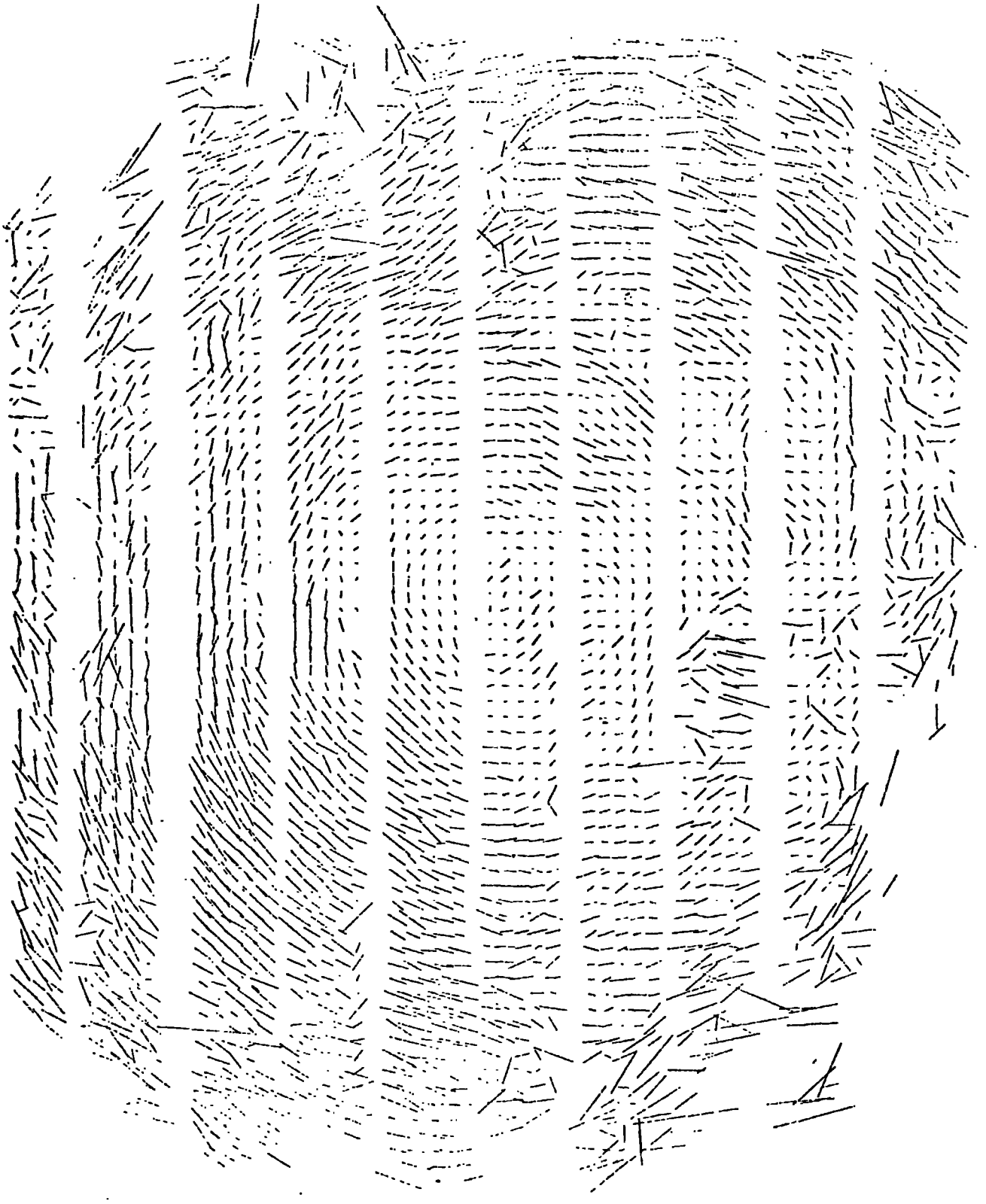

Figure 5.20: The polarisation map from electronographs 1-8 aligned by eye for central region of the Orion Nebula.

$$\alpha = A + BX + Cy \qquad (5.1)$$

$$\delta = D + EX + Fy \qquad (5.2)$$

the transformation coefficients will be found, where (α, δ, x, y) have been used for the stars in the field of view.

5.3 Results of the Present Observation of the Orion Nebula

In the present series of observations, the analysis of the results gave information on the degree and angle of polarisation for over 8550 points in the Orion Nebula. Figures 5.18 and 5.19 show the two halves of the map for the Central region of the Orion Nebula, and Figure 5.20 shows the both halves.

The polarisation map of the Central region, Dark Bay and Fan edge after sky subtraction in the (α, δ) system, are presented in Figures 5.21, 5.22 and 5.23 individually. Figure 5.24 shows the whole polarisation map of the Orion Nebula, which is a combination of the three sets of data results.

The length of each line is directly proportional to the degree of polarisation and is drawn parallel to the electric vector (E) of the linearly polarised component of the radiation and centred on the point observed. Each vector represents the integrated polarisation over an area 7" x 7".

The complete results are shown in Figure 5.25 superimposed on a photograph of the Orion Nebula taken in the red. The small square (Figures 5.24 and 5.25) shows the position of the Klunmann - Low nebula.

5.4 Errors on the Measurements

There is some difficulty involved in the determination of the

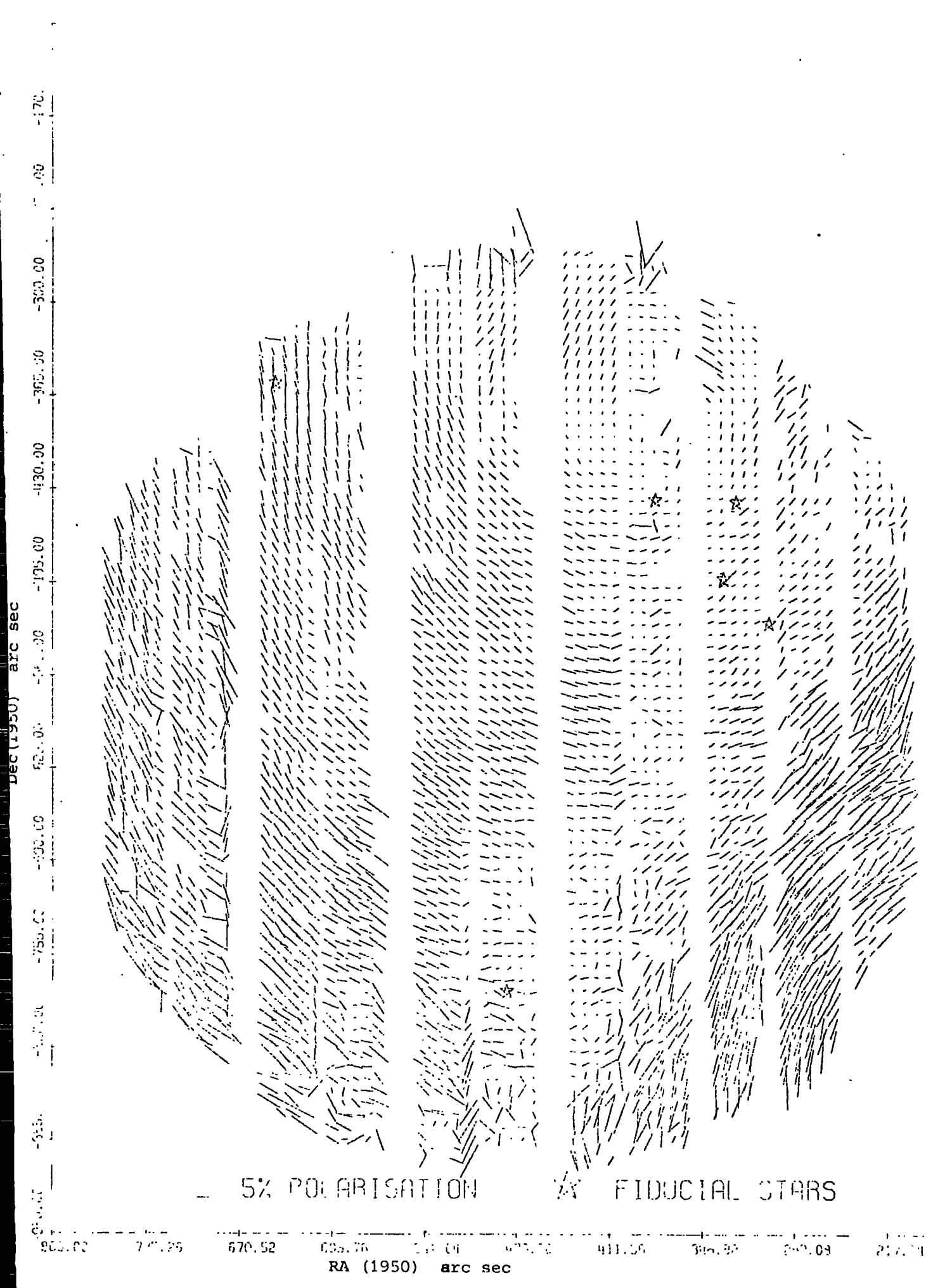

Figure 5.23: The optical linear polarisation map of the Orion Nebula (Fan Edge).
The origins are: RA 05h 33m 15s
Dec-05° 31′ 00.00″

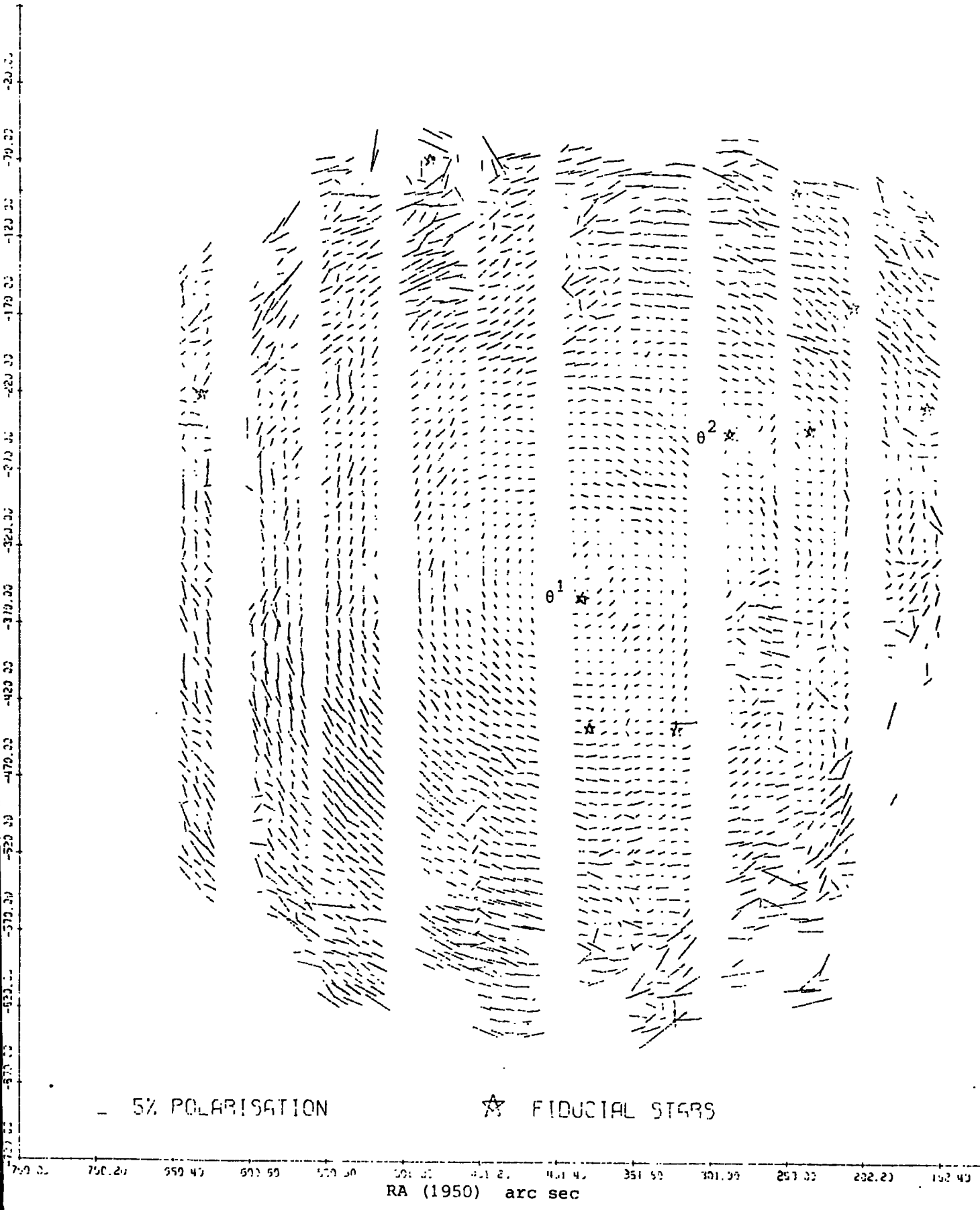

Figure 5.21: The optical linear polarisation map of the Orion Nebula (central region)

The origins are: RA 05h 33m 15s
Dec-05° 3' 00.

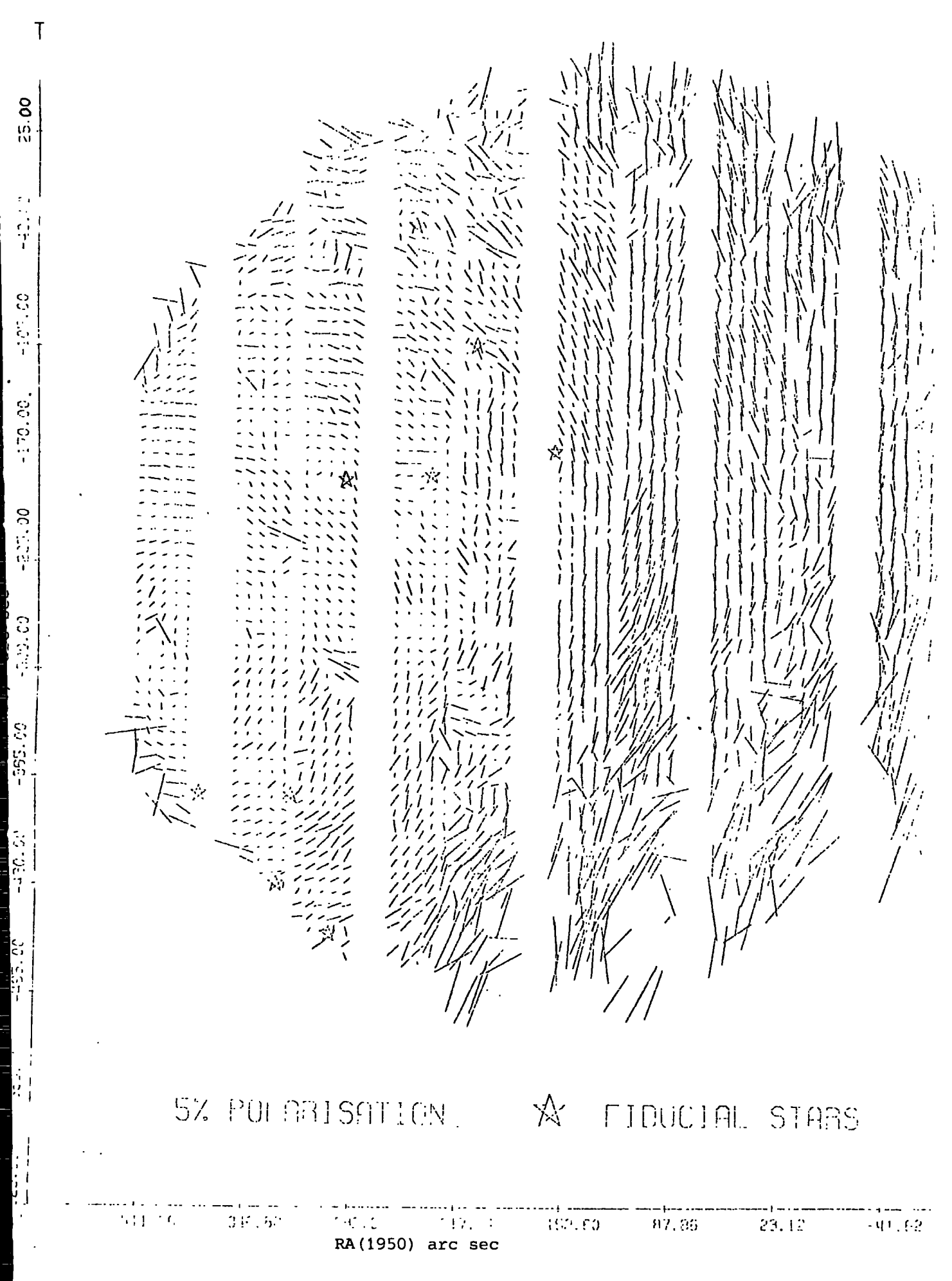

Figure 5.22: The optical linear polarisation map of the Orion Nebula (Dark Bay).
The origins are: RA 05h 33m 15s
Dec-05° 31′ 00.00″

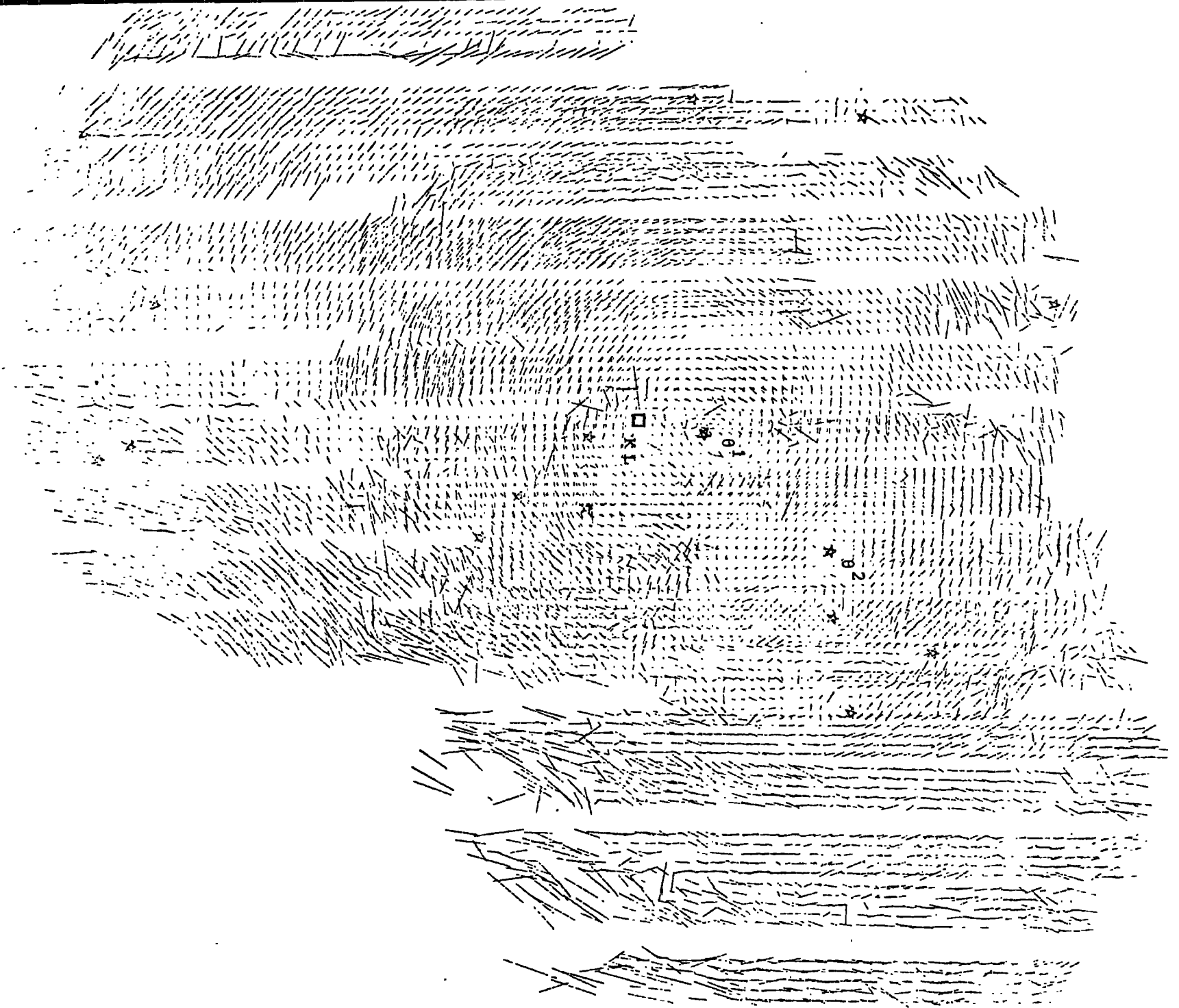
x1
θ1
θ2


θ2
θ1
KL

individual errors on each point of the polarisation map, because this needs detailed knowledge of the individual errors on the values $i_1 - i_8$. However some estimate of the relative errors on various points on the plate can be made by examining the variation of the difference between the two estimates of the degree of polarisation $P_1 - P_2$, and that between the angles, $\theta_1 - \theta_2$, with the intensity and degree of polarisation measured. It has been mentioned (Section 3.6) that the instrumental errors can be ignored.

Since $P = (Q^2 + U^2)^{\frac{1}{2}}/I$ and $\theta = \frac{1}{2} \tan^{-1} \frac{U}{Q}$, one would expect that the error on the degree of polarisation depends more strongly on the intensity than does the error on the angle.

If we consider the distribution of the values $P_1 - P_2$ against intensity (Figure 5.26) it can be seen that, with increasing intensity, the difference in the two estimates of the degree of polarisation falls off rapidly.

If we consider the difference in the two estimates of the degree of polarisation as a function not only of the intensity, but also of the degree of polarisation itself, we can obtain more detailed estimates of the error on the degree and angle of polarisation. The relationship between the difference between the two estimates of the degree of polarisation measurements, $P_1 - P_2$, with intensity, for various intervals of the degree of polarisation, P, less than 2%, between 2% and 4%, and greater than 4%, are shown in Figure 5.27. The intensity scale used is logarithmic, in order to show more clearly the information measured, since Figure 5.26 shows the distribution to be almost exponential.

From Figure 5.27 one can see that for all intervals of the degree of polarisation the difference in the two estimates, $P_1 - P_2$, is greater than for lower intensity regions, than for the more intense

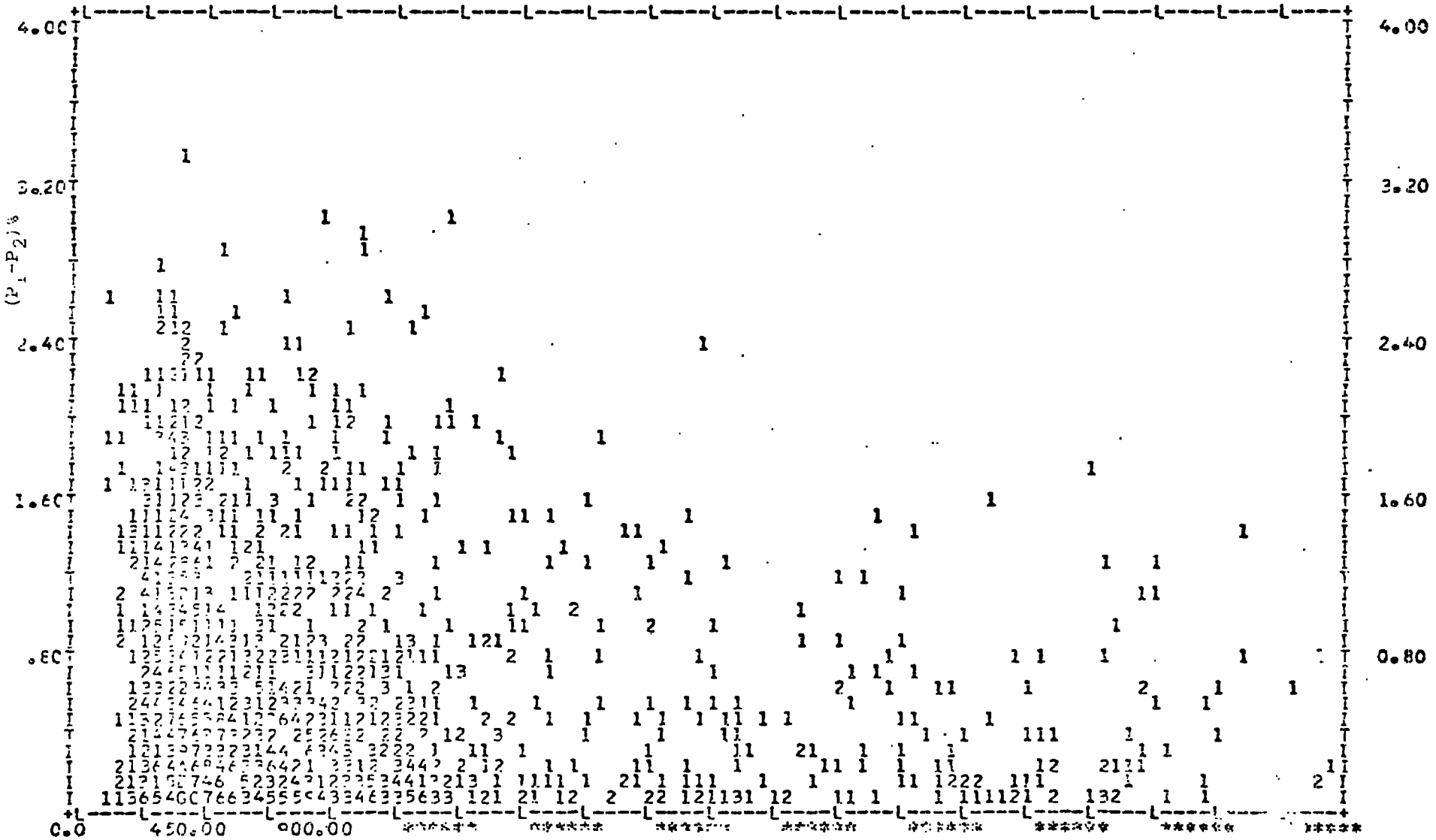

Figure 5.26: Distribution of $P_1 - P_2$ as a function of Intensity.

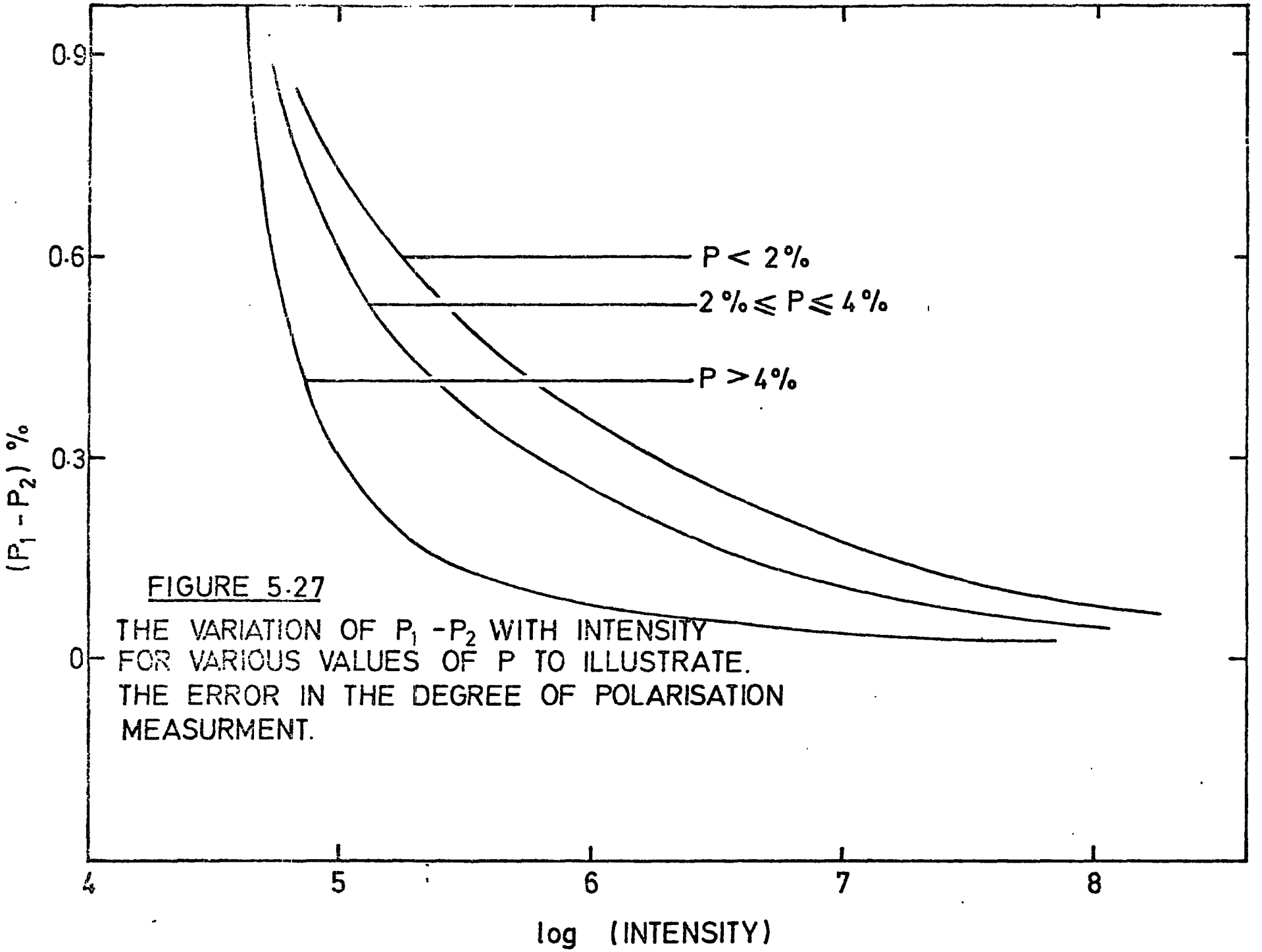

FIGURE 5·27

THE VARIATION OF $P_1 - P_2$ WITH INTENSITY FOR VARIOUS VALUES OF P TO ILLUSTRATE. THE ERROR IN THE DEGREE OF POLARISATION MEASURMENT.

brighter regions of the nebula.

For low values of the degree of polarisation $0\% \leqslant P \leqslant 2\%$, value of the $P_1 - P_2$ can be as great as 0.6% for the faint regions of the nebula, falling to less than 0.1% in the more intense regions. For the small values of polarisation the shape of the error line seems to be approximately linear, showing that the error is not so nearly dependent on the intensity as for higher values of the polarisation. As the degree of polarisation increases the value of $P_1 - P_2$ falls off more rapidly with the intensity.

As one can see from Figure 5.27, for the higher values of the degree of polarisation $P > 4\%$, even at the low intensity the polarisation is well determined, that is $P_1 - P_2$ is less than 0.1%.

The nonlinearity in the digitisation process of the electronograph is another factor. Although this effect is allowed for in the reduction technique, for large values of the degree of polarisation, this effect could cause systematic errors in the polarisation measured.

Now it can be concluded that the error on the degree of polarisation measured is intensity dependent and that the error decreases with increasing value of the degree of polarisation.

Figure 5.28 shows the relationship between the difference of the two estimates of the angle of polarisation measured, $\theta_1 - \theta_2$, with intensity for the same intervals of P as for Figure 5.27.

It can be seen from Figure 5.28 that the error on the angle measured is less dependent on the intensity, as would be expected, and more dependent on the degree of polarisation. But the less well determined values of the degree of polarisation are a function of the intensity and in fact $\theta_1 - \theta_2$ is slightly greater, of the order of 10°

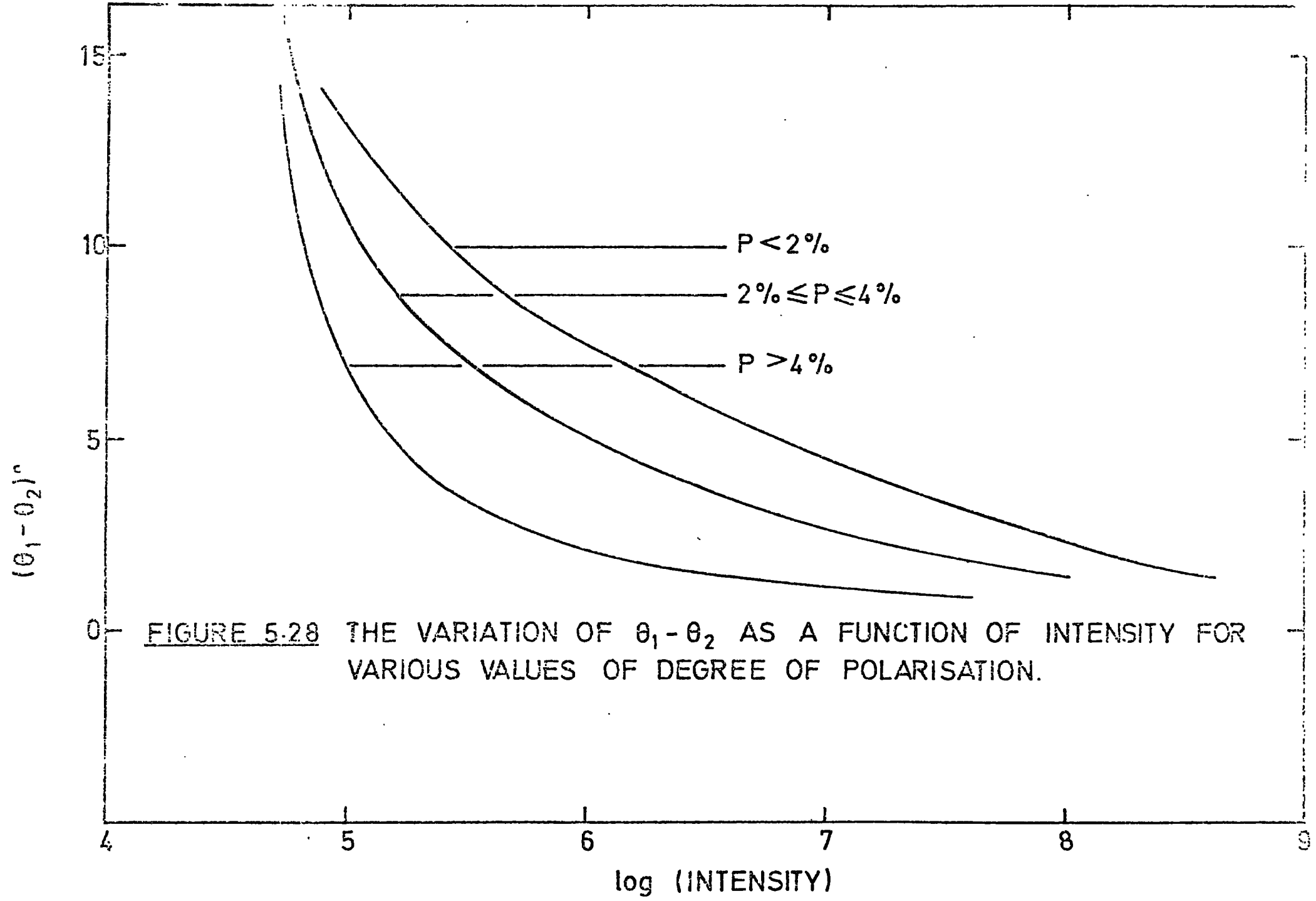

FIGURE 5·28 THE VARIATION OF $\theta_1 - \theta_2$ AS A FUNCTION OF INTENSITY FOR VARIOUS VALUES OF DEGREE OF POLARISATION.

for low intensity values falling to 3° at the higher intensity levels.

5.5 Description of the observed Optical Polarisation of the Orion Nebula

From Figure 5.25 which shows the results of the present series of observations, superimposed on a red photograph of the Orion Nebula, it can be deduced that the degree and angle of polarisation can be measured by this method for nearly whole areas of the nebula.

In the central region of the Orion Nebula (Figure 5.21), which is correlated to that measured in the B waveband of the UBV system by Pallister et al (1977), the general pattern of the polarisation vectors agree well. A more detailed comparison of the results of these two sets of observations will be discussed in the following chapter.

The most obvious feature of Figure 5.25 is the centrosymmetric pattern to the North, West and South of the Trapezium (θ^1ori), the vectors are mainly normal to the radius vector from the Trapezium and the point of observation. This effect is due to the scattering of light emanating from the Trapezium by the nebular material, the degree of polarisation depending mainly on the character of the particles and the scattering geometry.

As one can see from Figure 5.25, in the region around θ^2ori, the pattern tends to centre on θ^2 rather than on the Trapezium, also the position of the 'bar' said to be an ionisation front which runs north-east - south-west, is just below θ^2 on this picture. The pattern in the bottom and at the right corner of Figure 5.25 has been produced by NGC 1982 (M43). An optical polarisation map of this object will be presented in this chapter.

Furthermore, in order to see clearly the area illuminated by θ^2 ori and the position of the bar, figure 5.22à is presented here. This has a larger scale than figure 5.22. It can easily be seen that a larger area around θ^2 ori is illuminated by this star than is indicated by the work of Pallister et al (1977). This shows the important role of θ^2 ori in the illumination of the Orion Nebula, in addition to θ^1 ori. Also two solid parallel lines are drawn along the position of the bar, to show this region. The orientation of the polarisation vectors in this region indicates the transition of light in the area between two sources of illumination, θ^1 ori and θ^2 ori.

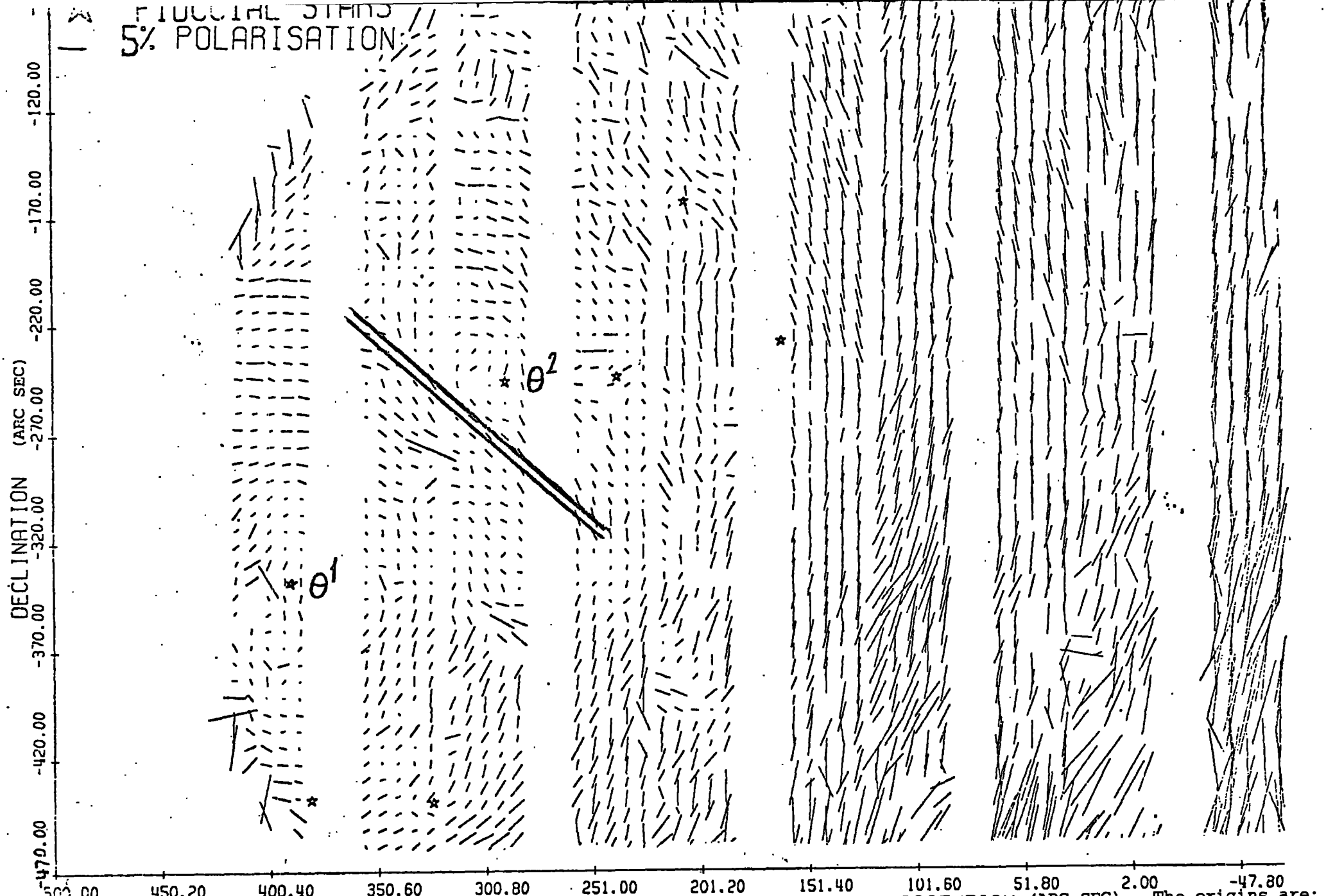

Figure 5.22 : Showing region illuminated by θ^2 ori, and position of 'bar'. RA 05h 33m 15s, Dec = 05° 31′ 00 0″

The degree of polarisation changes from nearly 1% for the inner regions to about 12% for outer regions. The fact that the degree of polarisation observed is small is due partly to the fact that the light we see is the sum of the scattered and emission components of the nebular light. Only the scattering effect is expected to show much polarisation.

5.6 Comparison of the present data of the Orion Nebula with Hall work

A comparison between the results of the present series of observation with those measured by Hall (1974) for central regions of the Orion Nebula shows that the degree and angle of polarisation agree well. As the number of points measured by Hall is small compared with the present data, there are not enough measurements to make a point to point comparison. It has been noted by Hall (1974), that ther is a general increase in polarisation at all wavelengths with increasing distance from θ^1ori.

To find this, a plot of percentage of polarisation against distance from θ^1ori has been drawn and is presented in Figure 5.29. The values of tbe error bars for percentage of polarisation are ± 0.10 to ± 0.58 in certain regions. From this plot one can see that the degree of polarisation for an area in the centre of the Orion Nebula is around 1% and increases towards the outer regions, which is in good agreement with Hall's results.

5.7 Comparison of the present data of the Orion Nebula with the work of Pallister et al

Optical linear polarisation has been measured at 3000 points in the central region of the Orion Nebula by Pallister et al (1977), using

To make further consideration in comparison of the present results with those measured by Hall (1974), a plot of percentage polarisation against distance from θ^1 ori has been drawn, using our results and an average of those measured in the continuum by Hall. From figure 5.29a it can be seen that in general the two plots agree, but there is some discrepancy, especially for those points near θ^1 ori. The difference in the two sets of data may be at least partially explained as a consequence of the different aperture size used. The present results were made with a 7 arc sec aperture, while those of Hall were made with a 27 arc sec aperture.

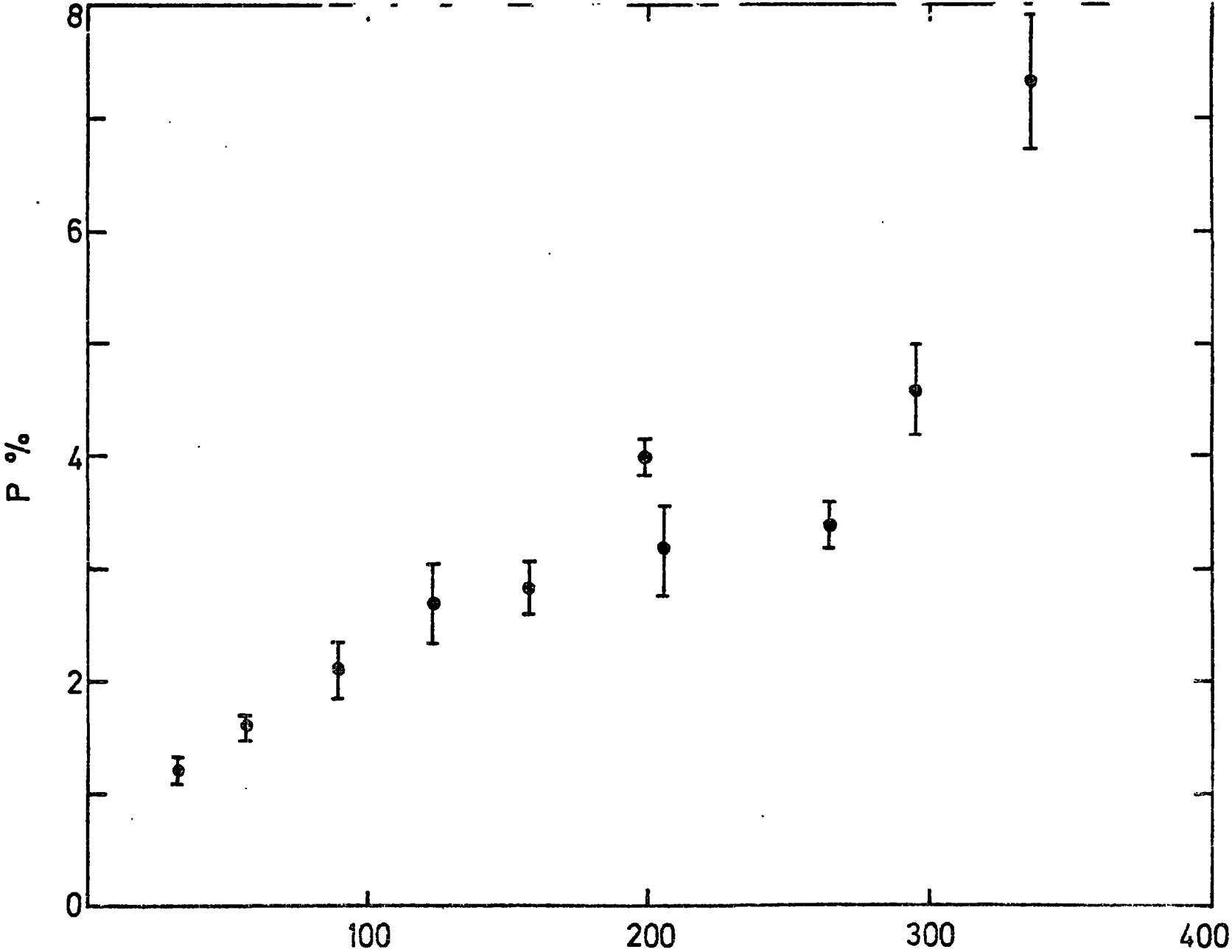

FIGURE 5.29 VARIATION IN PERCENTAGE POLARISATION FOR M42 WITH INCREASING DISTANCE FROM θ^1 ORI

To investigate whether the points which agree and disagree are randomly distributed, a plot o f degree of polarisation versus distance from the trapezium (in a north east - south west direction) has been drawn for the two sets of data, and is shown in figure 5.30a. The plot suggests that it is the region near the trapezium where the data disagree most.

Two explanations may be postulated for the poorer correlation for the degree of polarisation compared with that for the angle of polarisation. Firstly, the B measurements include a contribution from the H_β emission line, while the V waveband does not include any hydrogen emission lines. The emission radiation, which is unpolarised, will dilute the degree of linear polarisation observed without changing the observed orientation. Furthermore, because of the complex emission topography of the central part of the Orion Nebula (Elliot and Meaburn 1974†, and Scarrott 1978††) it will tend to increase the effective noise shown in a correlation plot of the one set of data against the other. Secondly, because the polarisation orientation is given as a ratio of the Stokes parameters U and Q, and the degree of polarisation is a sum, any errors in clear plate or sky subtraction will cause much larger errors in the latter parameter, as seen in figures 5.30 and 5.31.

---

† Elliott, K.H. and Meaburn, J. 1974, Astron & Astrophys. 34, 473

†† Scarrott, S.M. 1978, private communication, Physics Department, University of Durham

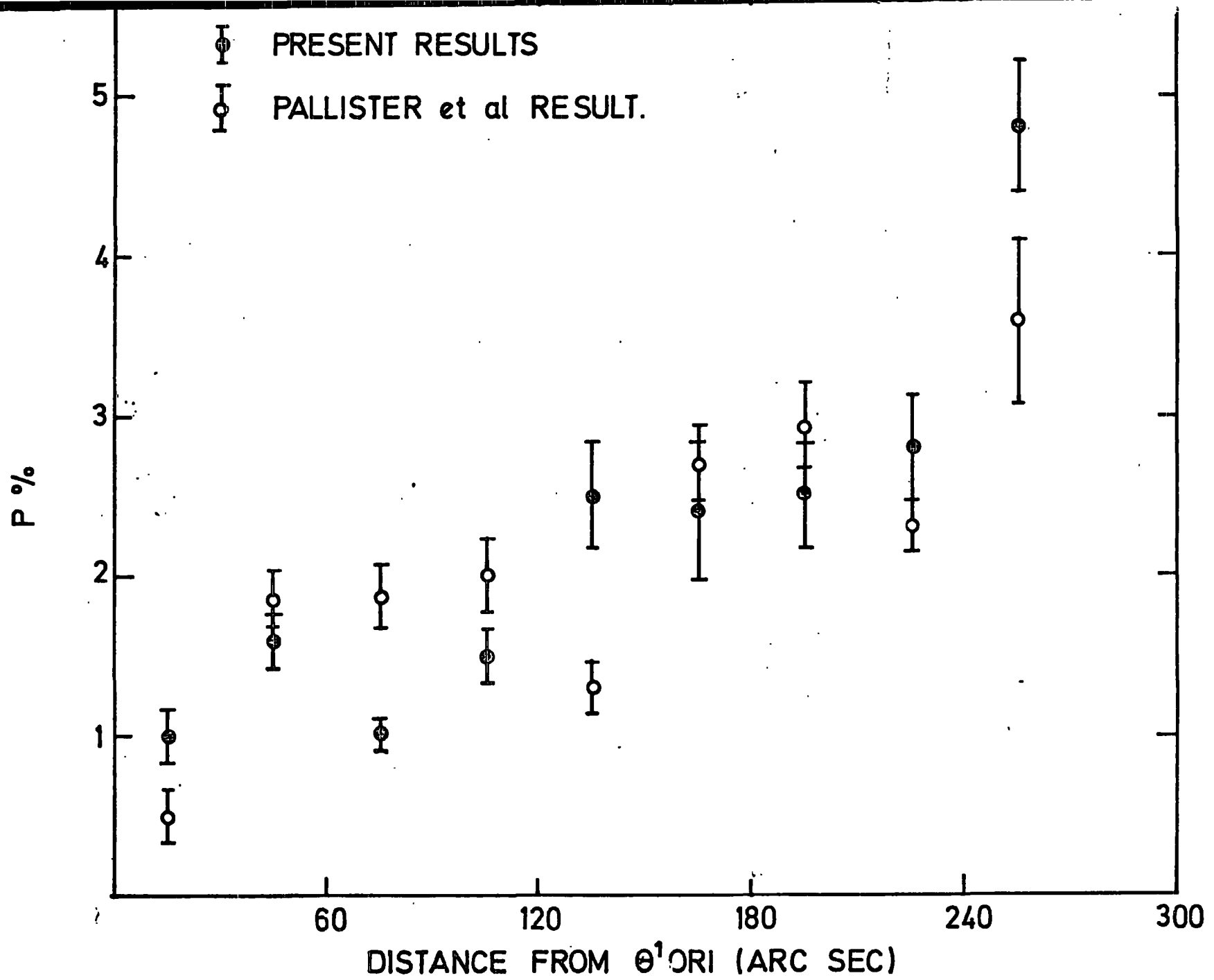
PRESENT RESULTS
PALLISTER et al RESULT.
P %
5
4
3
2
1
60
120
180
240
300
DISTANCE FROM θ¹ ORI (ARC SEC)

FIG. 5.30 a

the Blue Band of the UBV system and the same technique as for the present series of observations. Both measurements are over a 7 x 7 arc sec square which gives more validity in comparison.

To make a comparison between the two sets of results, it is necessary to compare the measurements of the polarisation obtained in each map, corresponding to the same point in the nebula. The present map was transformed to the co-ordinate system that Pallister et al used, using the field stars as fiducial marks, so that there was a one to one correspondence between measurements in the two sets of observations using B and V wavebands of the UBV system.

The scatter plots shown in Figures 5.30 and 5.31 show a general comparison between the two sets of results. Figure 5.30 shows, for each corresponding pair of measurements, the scatter plot of the degree of polarisation for the B and V measurements. If there is good agreement between the measurements the points should lie close to a line at 45% to the axes. Although the general trend is a line at 45°, the points are widely scattered about this line as shown in Figure 5.30, which indicates that there is some discrepancy between the two sets of measurements.

Either we consider the discrepancy to be due to errors in location of the comparison points, the two different sky levels in sky subtractions and the dependence on the waveband in which the observations were taken which has been noted by Hall (1974), or we assume that the measurements of the optical linear polarisation are wrong in places.

Figure 5.31 shows a similar plot for the angle of polarisation. There is excellent agreement between the two sets of observations in this plot.

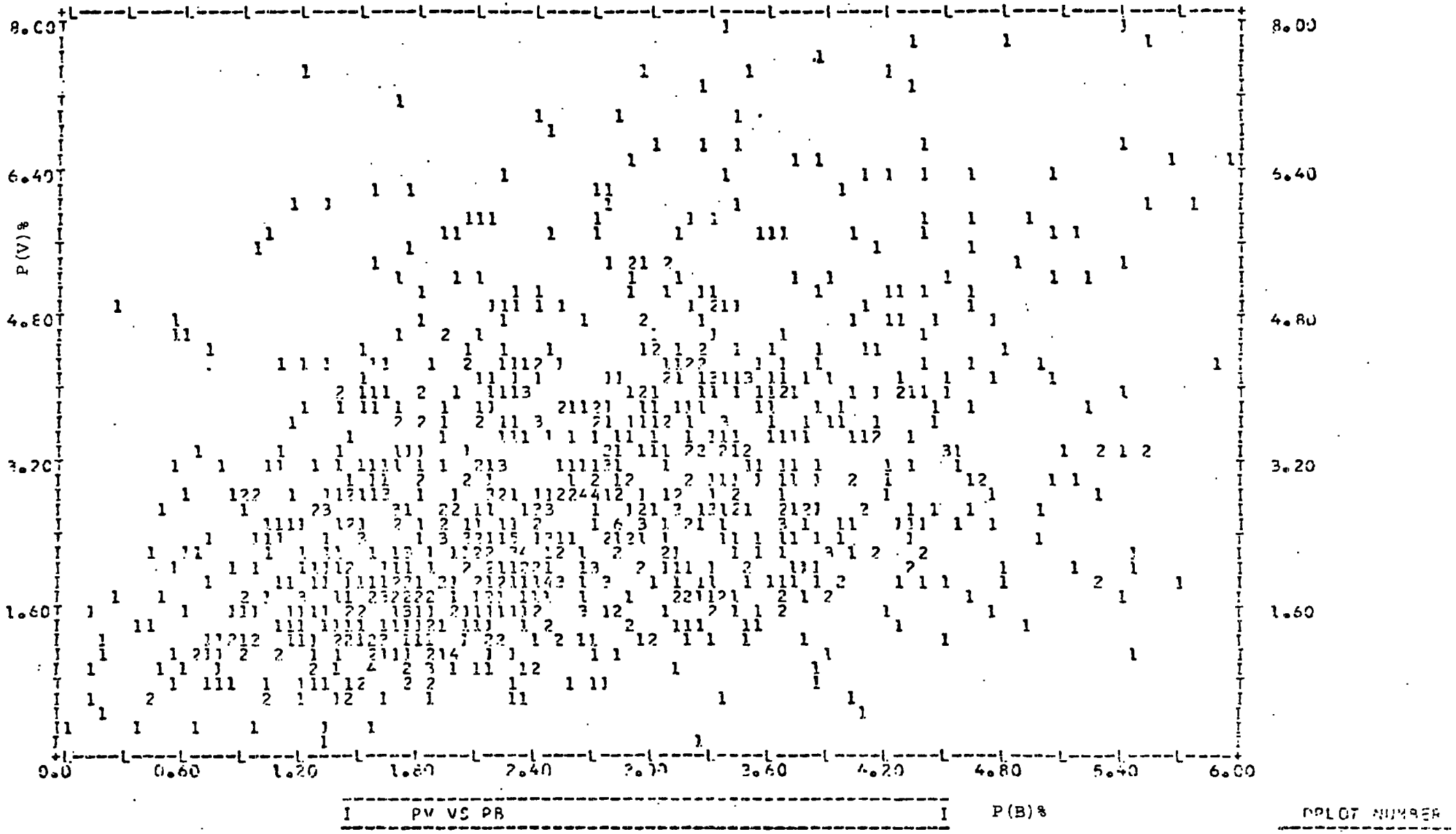

Figure 5.30: Scatter plot to compare the measurements of the degree of polarisation done by Pallister et al(B) with those of the present work (V)

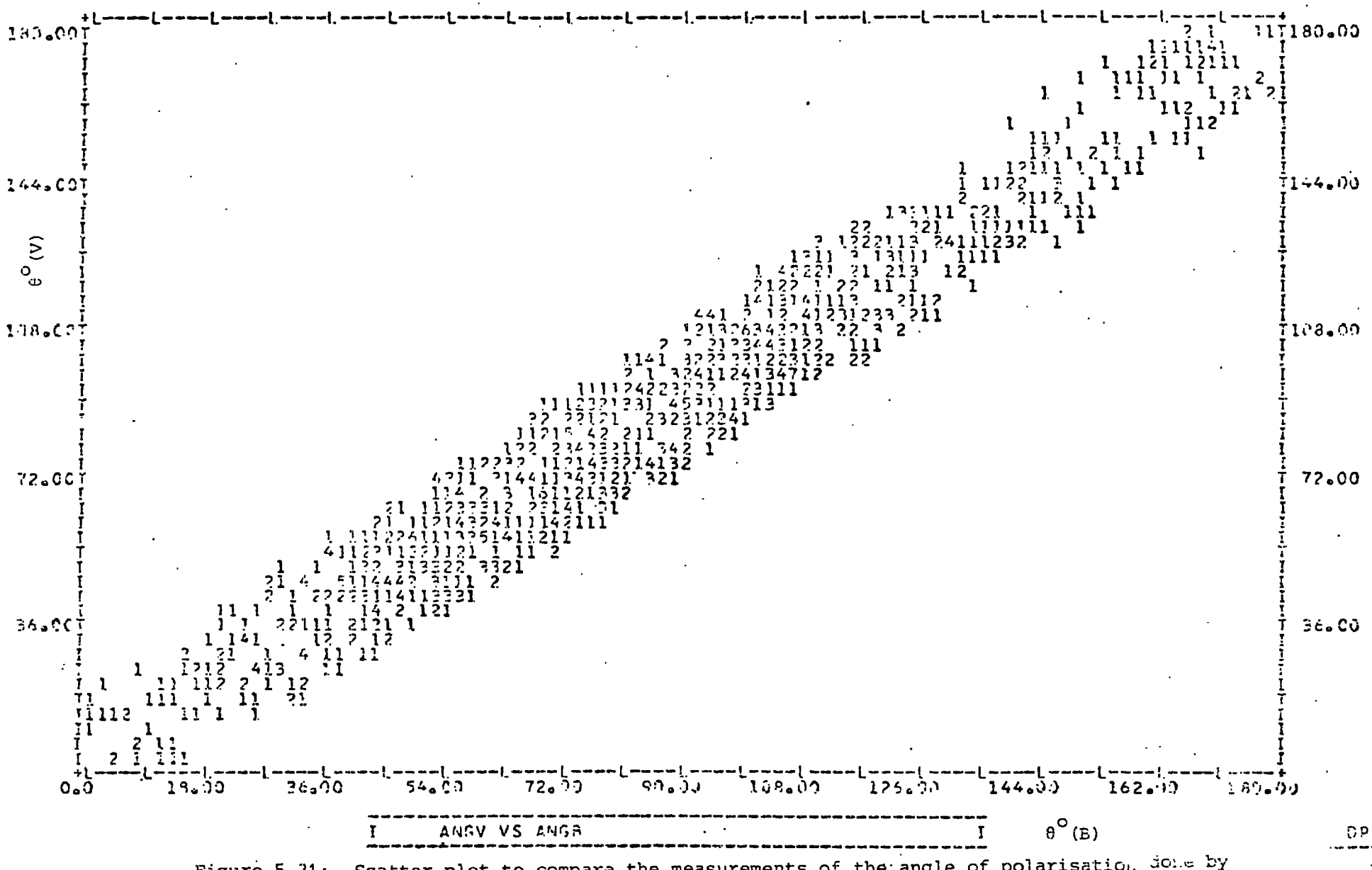

Figure 5.31: Scatter plot to compare the measurements of the angle of polarisation done by Pallister et al (B) with those of the present work (V).

This point to point comparison between the Pallister et al map (B) and the present map (V) is very informative as it gives further confirmation of the validity of the present technique to measure polarisation of extended astronomical objects.

5.8 Optical Polarisation Map of M43

The part of the Orion complex which is an HII region and is located at the NE of M42, is called M43 or NGC 1982. It is partly cut off from M42 by foreground extinction in the area of the Dark Lane which separates these two nebula from each other.

The observations involved in finding the optical polarisation map of M43 were obtained with the 1 m telescope of the Wise Observatory, Israel, in November 1977. The V waveband of the UBV system was used. The technique is the same as that used for M42.

The polarisation map is shown in Figure 5.32, superimposed on a photograph of the M43 taken in the red. Again, each measurement of polarisation is indicated by a line in the direction of the E-vector, proportional in length to the degree of polarisation and centred on the point observed. Typical errors in the body of the nebula are the same as described for M42. Each measurement is over a 7 x 7 arc sec square, and the 2000 data points give an essentially complete optical polarisation map of M43.

It can be seen from Figure 5.32 that the degree of polarisation changes from nearly 3% in the inner region (where the source of illumination is located) to 20% at the edge, particularly in the north where it seems that there is no emission.

Furthermore, as the diameter of an HII region is $2R_s = 0.56\ P_c$ (Table 4.2) or about 4.3′, the Strömgren sphere with this diameter

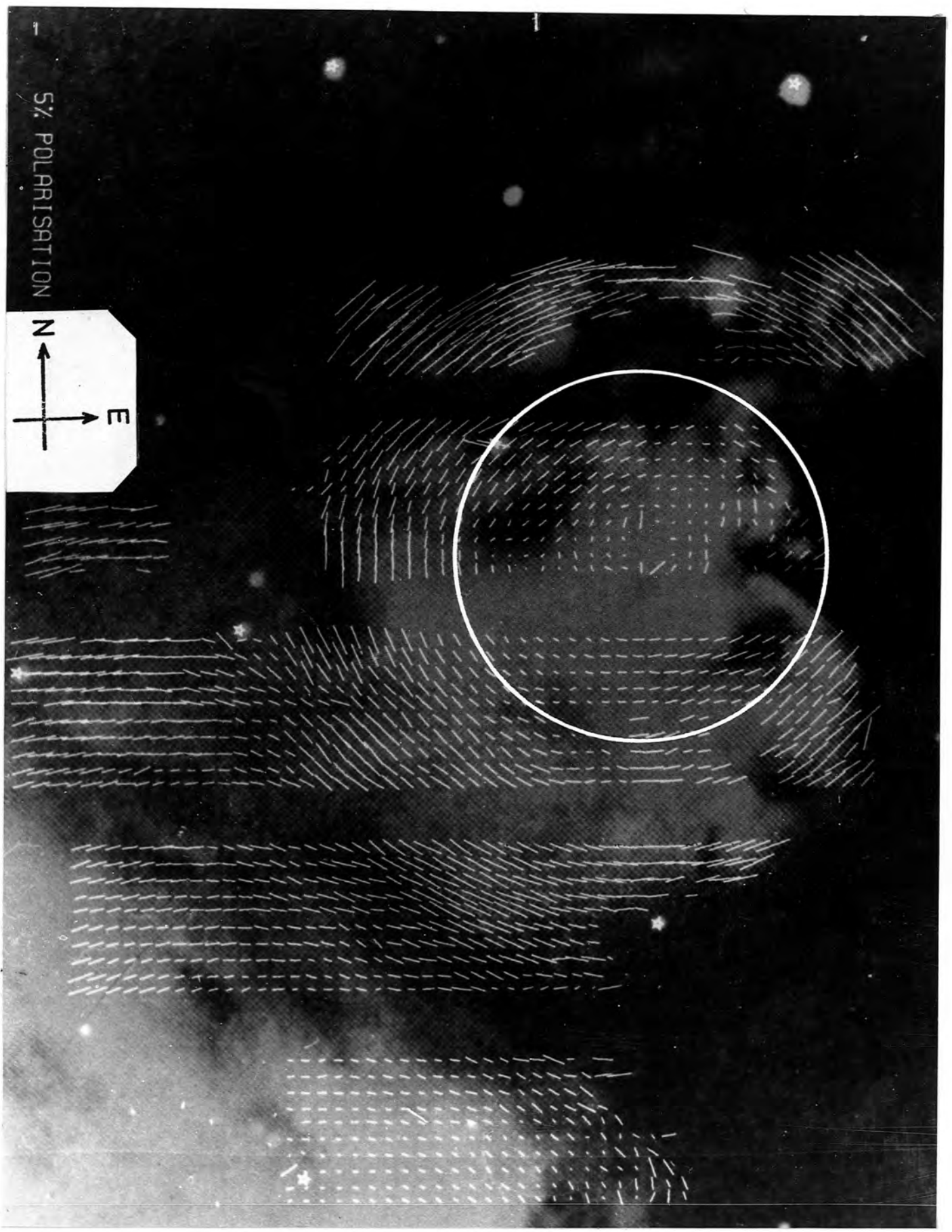

Figure 5.32: Results of the present observations of the linear polarisation of M43 superimposed on a red photograph. The white circle shows the extent of the Strömgren sphere.

can be discerned from Figure 5.32. The picture suggests that since the area running north-west - north-east, is located outside this sphere, there is no evidence for emission in this region and the degree of polarisation is relatively high.

REFERENCES

CHAPTER 5

Hall, R. 1974, IAU. Col. 23, Planets, Stars and Nebula, p.881, ed. T. Gehrels.

Osterbrock, D.E. 1974, Astrophysics of Gaseous Nebula, pub. Freeman and Company.

Pallister, W.S. et al, 1977, M.N.R.A.S. 178, 93P.

CHAPTER SIX

INTERPRETATION OF THE RESULTS

6.1 Geometry of the Orion Nebula and M43

The Orion Nebula has the advantage of presenting the regional variation of its physical characteristics, for observation because of its proximity (at a distance about 460 pc) as well as its relatively small interstellar extinction.

Many observations show that the large scale variations of the observed data are more or less circularly symmetric, and spherically symmetric models have been constructed by many observers (see, for instance, Osterbrock and Flather, 1959). According to the schematic picture of the Orion Nebula and molecular cloud presented in Figure 4.2, the nebula is ionisation bounded on the far side by the molecular cloud and a model present by Zukerman (1973) accounts for the high gas densities and substantial fluctuations in density and temperature observed within the Orion Nebula.

For the basic geometry of the nebula and surrounding material, to the first order, the model presented by Balick et al (1974) consists of a 'core' HII region surrounding θ^1ori which is an ionised 'cavity' partially imbedded in the near edge of a large neutral complex that contains the molecular clouds and infrared sources. Their model is a highly dynamic one where newly ionised gas flows into the nebular core from the nearby neutral gas, and then disperses into the lower density medium on the near side of the neutral complex.

All studies of the Orion Nebula are complicated by the problem of finding an adequate model of the geometry, for example for the relative

positions of the illuminating stars and scattering dust. In the present series of observations the optical linear polarisation map of the Orion Nebula (Figure 5.25) clarifies this primary problem of the structure of the nebula.

From Figure 5.25 one can see that polarisation values of ·5% dominate in most parts of the nebula. Over a large fraction of the map there is a centrosymmetric pattern of polarisation vector orientations. This pattern is centred on θ^1ori, and an interpretation of this effect is that the pattern is due to the scattering of light originating in θ^1ori by the nebular medium, where the character of the particles and the scattering geometry are the most effective parameters in determining the degree of polarisation.

It is obvious from the extent of the polarisation pattern that most of the Orion Nebula is illuminated by θ^1ori. However, in the region of θ^2ori where the polarisation pattern is more complicated, the pattern tends to centre on θ^2 rather than on the Trapezium, suggesting that this area of the nebula is mainly illuminated by θ^2. There is independent evidence of θ^2 contributing to the illumination of the nebula in the form of bright edges on small condensations near this star (the condensations are too small to be seen individually on the present map), discussed by Münch and Wilson (1962) and Taylor (1974). Their suggestion of the condensations being illuminated by θ^2 is supported by the pattern of the polarisation in this area and the results obtained by Pallister et al (1977).

The position of the Kleinmann-Low infrared nebula is indicated on Figure 5.25. The direction of infrared polarisation is similar to that observed optically.

From Figure 5.32 one can see again over a large fraction of the linear optical polarisation map of M43, that there is a centrosymmetric pattern of polarisation vector orientations tending to centre on the exciting star of M43. In the south-west quadrant near the Dark Lane, the orientations of the polarisation vectors differ from those expected, suggesting the possibility of a transition effect in this part of the nebula.

The higher degree of polarisation in M43 compared with M42 suggests that the effect of emission here is weaker than in M42, and/or the application of Rayleigh scattering is more applicable in this nebula.

6.2 A Simple Model of the Orion Nebula

Many observers have tried to find a theoretical model for the Orion Nebula to fit with the observations (see, for example, Zuckerman 1973, and Schiffer III and Mathis, 1974). A model is suggested by Wilson et al (1959) in which the gas is expanding as a spherical cloud centred on the Trapezium and Tamura (1975) constructed a model of the Orion Nebula based on an assumption that the nebula is composed of gaseous clumps surrounded by vacuum space.

The scattered light is diluted by direct nebular emission, which does effect the percentage of polarisation, but not the polarised intensity. We present a simple model of the Orion Nebula as a spherically symmetric optically thin dust cloud with θ^1ori at the centre. Then we compare the total and polarised intensity of our measurements with those predicted by the theoretical model. The scattering geometry of the model is shown in Figure 6.1, and Table 6.1 presents the parameters used in this model.

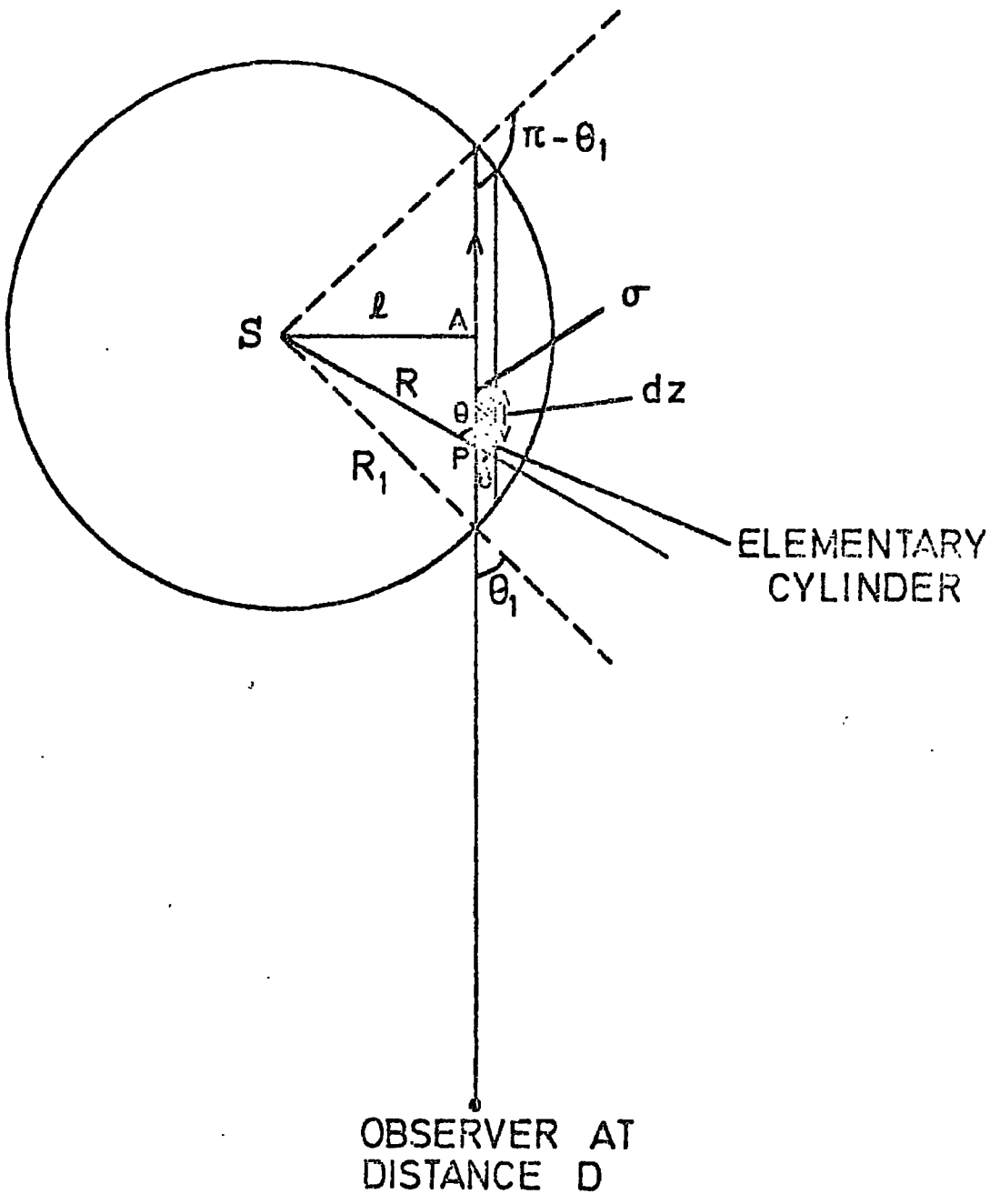

FIG. 6.1

SCATTERING GEOMETRY FROM A STAR IN AN OPTICALLY THIN SPHERICALLY SYMMETRIC DUST CLOUD.

R_1	Radius of dust cloud
R	Distance between the star and scattering particle
ℓ	Distance of the star from line of sight
θ_1	Scattering angle for a particular line of sight at the surface of the dust cloud
θ	Scattering angle
L	Luminasity of the star
z	Direction in line of sight
σ	Cross section of elementary cylinder
K	$= \frac{2\pi}{\lambda}$ wave number
D	Distance between observer and plane of scattering

Table 6.1: Parameters used in the present model of the Orion Nebula.

First we consider the number of dust particles per unit volume to be:

$$= n(R) \qquad \text{for} \qquad R < R_1$$

and

$$= 0 \qquad \text{for} \qquad R > R_1$$

The intensity of incident light at the point P in the optically thin case is:

$$I_R = \frac{L}{4\pi R^2} \quad \text{erg cm}^{-2} \text{ sec}^{-1} \tag{6.1}$$

The scattered intensity at the point of observation from a particular dust particle is given by Van de Hulst (1957) in the form of:

$$I_o = {}^1/_2 \frac{(I_1 + I_2)}{K^2 D^2} \cdot I_R \tag{6.2}$$

where

$$I_1 = |S_1(\theta)|^2 \tag{6.3}$$

and

$$I_2 = |S_2(\theta)|^2 \tag{6.4}$$

S_1 and S_2 are complex amplitude functions defined in Chapter 2. The number of particles in the elementary cylinder is equal to $n(R)\sigma \, d\, Z$. Therefore the total intensity at the distance ℓ (integrated along the line of sight) is:

$$I_o^T = \int_{-Z_o}^{Z_o} I_o \, n(R)\sigma \, dZ \tag{6.5}$$

Transforming from Z to θ for a given ℓ gives

$$Z = -\ell \cot\theta$$

and

$$dZ = \ell \cos \sec^2 \theta \; d\theta$$

Hence

$$I_o^T = \int_{\theta_1}^{\pi - \theta_1} I_o \, n(R) \, \sigma \, \ell \, \mathrm{cosec}^2 \theta \, d\theta \qquad (6.6)$$

At the observer, in terms of unit solid angle (solid angle $\equiv \frac{\pi}{D^2} = 1$) for the total intensity we have

$$I_T = D^2 \ell \int_{\theta_1}^{\pi - \theta_1} I_o \, n(R) \, \mathrm{cosec}^2 \theta \, d\theta \qquad (6.7)$$

Using equations (6.1) and (6.2):

$$I_T = D^2 \ell \int_{\theta_1}^{\pi - \theta_1} \frac{(I_1 + I_2)}{2K^2 D^2} \cdot \frac{L}{4\pi R^2} \cdot n(R) \, \mathrm{cosec}^2 \theta \, d\theta \qquad (6.8)$$

As, $R = \ell \, \mathrm{cosec} \, \theta$, using equations (6.3) and (6.4):

$$I_T = \frac{L}{8\pi K^2} \cdot \frac{1}{\ell} \int_{\theta_1}^{\pi - \theta_1} (|S_1(\theta)|^2 + |S_2(\theta)|^2) \, n(R) \, d\theta \qquad (6.9)$$

Where $S_1(\theta)$ applies to the electric vector perpendicular to the plane of scattering and $S_2(\theta)$ for parallel to the plane of scattering.

The polarised intensity is given by the difference between contributions from I_1 and I_2, so:

$$I_p = \frac{L}{8\pi K^2} \cdot \frac{1}{\ell} \int_{\theta_1}^{\pi - \theta_1} (|S_1(\theta)|^2 - |S_2(\theta)|^2) \, n(R) \, d\theta \qquad (6.10)$$

In the case of Rayleigh scattering for I_1 and I_2 Van de Hulst (1957) gives:

$$I_1 = |S_1(\theta)|^2 = K^6 |\alpha|^2 \qquad (6.11)$$

and

$$I_2 = |S_2(\theta)|^2 = K^6 |\alpha|^2 \cos^2 \theta \qquad (6.12)$$

where α is the polarisability.

Thus in this case we Have:

$$I_T = \frac{LK^4|\alpha|^2}{8\pi\ell} \int_{\theta_1}^{\pi-\theta_1} (1 + \cos^2\theta)\ n(R)\ d\theta \tag{6.13}$$

and

$$I_p = \frac{LK^4|\alpha|^2}{8\pi\ell} \int_{\theta_1}^{\pi-\theta_1} \sin^2\theta\ .\ n(R)\ d\theta \tag{6.14}$$

Assuming a power beam falls off in the form of:

$$n(R) = \frac{n_o}{R^m} \tag{6.15}$$

Therefore:

$$I_T = \frac{LK^4|\alpha|^2 n_o}{8\pi\ell^{m+1}} \int_{\theta_1}^{\pi-\theta_1} (1 + \cos^2\theta)\ \sin^m\theta\ d\theta \tag{6.16}$$

and

$$I_p = \frac{LK^4|\alpha|^2 n_o}{8\pi\ell^{m+1}} \int_{\theta_1}^{\pi-\theta_1} \sin^{m+2}\theta\ d\theta \tag{6.17}$$

Considering

$$C = \frac{LK^4|\alpha|^2 n_o}{8\pi}$$

the general equations for I_T and I_p will be:

$$I_T(\ell) = \frac{C}{\ell^{m+1}} \int_{\theta_1}^{\pi-\theta_1} (1 + \cos^2\theta)\ \sin^m\theta \cdot d\theta \tag{6.18}$$

and

$$I_p(\ell) = \frac{C}{\ell^{m+1}} \int_{\theta_1}^{\pi-\theta_1} \sin^{m+2}\theta\ d\theta \tag{6.19}$$

where,

$$\theta_1 = \sin^{-1}\left(\frac{\ell}{R_1}\right)$$

Evaluating these integrals for particular values of m gives:

m = 0

$$I_T(\ell) = \frac{C}{2\ell}(3\pi - 6\theta_1 - \sin 2\theta_1) \quad (6.20)$$

$$I_p(\ell) = \frac{C}{2\ell}(\pi - 2\theta_1) \quad (6.21)$$

m = 1

$$I_T(\ell) = \frac{2C\cos\theta_1}{\ell^2}(1 + \frac{1}{3}\cos^2\theta_1) \quad (6.22)$$

$$I_p(\ell) = \frac{2C\cos\theta_1}{\ell^2}(1 - \frac{1}{3}\cos^2\theta_1) \quad (6.23)$$

m = 2

$$I_T(\ell) = \frac{C}{16\ell^3}(10(\pi - 2\theta_1) + 8\sin 2\theta_1 + \sin 4\theta_1) \quad (6.24)$$

$$I_p(\ell) = \frac{C}{16\ell^3}(6(\pi - 2\theta_1) + 8\sin 2\theta_1 - \sin 4\theta_1) \quad (6.25)$$

The comparison between the total and polarised intensity of our measurements with those predicted by the model is shown in Figures 6.2 and 6.3 with m = 0 for constant dust density.

Figure 6.2 shows the variation of I_T (Logarithmic scale) with distance of each data point from θ^1ori in arc sec for both Theoretical and Observational cases, Figure 6.3 shows the same variation of I_p. We normalised the polarised and , total intensity of predicted data points with those obtained by the observation, where the normalisation factors are respectively

C_1 and C_2 ($C_1 = \frac{I_p \text{ observational}}{I_p \text{ theoretical}}$, $C_2 = \frac{I_T \text{ observational}}{I_T \text{ theoretical}}$) .

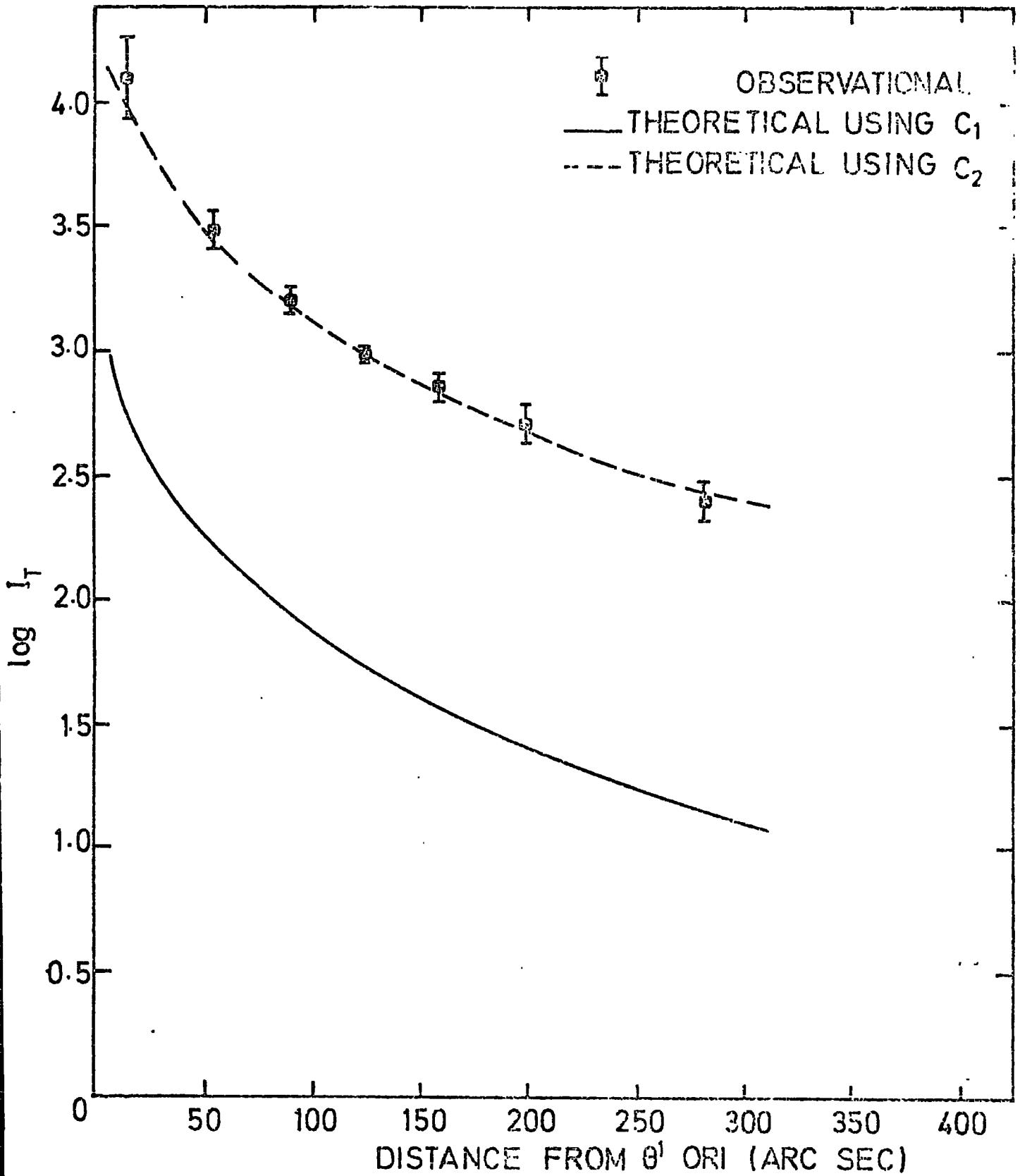

FIG. 6.2 VARIATION OF THE TOTAL INTENSITY (I_T) WITH DISTANCE FROM θ^1 ORI FOR BOTH THEORETICAL AND OBSERVATIONAL CASES.

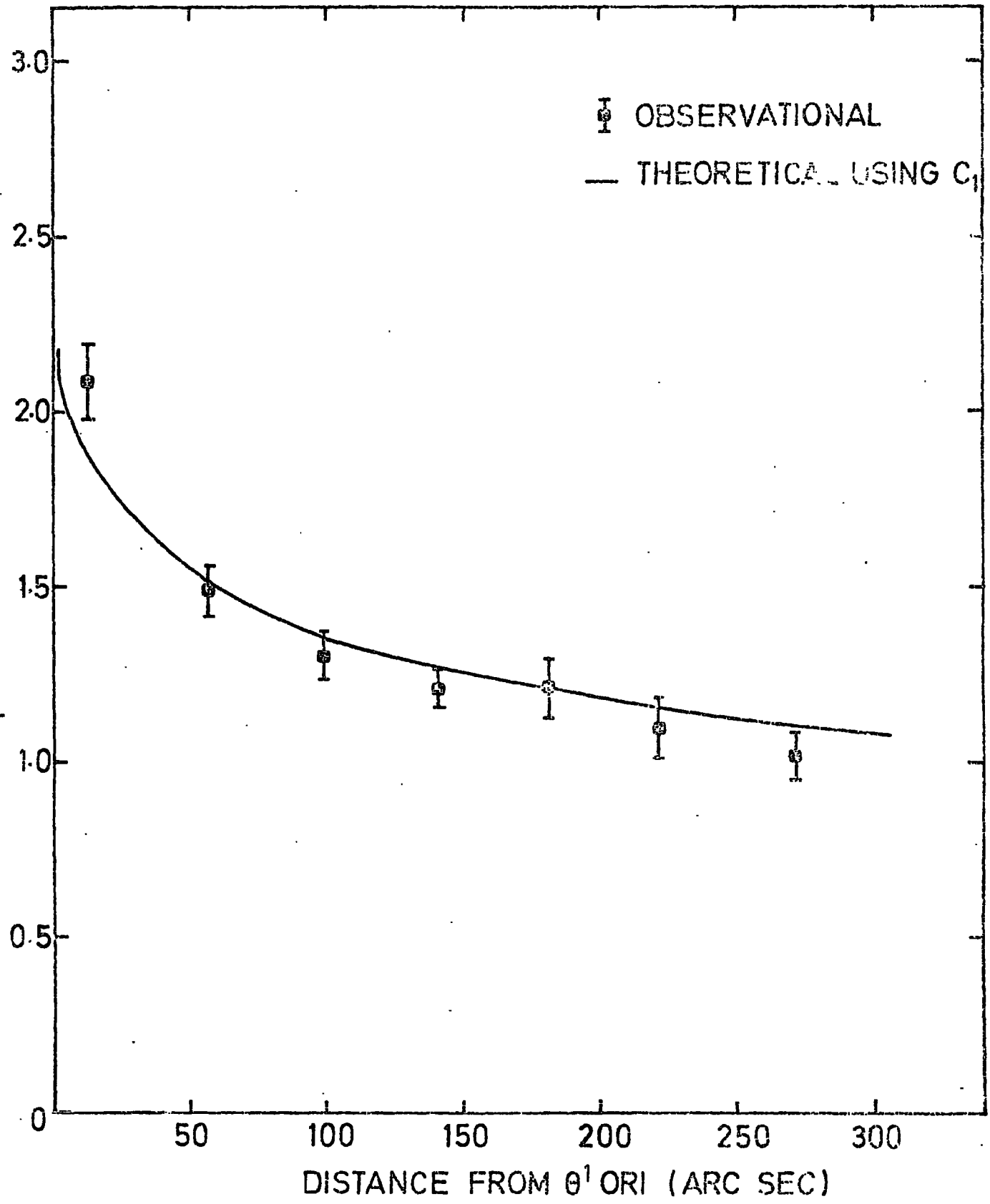

FIG. 6·3 VARIATION OF THE POLARISATION INTENSITY I_p WITH DISTANCE FROM θ^1 ORI FOR BOTH THEORETICAL AND OBSERVATIONAL CASES.

In these figures, the observed data points are represented by the squares, the size of error bars indicating the error. The predicted data points after normalisation by C_1 are represented by the solid line and those after normalisation by C_2 are represented by the dashed line.

As one can see from Figure 6.2, the predicted data points after normalisation by C_2 agree well with the observed data points, but those normalised by C_1 do not. This may be caused by the fact that we have used optically thin case and also by the geometry. Figure 6.3 shows a good agreement between the predicted data points after normalisation by C_1 and those obtained by the observation. Considering these, in conclusion it seems the present model is in reasonable agreement.

6.3 Possible causes of the Disagreement between the Present Model of the Orion Nebula and Observational Results

The discrepancy between the observational results and those predicted by the model could result either from one of the following effects or from a combination of them.

1. Either the measurements are wrong in places.
2. The optically thin case is not applicable here.
3. Geometry.
4. Predomination of Mie scattering rather than Rayleigh scattering.

So, to make a general model of the Orion Nebula in order to determine the precise geometry and the nature of the dust particles, which are important in star formation, one needs more information and detailed data.

REFERENCES

CHAPTER 6

Balick, B. et al, 1974, Pub. A.S.P. 86, 616

Münch, G. and Taylor, K. 1974, Ap. J. 192, L93

Münch, G. and Wilson, D.C. 1962, Z. Ap. J. 56, 127

Osterbrock, D.E. and Flather, E. 1959, Ap. J. 129, 26

Pallister, W.S. et al, 1977, New Scientist, 24 March

Schiffer III, F.H. and Mathis, J.S. 1974, Ap. J. 194, 597

Tamura, H. 1975, Sci. R. Eng. I, Vol. LVIII, p.23

Van De HULST, H.C. 1957, Light Scattering by Small particles.

Wilson, O.C. et al, 1959, Ap. J. Suppl. 4, 199

Zuckerman, B. 1973, Ap. J. 183, 863

CHAPTER SEVEN

GENERAL CONCLUSIONS

The use of the Durham polarimeter in conjunction with the Royal Greenwich Observatory electronographic camera provides a fast and accurate method of measuring the optical linear polarisation of a few thousand points simultaneously, in an extended astronomical object.

Our automated reduction techniques can be used to analyse the results of observations for many objects with only slight modifications necessary, corresponding to the requirements of the different individual sets of measurements, as has been illustrated in this thesis, for the optical polarisation studies of the nebulae, M42 and M43.

The results obtained with the present technique for the Orion Nebula are a considerable improvement both in quality and quantity on those previously available.

The comparison of the present results for the Orion Nebula with the earlier work of Hall (1974) and Pallister et al (1977), shows that the two sets of measurements agree well, in the same physical regions of the nebula.

In this work some physical properties of the nebulae, M42 and M43 are presented, and it is the first attempt to obtain the optical linear polarisation map of M43.

Centrosymmetric pattern of polarisation vector orientations which tend to centre on the exciting star in both nebulae, indicates that the polarisation is due to the scattering of light emanating from the exciting star by the nebular material. In the Orion Nebula in addition to θ^1ori in the centre, in the region around θ^2ori, the polarisation pattern tends to centre on this star rather than Trapezium, giving rise

to the assumption that this area of the nebula is mainly illuminated by θ^2ori.

~~Although~~ The direction of infrared polarisation is not similar to that observed optically in the Orion Nebula, the polarising mechanisms may differ, since the optical polarisation can arise from scattering of light by randomly aligned particles, whereas the infrared effect has been attributed, by Dyck and Beichman (1974), to a polarising screen of aligned dust grains. Those authors assumed that the alignment was caused by magnetic fields, but there is no evidence for this at optical wavelengths. There is no certainty that the infrared feature has an optical counterpart, and an alternative possibility is that the alignment is produced by radiation effects, the source of energy being the Trapezium. Such effects have been discussed in a different contest by Harwit (1970).

In addition to the geometry of the Orion Nebula and M43, we derived a simple model for the Orion Nebula which gave some disagreement between the observational results and the theoretical model. Considering the relatively small value of the degree of polarisation, particularly in M42, it seems that Mie scattering dominates in this nebula. More information is needed to find a general model for this astronomical object.

In conclusion, therefore, present technique provides a powerful tool for measuring optical linear polarisation of extended astronomical objects. Already technique is being developed which aims at increasing the accuracy of the results by first obtaining a map of the photocathode containing the defects therein and subtracting this before going on to obtain the Stokes parameters.

Dyck and Beichman (1974) have measured the infra-red linear-polarisation of the Kleinmann-Low nebula. Their results and the present measurements of the optical polarisation in terms of the angle of polarisation for the regions corresponding to each other in both observations are presented in Table 7.1.

Region	Infra-red			Optical		
	RA (1950)	Dec (1950)	θ^{o}	RA (1950)	Dec (1950)	θ^{o}
A	$5^{h}\ 32^{m}\ 46.^{s}4$	$-5^{o}\ 24'\ 17''$	109 ± 3	$5^{h}\ 32^{m}\ 46.^{s}2$	$-5^{o}\ 24'\ 19''$	165 ± 1
B	5 32 46.8	-5 24 22	106 ± 3	5 32 47.3	-5 24 28	171 ± 2
C	5 32 46.8	-5 24 28	77 ± 4	5 32 47.3	-5 24 36	159 ± 2
D	5 32 46.8	-5 24 33	106 ± 16	5 32 47.3	-5 24 45	166 ± 1

Table 7.1: Comparison between our measurements of the angle of polarisation (optical) and those of Dyck and Beichman (infra-red), 1974.

Table 7.1 shows that the orientations of the polarisation vectors in the Kleinmann-Low nebula do not agree at optical and infra-red wavelength. The present measurements (figure 5.21), and those of Pallister et al (1977) agree however, which suggests that the optical measurements are correct. Dyck and Beichman (1974) have suggested that the infra-red polarisation is caused by transmission of the infra-red radiation through aligned grains in the Orion Nebula. The present map shows no evidence for such a phenomenon as the pattern at optical wavelengths can be well explained by the scattering of light from θ^{1} ori from randomly aligned grains.

REFERENCES

CHAPTER 7

Dyck, H.M. and Beichman, C. A. 1974, Ap. J. 194, 57

Hall, R. 1974, I.A.U. Coll. 23, Plants, Stars and Nebula, p.881, ed. T. Gehrels

Harwit, M. 1970, Bull. Astr. Inst. Czechoslovakia, 21, 204

Pallister, W.S. et al, 1977, New Scientist, 24 March.

ACKNOWLEDGEMENTS

The author wishes to thank exceedingly Dr. S.M. Scarrott for his academic and moral guidance, and helpful suggestions given at all stages of this work.

He expresses gratitude to Dr. W.S. Pallister for his many critical comments both academically and as a friend whose advice has been of great value.

Many useful discussions on the modelling aspect ofthis work have been held with Dr. J. Chesterman for which the author is indebted to him.

Miss T.F. Carty is thanked for her meticulous proof reading of the thesis and the other members of the Astronomy group are thanked for their guidance and help in obtaining the data.

The facilities and expertise of the Royal Greenwich Observatory provided by Dr. R.G. Bingham are gratefully acknowledged as is his great help, and also that of Dr. D. McMullan and Dr. J. Pilkington, along with the staff of Wise Observatory.

Professors A.W. Wolfendale, F.R.S., and B.H. Bransden, sequentially the Heads of the Physics Department, are thanked for making the facilities of the Department readily available.

The University of Ferdossi (Mashhad), Ministry of Science and Higher Education, Iran, are greatly thanked for their official and financial support.

Finally, the author wishes to thank his wife, without whose support and encouragement, none of this would have been possible.